Electrolytes for Sodium Ion Batteries: The Current Transition from Liquid to Solid and Hybrid systems

ADVANCED MATERIALS
www.advmat.de

Electrolytes for Sodium Ion Batteries: The Current Transition from Liquid to Solid and Hybrid systems

Hamideh Darjazi, Marisa Falco, Francesca Colò, Leonardo Balducci, Giulia Piana, Federico Bella, Giuseppina Meligrana, Francesco Nobili, Giuseppe A. Elia, and Claudio Gerbaldi**

Sodium-ion batteries (NIBs) have recently garnered significant interest in being employed alongside conventional lithium-ion batteries, particularly in applications where cost and sustainability are particularly relevant. The rapid progress in NIBs will undoubtedly expedite the commercialization process. In this regard, tailoring and designing electrolyte formulation is a top priority, as they profoundly influence the overall electrochemical performance and thermal, mechanical, and dimensional stability. Moreover, electrolytes play a critical role in determining the system's safety level and overall lifespan. This review delves into recent electrolyte advancements from liquid (organic and ionic liquid) to solid and quasi-solid electrolyte (dry, hybrid, and single ion conducting electrolyte) for NIBs, encompassing comprehensive strategies for electrolyte design across various materials, systems, and their functional applications. The objective is to offer strategic direction for the systematic production of safe electrolytes and to investigate the potential applications of these designs in real-world scenarios while thoroughly assessing the current obstacles and forthcoming prospects within this rapidly evolving field.

1. Introduction

The current energy economy based on fossil fuels is accountable for dramatic environmental consequences to our lives and cannot be considered a feasible solution to guarantee the increasing global energy demand.[1–4] This scenario explains the progressively widespread application of clean, carbon-neutral, and sustainable energy systems as a feasible strategy to face the global challenges connected to the demands of our modern society.[5–7] It represents an imperative urgency for humankind and must go against economy-driven arguments.[8–10] The implementation of renewable energy, such as sun, waves, and wind, into energy production is increasing yearly. However, a more substantial penetration is limited by the energy production from renewable energy being diffused in space and variable in time. The latter issues can be mitigated by efficiently implementing large-scale electrical energy storage (EES) systems as a technology platform to smooth the intermittency of renewable energy harvesters/converters.[11–13] The principal EES systems are pumped-hydroelectric storage (currently covering 90% of the energy stored), flywheels, compressed-air energy storage, batteries, and capacitors. In recent years, massive attention has been paid to electrochemical energy storage due to its ability to combine low capital costs with high energy density, compactness with long cycle life, and simple

H. Darjazi, M. Falco, F. Colò[+], G. Piana[++], G. Meligrana, G. A. Elia, C. Gerbaldi
GAME Lab
Department of Applied Science and Technology – DISAT
Politecnico di Torino
Corso Duca degli Abruzzi 24, Torino 10129, Italy
E-mail: giuseppe.elia@polito.it; claudio.gerbaldi@polito.it

The ORCID identification number(s) for the author(s) of this article can be found under https://doi.org/10.1002/adma.202313572

[+]Present address: Stellantis Europe SpA, Corso G. Agnelli 200, Torino 10135, Italy

[++]Present address: Free2move eSolutions S.p.A, Piazzale Lodi 3, Milan 20137, Italy

DOI: 10.1002/adma.202313572

H. Darjazi, M. Falco, F. Colò[+], G. Piana[++], F. Bella, G. Meligrana, F. Nobili, G. A. Elia, C. Gerbaldi
National Reference Center for Electrochemical Energy Storage (GISEL) – INSTM
Via G. Giusti 9, Firenze 50121, Italy

L. Balducci, F. Nobili
School of Sciences and Technologies – Chemistry Division
University of Camerino
Via Madonna delle Carceri ChIP, Camerino 62032, Italy

F. Bella
Electrochemistry Group
Department of Applied Science and Technology – DISAT
Politecnico di Torino
Corso Duca degli Abruzzi 24, Torino 10129, Italy

maintenance with limited self-discharge.[14,15] Lithium-ion batteries (LIBs) are extensively used for portable electronic devices and in the mobility/transportation market, both for hybrid and electric vehicles.[16,17] However, relying on a single technology for electrochemical energy storage can constrain material supply, particularly considering critical raw materials (CRMs) such as Li, Co, Ni, and natural graphite.[18] Moreover, energy security concerns and geopolitical considerations in the supply chain are prompting nations to explore alternative battery chemistries.[10,19]

Sodium-ion batteries (NIBs) are among the most studied electrochemical storage systems,[20–23] generally considered a cheaper and more sustainable alternative for secondary battery needs. Similar to LIBs, NIBs also consist of three main components that allow their operation: a cathode, an anode, and a Na^+-conducting electrolyte. Besides the widely distributed and abundant natural resources (the sixth most abundant element, 2.36 versus 0.0017 wt.% for Na and Li, respectively), Na shows similar electrochemical properties to Li, the latter having a potential 0.33 V lower than Na.[24–26] The research on Na-ion batteries, motivated by sustainability, has garnered attention from the industry. This is because the raw material Na_2CO_3 is considerably cheaper and less prone to price volatility compared to Li raw materials like Li_2CO_3.[27] Moreover, in NIBs, the Cu current collector used in LIBs can be replaced by cheaper and lighter Al foil, which benefits the overall cell cost and energy density.[28] Additionally, the utilization of NIBs in a fully discharged state or their discharging to 0 V is considered safer when compared to LIBs. This safety advantage arises because there is no oxidation or dissolution of the current collector material used in NIBs (Al) as opposed to LIBs (Cu).[29–31]

On the other hand, the higher ionic radius of Na^+ (1.02 Å) compared to Li^+ (0.76 Å) renders it incompatible with certain conventional electrode materials.[32] This disparity also impacts phase stability, transport properties, and the formation of interphases.[33] When these issues are combined with the higher atomic weight of Na with respect to Li, Na demonstrates a significantly lower theoretical gravimetric/volumetric capacity compared to Li, with values of 1166 mAh g^{-1} and 1131 mAh cm^{-3} for Na, in contrast to 3861 mAh g^{-1} and 2062 mAh cm^{-3} for Li.[34] Given these challenges, the scientific community has produced thousands of articles on developing advanced electrode materials and novel electrolyte formulations.[35] In this respect, the reader can refer to several review articles covering state of the art on electrodes based on various elements and related compounds: antimony,[36] bismuth,[37] carbon,[38,39] iron,[40] manganese,[41] phosphorous,[42] tin,[43] titanium,[44,45] vanadium.[46,47] Moreover, electrodes for NIBs have also been proposed exploiting biomass-derived or cellulose-based materials,[48] conversion-type materials,[49,50] layered oxides and (di)chalcogenides,[51,52] metal oxide/carbon composites,[53,54] multi-electron reaction materials,[55] organic (carbonyl) compounds,[56,57] polyanionic insertion materials,[58,59] polymeric electrodes,[60] Prussian blue,[61] sulfides and selenides,[62,63] and super ion conductors.[64] Issues related to electrode design should also focus on electrode/electrolyte interfaces, sodiation/de-sodiation phenomena, Na metal chemical reactivity with organic solvents, etc. To this purpose, review articles on operando X-ray diffractometry and other diagnostic tools,[65–67] treatment of Na metal anodes,[68] interfaces and their engineering,[69,70] modeling and simulation,[71,72] cost analysis[73] and large-scale fabrication strategies[74–76] have been published in the last years to push NIBs closer to the widespread intrusion in the market for EES systems. Furthermore, several solvation structure-related interfacial models have been introduced, which integrate molecular-scale interactions among the alkali-ion, anion, and solvents at the electrolyte–electrode interfaces. These models serve to facilitate the interpretation of battery performance.[77–81]

As one of the three key components in an electrochemical cell, the electrolyte of NIBs typically consists of a solution of salts dissolved in aprotic solvents. Although this cell component often receives less consideration with respect to the electrodes, its role is fundamental for the proper operation of a battery system.

It is also responsible for safety issues in battery performance when temperature and charge/discharge current rates change. Thermal stability, strictly connected to flammability and explosiveness, remains one of the main issues of organic liquid electrolytes, analogously to the LIB technology.[82,83] The scientific community has recently started considering alternative concepts and the path toward solid electrolyte systems offering high thermal stability, no leakage and volatilization, low flammability, and no risk of fire and explosion (**Figure 1**).[84] This scenario covers both full- and half-cells, based on Na metal anodes (strongly enhancing the energy density), where mechanically robust solid electrolytes restrain dendrites formation.

Compared to traditional liquid electrolytes, utilizing solid-state electrolytes with high mechanical strength effectively prevents dendrite propagation, enhancing the safety and performance of batteries. Thus, in research, emphasis should be placed on achieving a stable solid-electrolyte interphase (SEI) layer, controlling dendrite formation, reducing "dead Na", and enhancing ionic conductivity, all within the context of electrolyte development. Some reviews were published on electrolyte systems for NIBs, focused on structure/property relationships[85–87] and basic concepts,[88,89] also covering additives,[90–92] ethers-based systems,[93–95] ionic liquids,[32,96–99] inorganic solid electrolytes[100–104] and investigation of the electrolyte effects on SEI formation.[105,106]

This review highlights the progressive transition from liquid electrolytes to solid and quasi-solid systems in NIBs, on which we discover that although significant advancements have been made, substantial challenges must be addressed before being commercially viable. Initially, an introductory overview outlines the electrolyte components and liquid systems, encompassing sodium salts, organic solvents, and additives. Subsequently, attention is directed toward the solvation structure and distinguishing characteristics of various electrolyte systems, including conventional liquid electrolytes, ionic liquids, polymer electrolytes, superconcentrated electrolytes, and localized high-concentration electrolytes. A thorough understanding is fostered through the exploration of fundamental equations and definitions, essential for delineating transport properties and conduction mechanisms across diverse Na-based battery electrolyte types. This comprehensive discussion elucidates the trajectory of advancements within the domain, encompassing a spectrum of electrolyte technologies aimed at enhancing the performance and viability of sodium-based energy storage systems. Continuing, the discussion delves into the pivotal role of separators and electrolyte

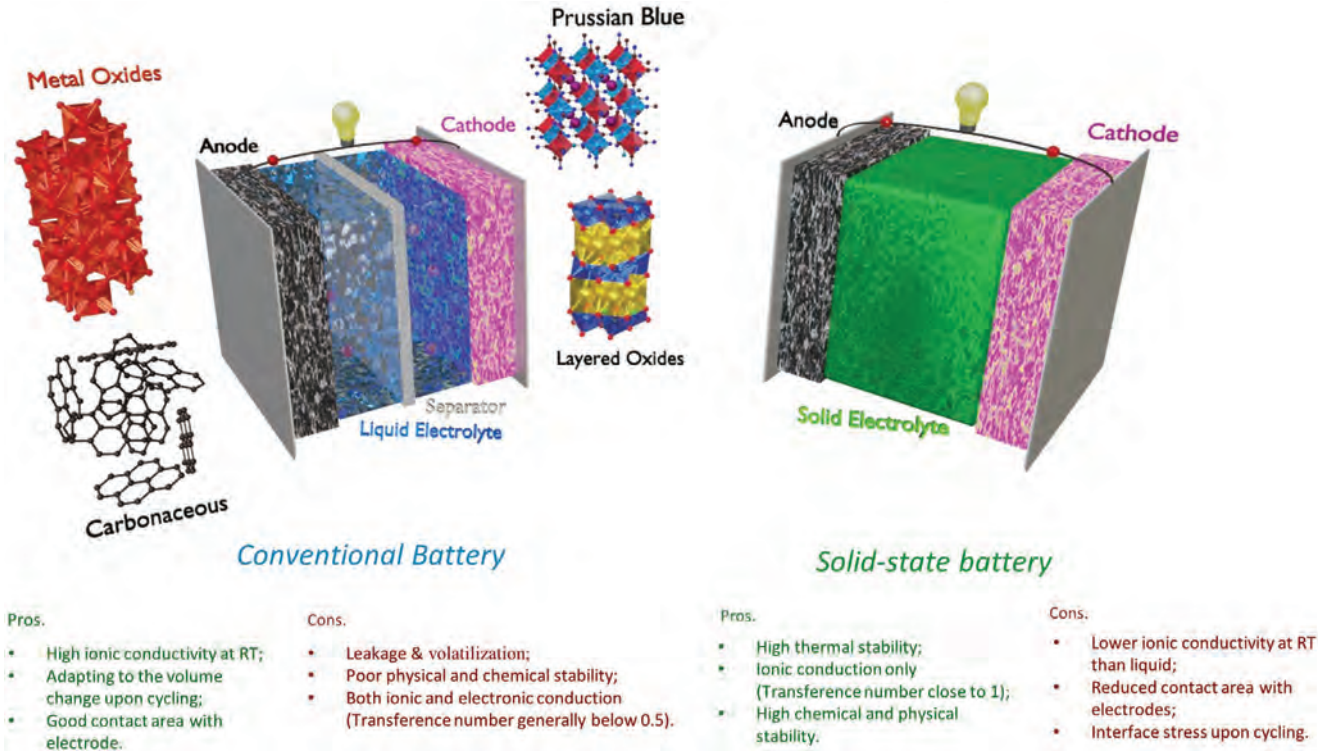

Figure 1. Schematic illustration of liquid NIB versus solid-state Na-based battery.

filling, underscoring the imperative of research endeavors aimed at transitioning away from liquid electrolytes. Recent advancements in ionic liquid systems are delineated, showcasing the ongoing progress in the field. Then, an extended elaboration is focused on the operational principles of solid-state batteries, ranging from truly solid-state electrolytes to hybrid polymer electrolytes, and ultimately to single sodium-ion conductors. Each topic is individually discussed, with specific attention to design principles, functional mechanisms, electrochemical performance, recent advancements, and remaining obstacles to practical exploitation, while also offering a comparative analysis of ionic conductivity across different solid-state electrolyte materials. This extensive overview serves as a cornerstone in offering novel data-driven insights, thereby presenting substantial value to the research community. Through meticulous analyses and critical evaluations, this review contributes fresh perspectives and invaluable findings, enriching the collective understanding within the field.

2. Fundamentals: Electrolyte Components and Liquid Systems

Liquid electrolytes have been the subject of extensive research for Na-ion systems due to their potential for high ionic mobility in the liquid state. These electrolytes typically involve dissolving a sodium-based ionic salt in either a single organic solvent or a mixture of organic solvents, or in water. As a result, they are categorized into two main types based on the solvent used: non-aqueous and aqueous electrolytes. However, this review exclusively focuses on non-aqueous electrolytes for applications in aprotic NIBs in the upcoming sections.[107] The practical use of electrolytes in an electrochemical system requires a precise list of features, which can be summarized as follows:

a) it should be ionically conductive and electronically insulating in order to facilitate the Na^+ ions transportation during cell operation and minimize the self-discharge;
b) it should be chemically stable, thus, no chemical reactions occur during cell operation within itself, with the separator and the electrodes in use, and with the other cell components, like packaging materials and current collectors (Al foils are typically used for NIBs);
c) it should be thermally stable, so the melting should be lower and boiling points should be higher than the operating temperature of the battery;
d) it should have a wide electrochemical stability window (ESW), meaning no degradation occurs within the range of electrode working potentials;
e) it must induce morphologically stable protective film (i.e., the SEI layer) on the electrode's surface.

Besides these operational requisites, an NIB electrolyte should also be formulated in order to meet other market criteria:

a) it should be eco-friendly, with low toxicity and limited environmental hazards;
b) it should be based on sustainable chemistries, which means abundant elements and synthetic processes with as low impact as possible;

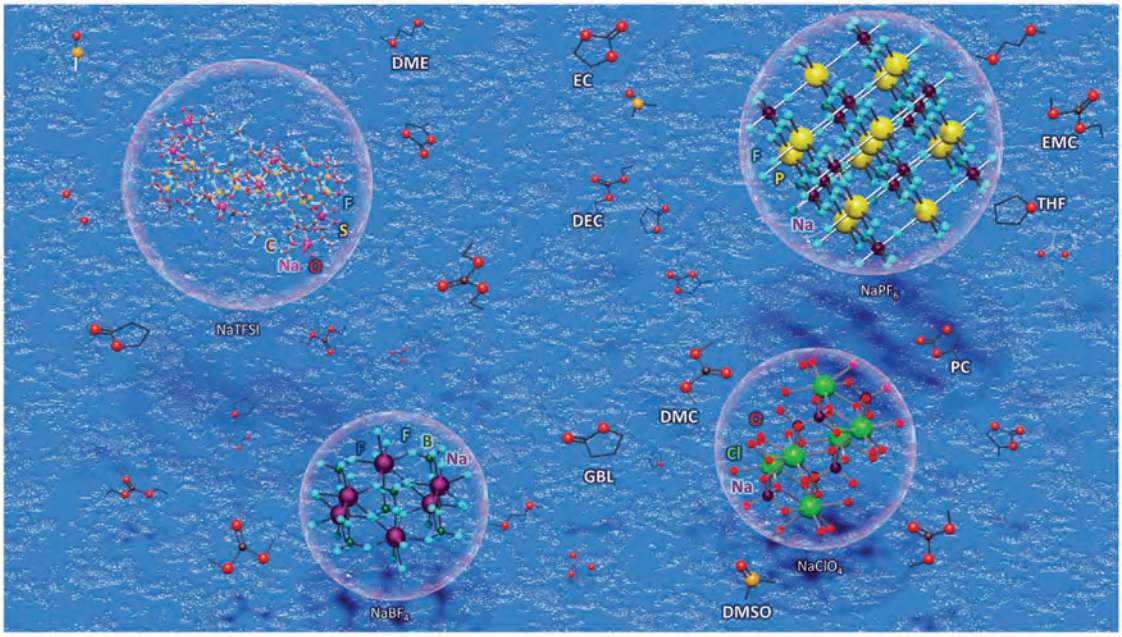

Figure 2. Schematic illustration of common Na salts and organic solvents.

c) it should be cheap in terms of materials and production not to increase the final prototype's overall cost.

The above requirements are generally valid for any electrolyte because the specific characteristics must be considered based on the kind of electrode chemistries involved and the final envisaged application. Non-aqueous liquid electrolytes typically consist of three primary components: solvent, salt, and additives. These elements will be further discussed in the following sections.

2.1. Sodium Salts

Soluble sodium salts are added to the solvent(s) (see **Figure 2**), and they act as charge carriers of the current passing in the electrochemical cell during operation (charge and discharge processes). An ideal electrolyte salt should meet the following requisites:

a) high solubility in the solvent(s) used, attaining a favorable level of ionic conductivity. In particular, the anion should be inert to the solvent(s);
b) elevated stability against electrochemical oxidation and reduction to ensure a wide ESW. ESW is defined as the difference between the energy levels of the lowest unoccupied molecular orbital (LUMO) and the highest occupied molecular orbital (HOMO). In particular, anions with lower HOMO levels are less susceptible to electron loss and decomposition;
c) elevated chemical stability against the other cell components. Na salt anions exert dual effects on electrolyte chemical stability in NIBs. First, the HOMO level of the anions can restrict the upper electrochemical window of NIBs. Second, the LUMO level of the anions can facilitate the formation of the SEI layer, which acts to prevent further decomposition of the electrolyte;

The characteristics just mentioned drastically reduce the number of Na salt candidates. The role played by the anion is fundamental because it must have a central atom with ligands withdrawing electron density, which delocalize the negative charge and, thereby, to easily "free" the Na^+ cation mobility, e.g., $[ClO_4]^-$, $[CF_3SO_3]^-$, $[AlX_4]^-$ (X = Cl–I), $[MF_6]$ (M = P, As, Sb, etc.), $[BF_4]^-$, or $[MCTFSI]^-$.[86] As a result, the most commonly used Na salts are $NaClO_4$, $NaBF_4$, $NaPF_6$, NaFSI ($N(SO_2F)_2^-$), NaTf ($CF_3SO_3^-$), and NaTFSI ($[N(CF_3SO_2)_2]^-$).

Table 1 summarizes some examples of these salts with some basic properties. In general, sodium salts have higher melting points than the corresponding Li salts, so they are more thermally stable, thus improving overall safety. Na perchlorate ($NaClO_4$) is one of the most commonly used due to its abundance (it is the most soluble among the common perchlorate salts), which renders it very cheap. Regarding thermal stability, it outperforms all other salts (from thermogravimetric analysis (TGA) and differential scanning calorimetry (DSC) studies, it shows decomposition temperatures of 500 and 474 °C, respectively). However, this salt use is restricted to academic research because, even after drying at 80 °C under vacuum for 12 h, the water content is relatively high (>40 ppm); moreover, it is explosive in the dry state.[88] It is more susceptible to oxidation due to the high HOMO level, which restricts its anodic stability. Na hexafluorophosphate ($NaPF_6$) is also widely implemented; it exhibits, in general, enhanced ionic conductivity with respect to $NaClO_4$ (1 M $NaPF_6$ in PC at 25 °C shows 7.98 mS cm^{-1}, while $NaClO_4$ provides an ionic conductivity of 6.4 mS cm^{-1}). Although $NaPF_6$ provides a better ionic conductivity than other salts, it is susceptible to moisture and suddenly reacts in the presence of water traces, evolving corrosive HF.[108] Besides, the PF_6^- ion possesses the lowest HOMO energy level, approximately at −11.67 eV, making it resistant to electron loss and decomposition.

Table 1. Sodium salts employed in NIBs and principal characteristics (the data in brackets are available only for the corresponding Li-salt).[86,88]

Salt	Chemical structure	Melting point, T_m [°C]	Molecular weight [g mol^{-1}]	Ionic conductivity in PC, σ [mS cm^{-1}]	HOMO level in EC/DEC [eV]
$NaClO_4$	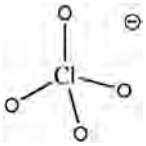	468	122.4	6.4	−7.89
$NaBF_4$	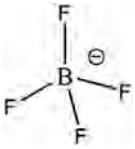	384	109.8	(3.4)	−10.45
$NaPF_6$	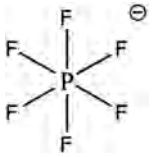	300	167.9	7.98	−11.67
NaTf	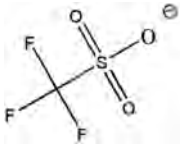	248	172.1	(1.7)	−7.5
NaTFSI		257	303.1	6.2	−8.6
NaFSI	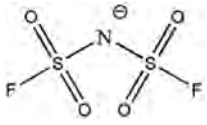	118	203.3	–	−8.66

Imide-based salts (NaFSI, NaTFSI) also show good ionic conductivity and, in some reports, they were compared in different solvent media to investigate their anodic stability and passivation/corrosion behavior towards Al.[109]

Huang et al. synthesized the Na-difluoro(oxalate)borate ($NaC_2O_4BF_2$, labeled NaDFOB), which is an evolution of the Na-bis(oxalate)borate (NaBOB) that has limited solubility in conventional carbonate-based solvents.[110] The replacement of an oxalate subunit by fluorides improves the solubility, thanks to the electron-withdrawing effect of fluorine. This new salt shows very high anodic stability over 5.5 V versus Na^+/Na in different solvents. Thus, it can be potentially used in combination with a high working voltage cathode.

Further studies were performed to find new tailored Na salts; for example, Plewa-Marczewska and coworkers published a work on Na 4,5-dicyano-2-(trifluoromethyl)-imidazolate (NaTDI) and Na 4,5-dicyano-2-(pentafluoroethyl)-imidazolate (NaPDI). The performance of both the salts were limited in terms of ionic conductivity with respect to the other commonly used salts, but having the advantage of being fluorine free, and with a good thermal and electrochemical stability.[111]

When considering factors such as oxidation, reduction, thermal stability, and toxicity together, our analysis suggests that $NaPF_6$ represents the most suitable compromise.[86] In addition, the solvation structure associated with PF_6^- induces preferential decomposition of the anion, resulting in the formation of a thin, inorganic compound-rich cathode–electrolyte interphase. The resulting protecting layer enhances interface stability and suppresses solvent decomposition, thereby ensuring electrode stability and facilitating charge transfer kinetics. Thus, $NaPF_6$ is not only more compatible with industrial processes, but also enhances battery performance. The adoption of commercial electrolyte designs incorporating $NaPF_6$ is expected to accelerate the industrialization of NIBs.[112]

The performance of the salts is not independent of the solvent(s) in which they are dissolved; thus, a brief overview of the most commonly used solvents is detailed below.

Table 2. List of solvents commonly used in battery electrolytes. T_m, T_b, T_f, η, and ε stand for melting point, boiling point, flash point, dynamic viscosity, and dielectric constant, respectively.

Solvent	Chemical structure	T_m [°C]	T_b [°C]	T_f [°C]	η at 25 °C [cP]	ε at 25 °C
Ethylene carbonate (EC)	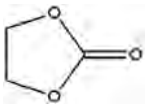	36.4	248	160	1.9	89.78
Propylene carbonate (PC)	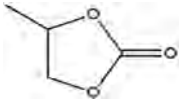	−48.8	242	132	2.53	64.92
Dimethyl carbonate (DMC)		4.6	91	18	0.59	3.107
Diethyl carbonate (DEC)	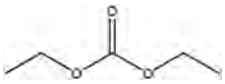	−74.3	126	31	0.75	2.805
Ethylmethyl carbonate (EMC)	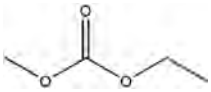	−53	110		0.65	2.958
Triethylene glycol dimethyl ether (TEGDME)		−46	216	111	3.39	7.53

2.2. Organic Solvents

The commonly used solvents in NIBs are generally derived from the knowledge accumulated in LIBs over the years. The main characteristics of an electrolyte solvent are listed below:

a) high dielectric constant (ε) in order to dissolve a sufficient amount of salt(s);
b) low viscosity to facilitate ionic mobility;
c) it should remain in the liquid state in a wide temperature range (typically, from −20 to +60 °C), meaning low melting and high boiling points;
d) non-toxicity, elevated safety content (low vapor pressure and flammability), and low cost.

All the above-reported features are challenging to meet with just one solvent; thus, using a mixture of two or three solvents, generally aprotic organic ones such as carbonates (both linear and cyclic), esters, and ethers are often preferable. Indeed, single cyclic carbonates (propylene carbonate (PC), ethylene carbonate (EC)), which have high ε and wide ESW, exhibit a relatively high viscosity; consequently, the ion mobility is reduced. On the other hand, other solvents (linear carbonates), such as diethyl carbonate (DEC) and dimethyl carbonate (DMC), have lower viscosity, but their dielectric constants are very low, limiting the salt solubility. Therefore, combining solvents with different characteristics is common to obtain a solution with suitable properties for high-performing batteries. The most popular solvents are listed in **Table 2** with the relative main physical characteristics.

The selection of solvent(s) is crucial and depends on the intrinsic features and compatibility with the other cell components. When a battery is designed, one should first consider its field of application. This assessment selects electrodes to meet specific energy requirements, power density, and working temperature. Once the electrodes are established, the choice of the solvent is crucial because the performances of the active materials strongly depend upon the electrolytes. In general, polar aprotic solvents and Na salts are reduced during the first oxidation/reduction process in the cell, forming insoluble Na compounds, which precipitate onto the surface of the electrodes, forming a passivating layer, typically called SEI. This thin film, which acts as a protective layer between the electrode and the electrolyte solution, is permeable to metal ions that can cross it and avoid electron's passage. The formation of the SEI layer is fundamental and influences different figures of merit, such as safety, shelf life, cycle life, and power capability of the device. Furthermore, it is essential when using native Na metal anode because of its high reactivity. Stable and homogeneous SEI is particularly relevant for Na metal batteries, where an inhomogeneous and unstable SEI can lead to uneven Na metal deposition and dendrites formation, with detrimental effects on the cell behavior.[113] Some studies highlight how to prevent dendrites growth by designing an artificial passive layer on the metal electrode.[114] Several research groups have investigated the nature, composition, and thermal stability of the SEI in half-cell systems utilizing carbonate-based electrolytes for both LIBs and NIBs.[109,115] However, the findings were not extended to full-cell configurations, nor the impact of varying the operational electrochemical window or examining different carbonate compositions was explored in detail. Tarascon et al. conducted research into the effect of various $NaPF_6$-based electrolytes containing different carbonates on the stability of the SEI formed in full $Na_3V_2(PO_4)_2F_3$ (NVPF)/hard carbon (HC) cells. This

investigation utilized complementary in situ UV–vis spectroscopy (UV), in situ cyclic voltammetry (CV) measurements, and galvanostatic charge-discharge tests. The results revealed the detrimental effect of linear carbonate-based electrolytes, which undergo reduction at the HC electrodes, leading to the release of soluble species that adversely affect cell performance.[116] This group has also made significant observations, discoveries, and correlations regarding the zero-volt stability, which are valuable for consideration by battery scientists and users, depending on the targeted application. They found that the best performances were achieved when either sodium-layered oxides or NVPF were combined with PC-based electrolytes. Similarly, highly oxidized NVPF in EC-PC-DMC-based electrolytes exhibited excellent performance, with the latter being particularly attractive in terms of system performance. However, due to the presence of linear carbonate (DMC), known to have detrimental effects on high-temperature performance, suitable electrolyte additives are necessary to stabilize the SEI and CEI to make this solution more practical.[31] Therefore, the incorporation of a small amount of foreign molecules, known as additives, provides significant benefits to electrolytes. Progresses made in electrolyte additives for NIBs are outlined in the following sections.

2.3. Additives

Additives are encompassed in the electrolyte solutions to improve the battery performance (in both LIBs and NIBs) (**Figure 3a**). They are added in small amounts, usually not exceeding 5 wt% of the whole electrolyte solution.[117,118] In general, additives must be affordable, easy to use, environmentally safe, non-combustible, and with a reasonably wide operating voltage. They often serve to improve the characteristics of the electrode–electrolyte interface, mainly modifying the SEI by increasing the wetting of the electrode surface and protecting it from overcharging (e.g., by redox shuttles that store the extra charge). Additives are also occasionally employed as flame-retardants or to enhance the physico-chemical properties of the electrolyte (e.g., decrease the viscosity, radical scavengers, etc.).

The most frequently used additive in NIB electrolytes (widely used also in LIBs) is fluoroethylene carbonate (FEC). It is the most common SEI layer enhancer, particularly for fast-rate charging. FEC improves the capacity retention of anodes and mitigates the irreversible reactions at the interface with the Na metal electrode.[119] However, the addition of FEC in the electrolyte solution often causes anomalies in the potential versus time profile, which have been recently explained. Dugas et al. demonstrated the beneficial effect of FEC on the minimization of the irreversible capacity of a Na half-cell. However, they found a continuous release of small quantities of gases, clearly detrimental to the cell performances upon long-term cycling.[120]

Komaba et al. investigated several additives, including not only FEC but also vinyl carbonate (VC), ethylene sulfite, and the doubly fluorinated EC. Actually, FEC was found to be the additive that gave the best response. In the same study, VC, widely employed in LIBs, was demonstrated to have limited improvement in the NIBs performance.[119] Some years later, for the first time, Komaba's group reported the obtainment of high capacity and cyclability for black Phosphorus (P) electrode materials with the inclusion of VC in Na cells. In their work, it is demonstrated that the SEI layers modified by FEC and VC additives contribute to extended cycle life and enhanced reversibility during the desodiation/sodiation processes of the electrode[121] (Figure 3b).

Shi et al. studied the impact of adding VC to the $NaCF_3SO_3$-diglyme (DGM) electrolyte. They reported that VC, which shares a similar HOMO level with DGM, collaboratively undergoes oxidation with diglyme, leading to the beneficial formation of a cathode electrolyte interface (CEI) layer on the $Na_3V_2(PO_4)_3$@C cathode. Consequently, this enhances the oxidation stability of the ether-based electrolyte, enabling a compatible match between the electrolyte and the cathode. Concurrently, it maintains compatibility with the FeS@C anode. As a result, the electrolyte containing 5 wt% VC was effectively used in FeS@C || $Na_3V_2(PO_4)_3$@C full cells without requiring prior cathode or anode pre-activation in their respective preferred electrolytes. This system demonstrates outstanding cycling performance, retaining 67% of its capacity after 1000 cycles at 0.5C (Figure 3c).[122]

Recently, Zhang and co-workers showed that N-phenylbis(trifluoromethanesulfonimide) (PTFSI) as a novel film-forming electrolyte additive improved the cycling stability of hard carbon (HC) anode in half-cell versus Na due to passivation film generated from the preferential reduction of PTFSI. The improved stability of the SEI on the anode leads to a remarkable 52% increase in capacity retention for HC/$Na_3V_2(PO_4)_3$ full cells after 100 cycles (Figure 3d).[123]

Although liquid organic solvents are the most useful in batteries, their volatile nature is one of the most significant issues associated with the somewhat limited safety of rechargeable batteries. The most recent event of a wretched failure in terms of explosion is the Samsung Note 7, in which an entire batch of mobile phones had overheating problems and even caught fire. For this reason, the famous brand was forced to withdraw the products from the market. To guarantee a safe device, it is fundamental to solve these issues for portable technologies and large-scale EES (both electric vehicles and stationary), where explosion hazards must be avoided. Regarding safety, room-temperature ionic liquids (RTILs) have attracted much attention in the last few years; thus, a distinct section labeled Section 6 is allocated specifically to explore ionic liquid-based electrolytes.

3. Solvation Structure and Characteristics of Electrolytes

In liquid electrolyte solutions, the solvent lessens the electrostatic attraction force F between ions with opposite charges depending on its dielectric constant ε (F is inversely proportional to ε per Coulomb's law). Common organic solvents for battery electrolytes include ethers and carbonate esters containing oxygen as the electronegative heteroatom, inducing a dipole moment. These solvents are also Lewis bases, with oxygen conveying a hard character compared to other heteroatoms, such as nitrogen. Their lone-pair coordination with alkali metal cations is a strong component of the ion-solvent interaction, besides the ion-dipole interaction, resulting in highly directional solvation structures with defined coordination numbers (CN). Since the coordination environment is dynamic, the CN is generally given as the average of coordinating ligands to one ion, i.e., mostly Na^+ in electrolytes for NIBs.

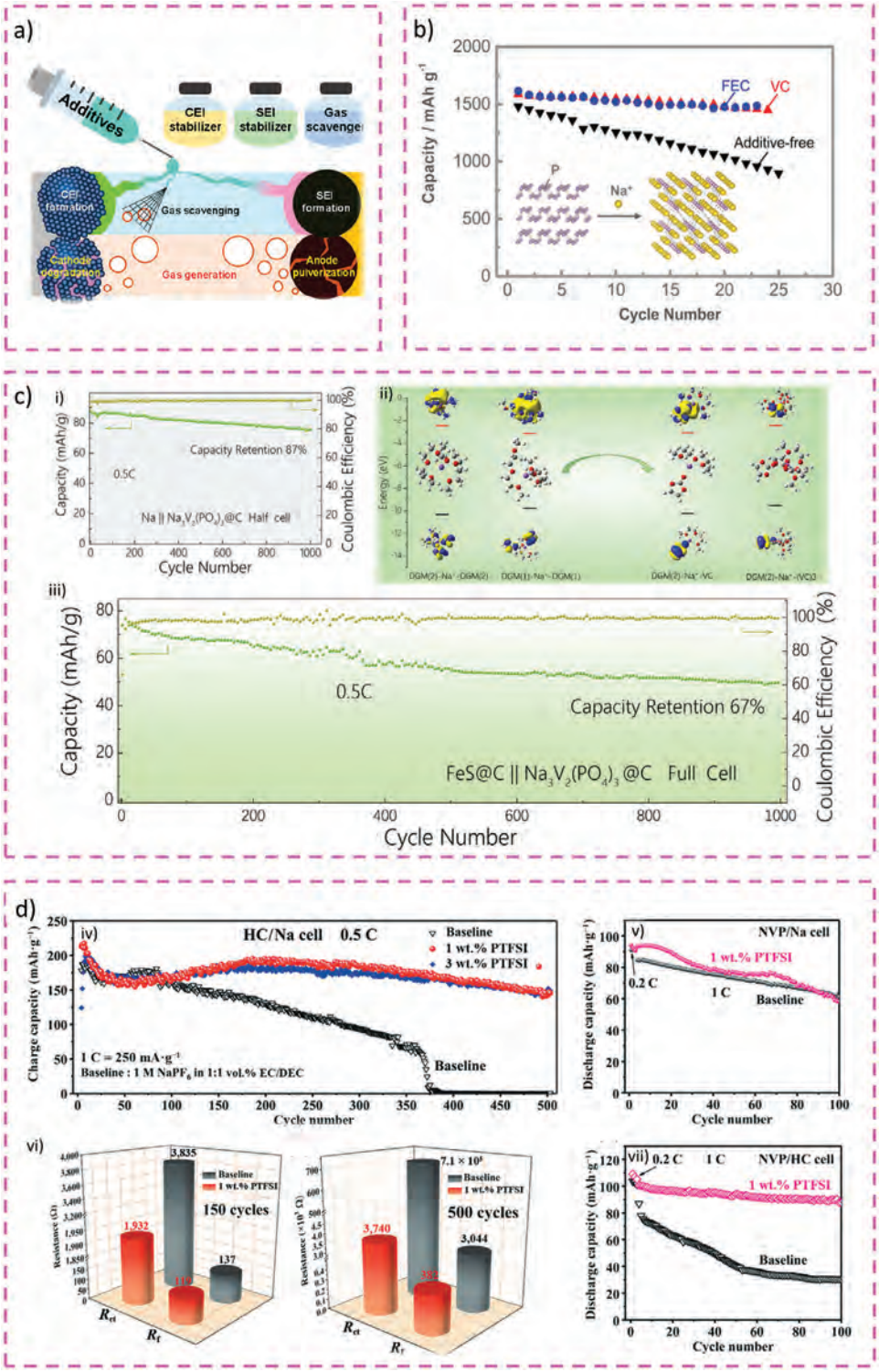

Figure 3. a) Schematic illustrating the impact of additive moieties on interfacial layers and gas generation. Adapted with permission.[124] Copyright 2020, American Chemical Society. b) Electrochemical properties of phosphorus electrodes in Na cells in 1 mol dm^{-3} $NaPF_6$/EC/DEC/electrolyte without additive, with FEC, and with VC. Adapted with permission.[121] Copyright 2016, American Chemical Society. c) Cycle performance of $Na_3V_2(PO_4)_3$@C cathode at 0.5C (i), the schematic representation of the change of solvation Na^+ sheath structure with the addition of VC and the energy variation (ii), and cycle performance of FeS@C|| $Na_3V_2(PO_4)_3$@C full cell at 0.5C (iii). Adapted with permission.[122] Copyright 2020, Elsevier. d) Cycling performance of the HC/Na without and with PTFSI additive (iv), resistance values of HC half-cell at desodiated sate for 150th and 500 cycles at C/2 with and without additive, calculated by electrochemical impedance spectroscopy (EIS) (v), and cycling performance of $Na_3V_2(PO_4)_3$/Na half-cell (vi) and NVP/HC full cell (vii). Adapted with permission.[123] Copyright 2022, Springer Nature.

The local structure in battery electrolytes is usually described in terms of alkali metal CN, solvent-separated neutral ion pairs (SSIPs), contact neutral ion pairs (CIPs), and charged aggregates of different ions (eg. M_2X^+, MX_2^-, where M is the alkali metal and X is the anion).[125] Nanoaggregates (n-AGG) of tens or hundreds of ions (size >1 nm) can be observed at a high salt concentration (see section 3.4), with multivalent ions, and when poor solvents (having low compatibility) are employed.[126] The development of n-AGGs is driven by ion-solvent (coordination and ion-dipole) and ion-ion interactions, and is controlled by a complex balance between many forms of interactions, including H-bonding, electrostatic, $\pi-\pi$ stacking.[126]

Ion speciation affects the transport properties fundamental for battery operation, giving scope to its computational and experimental characterization. Considering each aggregate as a charge carrier having a distinct diffusion coefficient, it is possible to compute the ionic conductivity. Yet, the static picture of ion speciation (e.g., snapshots from molecular dynamics (MD) simulations) may be inadequate as the basis to model how ion-ion correlation affects the experimental transport properties. Alternative analyses are time-dependent and take into account the flux–flux correlation[127] (see section 4).

In the following sub-sections, insights from literature addressing solvation in different Na-based electrolyte systems are overviewed, as it affects fundamental properties such as ion-transport and SEI forming ability.

3.1. Solvation in Conventional "1M" Liquid Electrolytes

Conventional electrolytes have typical concentrations near 1 M to ensure proper wetting of the electrode material and high ionic conductivity, relying on vectorial ion transport (see conduction mechanism).[125] The solvent molecules in the solvation shell (5-6 solvent molecules per Na^+ ion)[126,128] can move along with Na^+ ion due to the attractive ion–solvent interaction, depending on its balance with the thermal energy of the solution (this latter drives solvent molecules away from ions and into the bulk). The ion-solvent interaction is weaker when large soft ions with delocalized charge are involved, which is the case of anions in battery electrolytes.

Semi-empirical quantum mechanical models (Hartree-Fock based PM7) of diluted and concentrated $NaPF_6$ and $LiPF_6$ solutions in PC and ACN revealed that Na^+ containing electrolytes typically have more fluorine atoms in the first solvation shell, longer cation-solvent and cation-anion distances, higher CNs, and bigger CN variance.[126]

Based on density functional theory (DFT) calculations, both Li^+ and Na^+ cations show a preference for a solvation shell rich in cyclic carbonates over linear and fluorinated ones, in both the gas and liquid phases. Based on the estimated binding energy, monodentate binding is favored in Na^+-PC. Different IR signals owing to PF_6^- anion interactions were observed, with Na^+ having a higher tendency to form CIPs than Li^+ in linear DMC. A decreased influence of Na^+ on C=O stretching compared to Li^+ was detected by both Fourier transform infrared spectroscopy (FTIR) and DFT calculations, and attributed to weaker interaction between Na^+ and DMC with relatively low dielectric constant.[128] PFG-NMR investigations of self-diffusivities in $NaPF_6$ solutions in mixtures of cyclic and carbonate ester solvents also evidenced better Na^+/PF_6^- separation in PC-rich solutions over EC-rich ones, and an increase of ion-pairing with decreasing the amount of cyclic solvents.[128] Bidentate solvation and stronger ion-solvent interactions were evidenced by NMR in $NaPF_6$ solutions in DME ether solvent compared to carbonate ester solvents, with a larger downfield shift of the ^{23}Na signal in the former.[128]

Several studies recently collected in review articles addressed the influence of solvation on the SEI structure,[129] also taking into account solvation at the electrode/electrolytes interface,[130,131] leading to new concepts such as superconcentrated and locally concentrated electrolytes.[125,132]

In dilute electrolytes, where SSIP is the most abundant species, the LUMO is dominated by solvent molecules, which are reduced first at the negative electrode, leading to the SEI formation. Unlike the Li-based electrolytes, the organic sodium components are more soluble in the electrolyte solution, causing self-discharge and affecting the long-term stability of NIBs.[132]

Based on DFT models of $NaPF_6$ solutions in carbonate esters, the HOMO levels of EC and DEC molecules coordinated to Na^+ ions shift towards lower energies compared to free solvent molecules, meaning that the complexes are oxidized at higher potentials versus Na^+/Na. Conversely, the HOMO level of solvent-coordinated PF_6^- anion shifts towards higher energy, thus decreasing the oxidative stability. In this system, trimethoxy(pentafluorophenyl)silane (TPFS) as dual additive (DA) was found to affect PF_6^- coordination environment according to MD simulations, supported by the NMR analysis of ^{19}F chemical shift, facilitating its desolvation at the interface with NVPF and improving the oxidative stability (**Figure 4a**). Additionally, the water-scavenging ability of TPFS evidenced by NMR analysis is beneficial to prevent HF formation upon PF_6^- hydrolysis.[133]

The role of ions and solvent molecules arrangement at the electrode/electrolyte interface has also been taken into account. The formation of an anion-driven SEI has been proposed to explain the poor quality of the passivation layer formed on Na metal with ClO_4^- and $SO_3CF_3^-$ (triflate) anions, which can get close to the metal interface because of low steric hindrance and strong pairing with Na^+, respectively, as opposed to PF_6^-, which is located far away from the interface, based on MD simulations and XPS analyses (Figure 4b).[130] A targeted study on the solvation structure of $NaPF_6$ in different organic carbonate ester solvents at the interface with different electrode surfaces (NVP, NVPF, and graphite) was carried out by MD. It was found that surface-specific directional interactions cause the arrangement of solvent molecules in a packed layer close to the electrode surface, where the Na^+ ion loses part of its solvent shell upon crossing through. In particular, because of the presence of coordination sites, this effect is more pronounced at the NVP surface, where the highly ordered initial solvent layer is responsible for the highest energy barrier preventing Na^+ ions from diffusing back into the bulk. Solvent packing at the NVPF surface is less pronounced due to non-polar fluorine atoms, and absent at the graphite surface, where Na^+ ions may intercalate together with their solvation sheath.[131]

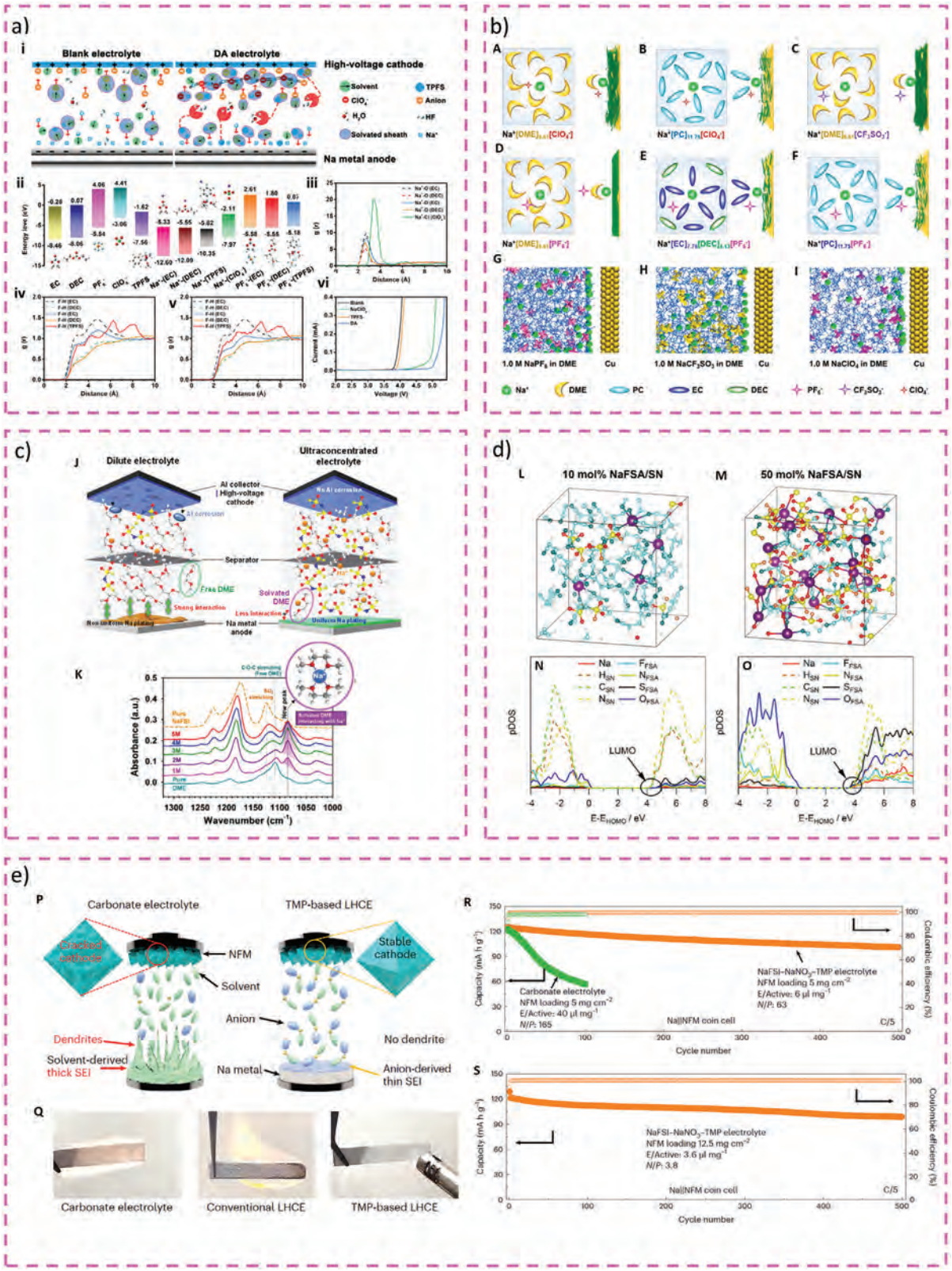

Figure 4. a) The dynamic high-voltage resistance and self-purifying mechanism (i), LUMO and HOMO energy levels of individual molecules and Na^+ and PF_6 -complexes (ii), Na^+ (iii) and PF_6 (iv)–(v) RDFs g(r) acquired from MD simulations of blank (dashed lines) TPFS (iv) (solid lines) and DA (v) (solid lines) electrolytes, LSV test (vi) of various electrolytes at a scanning rate of 2 mV s^{-1}. Adapted with permission.[133] Copyright 2022, John Wiley and Sons. b) Anionic interfacial model describes the interface between the electrolyte and the sodium anode in a battery system. The model for

3.2. Solvation in Polymer Electrolytes

Polymer-based electrolytes macroscopically exhibit solid-like properties, including the ability to act as separators, yet ions from the salt interact with a solvation environment similarly to liquid electrolytes on the microscopic scale.[125]

In accordance with Coulomb's law, a polar polymeric medium with a high dielectric constant contrasts ion association due to attractive electrostatic interactions. Under this condition, the degree of dissociation is high, and the ion-polymer coordination strongly affects the self-diffusivity of the cations, when their motion is correlated to the segmental relaxation dynamics of the polymer chains.[127] A relatively low cation transference number can arise from strong coordination between the ligands and alkali metal cations, notably evident with poly(ethylene oxide) (PEO). Consequently, carbonyl-based polymers such as polycaprolactone (PCL) and poly(trimethylene carbonate) (PTMC) have been investigated as alternative matrixes. This is due to their weaker coordination strength with alkali metal cations[134] (see section 4 for more information).

Ion coordination strength consists of the contribution of the CN and that of the ion–dipole interaction between the cation and the coordinating ligands. Bond distances, the coordination enthalpy and the CN depend on the ligand chemistry and the structure of polymer, as well as the size and charge of the ion.[134]

Na^+ ion coordination in several NaTFSI-based systems with PEO, PTMC, and PCL has been recently investigated by NMR, tracking the changes in the chemical shift of the ^{23}Na signal occurring at different polymer concentrations. Strong interactions between Na^+ and the ligands result in the increase of the electron density shielding ^{23}Na nucleus, thus shifting the signal upfield towards lower chemical shift values. A comparison with Li^+ was also provided. The coordination strength for Li^+ follows the order PEO >> PCL > PTMC, whereas in the case of Na^+ it is PEO > >PTMC > PCL. An initial downfield shift of the ^{23}Na signal at low PTMC or PCL concentrations, not observed with ^{7}Li, was interpreted as a sign of weaker coordination in the Na-based systems compared to their lithium counterparts.[134] The thermodynamic parameters for salt dissociation were also extracted from the FTIR analysis of salt-polymer systems at different temperatures, by exploiting the different signals due to associated and non-associated $TFSI^-$. The free energy for salt dissociation, which is an indicator of the ion-ligand coordination strength driving the salt dissolution, was found to be negative in all cases, with moduli following the order PEO>PCL>PTMC. In the case of PEO, the entropic contribution was found to be relatively more important compared to the carbonyl-containing systems, where dissolution seems to be more enthalpy-driven. The free energy for salt dissociation in PEO was found to be more negative for LiTFSI than NaTFSI, implying that Na^+ is more weakly coordinated to the polymer matrix, and thus more prone to ion association in pairs and aggregates.[134]

3.3. Solvation in Ionic Liquids

Ionic liquids (IL) are systems solely consisting of ions, where ion correlation cannot be neglected, often deviating from the standard diluted solution behavior.

The ratio between the mobility measured under an applied electric field (from electrophoretic NMR) and the mobility derived from the apparent self-diffusion coefficient (from PFG-NMR) quantifies the effective charge of the species containing the nucleus under study, i.e., an apparent degree of dissociation (see section 4). The overall apparent degree of dissociation for a number of different ionic liquid was found to follow the order 1-ethyl-3-methylimidazolium bis(trifluoromethylsulfonyl) imide (EmimTFSI) ≈1-ethyl-3-methylimidazolium tetrafluoroborate ($EmimBF_4$) ≈1-butyl-3-methyl imidazolium bis(trifluoromethylsulfonyl)imide (BmimTFSI) ≈1-butyl-1-methyl piperidinium bis(trifluoromethylsulfonyl)imide ($P_{14}TFSI$) ≈1-butyl-3-methylimidazolium hexafluorophosphate ($BmimPF_6$) > 1-butyl-1-methyl pyrrolidinium bis(trifluoromethylsulfonyl)imide ($Pyr_{14}TFSI$) ≈N,N,N-trimethyl-N-butyl-ammonium bis(trifluoromethylsulfonyl)imide ($N_{1114}TFSI$). Notably, for each IL the effective charge of anions was found be higher than that of the cation (even above 1 in the case of BMImTFSI and $BMImPF_6$), implying that besides neutral pairs there are asymmetric clusters $[M_aX_b]^{a-b}$ ($a \neq b$), and when these latter are dominated by the anions, they show higher mobility under an applied electric field, but lower self-diffusivity, compared to those dominated by the cations.[135]

In IL-based electrolytes for sodium batteries, the short T_2 spin-spin relaxation times make it difficult to measure Na^+ self-diffusion coefficient by PFG-NMR.[136] Nevertheless, information on the chemical environment of Na^+ ions can be extracted from ^{23}Na chemical shift. At the relatively high NaFSI concentrations in $Pyr_{13}FSI$, the ^{23}Na resonance was found to shift upfield towards lower values, attributed to larger shielding

1.0 M DME-based electrolyte using different metal salts including A) $NaClO_4$, C) $NaCF_3SO_3$, and D) $NaPF_6$, respectively. The model of $NaClO_4$-based electrolyte using PC (B). The model of $NaPF_6$-based electrolyte using different solvents: E) EC/DEC, and F) PC, respectively. The model in 1.0 M $NaClO_4$ in PC solution. Interfacial behavior of molecules on the anode surface, G) 1.0 M $NaPF_6$ in DME, H) 1.0 M $NaCF_3SO_3$ in DME, and I) 1.0 M $NaClO_4$ in DME, respectively (The green sphere represents a Na^+ ion. The yellow plates and spheres represent the Na metal anode at the microscopic and atomic scale. The dark green surface features on the Na metal anode represent products of the side reactions). Adapted with permission.[130] Copyright 2020, American Chemical Society. c) Illustration of superhigh and ultralow concentration electrolytes. Solvation behavior and interface model in the electrolyte of 5 M NaFSI in DME (J), FTIR spectra of xM NaFSI-DME (x = 0, 1, 2, 3, 4, or 5) and pure NaFSI salt (K). Adapted with permission.[146] Copyright 2017, American Chemical Society. d) Typical snapshots of the equilibrium trajectories (L,M) and the corresponding PDOS profiles (N,O) obtained by DFT-MD simulations on (L,N) dilute 10 mol% (4 NaFSA/36 SN) and (M,O) superconcentrated 50 mol % (20 NaFSA/20 SN) solutions (Atom color: Na, purple; H, white; N, blue; O, red; S, yellow; F, orange; C, light blue). Adapted with permission.[147] Copyright 2017, American Chemical Society. e) Illustration of the components with a Na-metal battery after long-term cycling in carbonate-based electrolyte (left) and NaFSI–$NaNO_3$–TMP electrolyte (TMP-based LHCE, right) (P), Flammability tests of carbonate-based electrolyte, conventional LHCE and NaFSI–$NaNO_3$–TMP electrolyte (Q), Cycling performance of NFM with different active-material loading (R, S). Adapted with permission.[155] Copyright 2024, Springer Nature.

of the Na^+ cation due to strong interaction with FSI^- anions, consistent with clustering.[137]

Sodium coordination in NaFSI solutions in $Pyr_{13}FSI$ at different concentrations was investigated by computational techniques in several studies.[137–140] In particular, MD simulations were run at 85 °C, taking into account inter- and intra-species correlation to analyze trajectory data, based on concentrated solution theory. It was found that oxygen plays a major role in the coordination of Na^+, which on average includes 5–6 oxygen atoms in its primary coordination environments, with a rise of variance at high concentrations, indicating an increase in the possible different coordination environment. Fast exchange of the anions coordinating Na^+ was evidenced by tracing the oxygen atoms in the primary coordination cage over time, particularly at low NaFSI concentration. Ion clusters were also characterized, revealing the absence of neutral pairs, and the dominant presence of small asymmetric agglomerates, such as $[M_1X_5]^{-4}$ and $[M_2X_8]^{-6}$ (circled by Pyr_{13}^+ compensating their charge) up to a molar fraction of 0.2 NaFSI, above which large agglomerates including all the Na^+ ions manifest frequently in alternative to the population of small clusters.[140]

A particular case is that of solvated ILs, where short-chain methyl ether terminated ethylene glycols (glymes) form chelates with alkali metal in solutions having a salt-to-solvent molar ratio equal to 1. The analogy with ILs relies on a picture where there are no free solvent molecules in the system, which is entirely composed of anions and cations, where the cation is chelate. These systems show extended liquid range upon supercooling, wider electrochemical stability window, and decreased vapor pressure compared to dilute solutions.[141] The properties of different glyme-based electrolytes in combination with Li and $NaPF_6$ at different concentrations were investigated by vibrational, impedance, and PFG-NMR measurements, evidencing the inverse relationship between ion association and glyme chain length. Interestingly, the increase in ion association with increasing temperatures was attributed to the simultaneous decrease in the solvent dielectric constant, also previously observed with Na salts in polyether polymer electrolyte.[142,143]

Equimolar mixtures of Na salts and ILs and several other superconcentrated systems have been explored, highlighting many differences in fundamental properties arising from the different coordination environment.[125]

3.4. Solvation in Superconcentrated Electrolytes

Evidences of strong ion-solvent and ion-ion interactions in superconcentrated electrolytes have been reported for a number of Na-based systems.

A comparison of $LiPF_6$ and $NaPF_6$ coordination in PC and ACN via PM7 computational studies evidenced the increase of F atoms in the primary coordination shell at high concentration, with an increased variance in the CN pointing at a more flexible coordination structure, attributed to the high charge delocalization of the anions involved in the ion-ion interactions. High CN variance and flexible coordination were related to an increase in the temperature range in which the electrolyte is in the liquid state, particularly with Na^+.[144]

Solutions of NaFSI in flame retardant trimethyl phosphate (TMP) have been investigated as non-flammable electrolytes up to 3.3 molar concentration. Based on DFT-MD investigations, at this high concentration, almost all TMP molecules are coordinated with Na^+ cations, supported by the large shift towards lower chemical shifts of both ^{17}O and ^{31}P NMR signals attributed to the shielding effect of Na^+ with increasing NaFSI concentration.[145] Similarly, the FTIR signal arising from the coordination between C–O–C moieties and Na^+ ions, distinct from that of the pure solvent, was found to increase as a function of NaFSI salt concentration up to 5 M in DME (see Figure 4c).[146] A shift of the distinct Raman signal due to FSI^- towards higher wavenumber was observed upon increasing NaFSI concentration in TMP, attributed to the formation of anionic clusters. DFT-MD computations showed the extensive presence of large agglomerates sharing at least 2 Na^+.[145] This system showed negligible volatility up to 150 °C, and flash-point above the boiling temperature (>200 °C) at NaFSI 3.3 M. These effects were ascribed to the strong interactions among Na^+, FSI^- and TMP, leaving few free solvent molecules, coupled with the high boiling point of TMP (197 °C).

Raman vibrational bands in the range of 720–750 cm^{-1} were examined for NaFSI solution in plastic crystal succinonitrile up to 1:1 molar ratio, together with the signal due to C≡N stretching. The contributions of CIPs and aggregates to the deconvoluted FSI^- band were found to increase up the disappearance of the free FSI^- at 50% mol NaFSI. Similarly, the C≡N stretching band was found to be dominated by the blue-shifted contribution attributed to ion-solvent coordination at high NaFSI concentration.[147] In this system, an extended liquid range was observed from below −50 °C at NaFSI molar ratio above 20%. Additionally, DFT-MD computations evidenced a downward shift of the LUMO energy level of FSI^- well below that of SN in concentrated solutions, due to the change in the coordination environment with respect to dilute solutions, where the LUMO depends on the solvent instead (Figure 4d). The simulated reduction mechanism at 50% by moles of NaFSI, in excess of electrons due to aggregation, predicts the formation of a singly occupied molecular orbital in FSI, and subsequent cleavage of the S-F bond, with the release of F^- coordinated by Na^+. Postmortem XPS analysis of Na//HC cells revealed a remarkable increase in NaF and inorganic sulfur-containing compounds on HC at high NaFSI concentration, pointing at the formation of an anion-derived SEI layer, way more effective than that formed in dilute solutions. This latter was dominated by SN decomposition products up to 20% by moles of NaFSI. This aspect is particularly important for Na-based systems, where many SEI components (e.g., derived from EC-based solutions) are more soluble compared to lithium-based systems.[132]

Alternatively, a shift of the redox potential to higher values (and lower energy) has been proposed based on the Nernst equation considering the redox reaction as follows:

$$host + Na(solv)_n^+ + e^- \leftrightarrow host{:}\ Na + n(solv) \quad (1)$$

$$E = E^0 + \frac{RT}{F} ln\left(\frac{a_{Na}}{a_{solv}^n}\right) \quad (2)$$

where a and n are the activity and the solvation number, respectively. Here, a decrease in the number of solvent molecules in

the solvation sheath causes an increase in the equilibrium redox potential, lessening the possible decomposition reactions upon reduction.[148]

Interestingly, higher oxidation stability (measured versus Pt) and diminished Al corrosion was observed with NaFSI 5 M in DME during LSV experiments. The increased oxidation potential was ascribed to a decrease in the HOMO energy level of the ether solvent due to the coordination with Na^+, like in solvate ionic liquids (see section 3.3). The suppression of Al corrosion was ascribed to the lack of free DME molecules able to dissolve the FSI-based passivation products (Al-FSI complexes and S-F compounds detected by postmortem XPS analysis) formed on Al surface upon oxidation at ≈4.2 V vs Na^+/Na.

As stated in section 3.3, Na^+ coordination environment at high NaFSI concentration in $Pyr_{13}FSI$ ionic liquid has also been investigated. It has been proposed that rapid exchanges in the average coordination environment of Na^+ ions with high variance in extensive agglomerates may result in a transport mechanism relying on structural rearrangement (somewhat similar to Grotthus mechanism) superior to vehicular transport.[137] Additional studies were dedicated to superconcentrated tetralkylphosphonium PF_6 ionic plastic crystal ($P_{1224}PF_6$) and linear tetralkylammonium borate ($[N_{2(2O2O1)3}][B(hfip)_4]$) IL systems in combination with $NaPF_6$ and NaFSI salts, respectively. In the system with $P_{1224}PF_6$, closer packing was observed with increasing the salt concentration, described as the formation of bulky $[M_a[(X)_b]^{a-b}$, which could further aggregate by sharing neighboring alkali metal ions, with the larger aggregates growing from 3 to >100 of atoms at the highest $NaPF_6$ concentration (50% by moles). From a comparison with $LiPF_6$, the largest aggregates were found in the Na system, which also showed less variability in terms of size, and higher persistence over time, pointing at a more interconnected structure.[149] The FTIR absorption signal due to C—O—C stretching in the trans conformation upon Na coordination was detected in the presence of NaFSI, and found to increase with increasing concentration. Several signals were found to be compatible with those sensitive to FSI^- coordination in ether solvent and interpreted in terms of neutral ion pairs and ion-clusters of Na^+, $[N_{2(2O2O1)3}]^+$ and FSI^-. These latter were found to increase with increasing NaFSI concentration. The analysis of ^{19}F signal linewidth evidenced a broadening indicative of mixed coordination and increased heterogeneity only at 50% by moles of NaFSI.[150] The electrochemical and transport properties in this latter system were found to be improved at 50 °C. Indeed, most superconcentrated electrolytes show high viscosity, requiring temperatures above room temperature to achieve optimal electrode wetting and ionic conductivity. In this respect, it is worth noting that the improved rate performance often observed with superconcentrated electrolyte is mostly attributed to the improved quality of the SEI layer, and the easier alkali metal desolvation at the interface with the electrode, due to a higher amount of anions in its coordination environment compared to diluted electrolytes.[132,144]

A subsequent advance aimed at decreasing the viscosity and cost, while improving the ionic conductivity and keeping the advantages of superconcentrated electrolytes in terms of interfacial chemistry and safety consisted in the introduction of non-solvating diluents, in the localized high-concentration approach.[125]

3.5. Solvation in Localized High-Concentration Electrolytes

This approach was first reported for NaFSI-based electrolytes in DME,[151] which showed excellent properties in superconcentrated solution up to NaFSI 5 M (see section 3.4). The addition of bis(2,2,2-trifluoroethyl) ether (BTFE) diluent allowed decreasing the concentration of costly NaFSI, while keeping the structure of the superconcentrated electrolyte at different diluent to DME molar ratios up to 3. The Raman spectra of NaFSI 5.2 M in DME and NaFSI 2.1 M in DME/BTFE showed similar characteristics, in particular, the disappearance of the band due to free DME, and the dominance of the blue-shifted contribution at 751 cm^{-1} due to aggregates in the band sensitive to FSI coordination. Additionally, the Raman band of BTFE was preserved regardless of concentration. This strategy allowed decreased viscosity, increased conductivity, and obtainment of excellent performance in Na metal cells at BTFE:DME ratio equal to 2, corresponding to a decrease in NaFSI concentration to 2.1 M compared to the reference superconcentrated solution.

Other hydrofluoroethers have been proven effective in realizing the localized high-concentration (LHCE) approach for sodium electrolytes, e.g., 1,1,2,2-tetrafluoroethyl-2,2,3,3-tetrafluoropropylether (TTE).[152] Hydrofluoroethers are effective diluents in virtue of their low DN (poor Lewis basicity) and dielectric constant, resulting in poor solvents for the sodium salt. A maximum threshold for the electrostatic potential energy (i.e., a computable parameter quantifying the strength of the interaction between the diluent and the anion) of 25 kcal mol^{-1} was proposed to select effective diluents for electrolyte design.[153]

Ab initio molecular dynamics (AIMD) simulations of NaFSI/DME/TTE systems evidenced a slight preference for FSI over DME in Na^+ coordination environment, with CN analogous to those observed in superconcentrated NaFSI/DME system devoid of diluent. The calculated CN for Na-TTE coordination was found to be negligible, evidencing its role as a non-solvating diluent. The statistical analysis evidenced the extensive presence of aggregates in both the superconcentrated electrolyte or solution and the LHCE, with a higher percentage of $[NaFSI_2(DME)_n]^-$ with n equal to 1 and 2, respectively.[152]

It has been proposed that a high number of small clusters with high diffusivity in LHCE could be achieved by increasing the free energy of solvation by decreasing the entropic contribution. In general, the segregated diluent phase is characterized by a low entropy, thus, electrolyte engineering aimed at increasing it (e.g., by mixing different diluent) could be an effective strategy to improve the transport properties. Artificial intelligence may be highly helpful in the formulation of these systems.[153,154]

Besides hydrofluoroethers, other species can be used as diluents. For example, $NaNO_3$ was found to be an effective diluent for the superconcentrated 3 M NaFSI-TMP system, further decreasing cost. The diluted system consists of 1.4 M NaFSI, 0.6 M $NaNO_3$ in TMP. The FTIR absorption signal due to (P-O)-C vibration, sensitive to TMP conformation and coordination, showed a blue-shifted contribution upon the addition of the sodium salt. Its contribution was evaluated upon deconvolution against the signal due to free TMP, yielding very similar ratios for 3 M NaFSI-TMP and 1.4 M NaFSI, 0.6 M $NaNO_3$ in TMP. Multiple peaks attributed to the presence of aggregates with different coordination were observed in the

^{31}P NMR spectrum of the ternary system. AIMD study showed the formation of aggregates with the presence of anions in the primary coordination environment in both the NaFSI-TMP and the NaFSI-$NaNO_3$-TMP systems. Further analysis indicated that the highest LUMO energy level is located on TMP, enabling the formation of anion-based SEI, in analogy to the superconcentrated and localized high-concentration electrolytes. Together with the decrease in cost, the ternary systems showed a doubled ionic conductivity compared to 3 M NaFSI-TMP, and improved electrochemical performance (Figure 4e).[155]

Lastly, the concept was extended to the dilution of ionic liquid battery electrolytes (e.g., with highly viscous $PP_{13}FSI$), and to quasi-localized high-concentration electrolytes, where weakly solvating compounds (e.g., fluorinated organic carbonate esters) instead of a diluent, participating to the alkali metal coordination in the primary solvation sphere. Examples of these systems were demonstrated for LIB application and will probably soon be reported for Na-based systems.[153]

4. Conduction Mechanism

4.1. Metrics

Here below, a table follows, which summarizes the basic equations and definitions useful to discuss the transport properties and conduction mechanisms in electrolytes for Na-based batteries (**Table 3**).

4.1.1. Various Types of Ion Transport

This section delves into the diverse ion transport mechanisms found in various electrolyte systems.

Vehicular Transport: In dilute liquid electrolyte solutions, vehicular motion serves as the primary mechanism for ionic diffusion. It consists of ion diffusion together with the solvation shell as one entity.[126]

The liquid-like mechanism usually exhibits a Vogel–Tammann–Fulcher (VTF) temperature dependency, following that of the fluidity ϕ, viz. the reciprocal of the viscosity η:

$$\phi = \phi_0 \; e^{\left(\frac{B}{T-T_0}\right)} \tag{3}$$

where the pre-exponential factor ϕ_0, B and T_0 are material-dependent parameters. The parameter B is related to the activation energy, whereas T_0 is related to the glass transition temperature (T_g). T_0 is the "ideal glass-transition temperature" at which the medium motion is frozen and is usually lower (30-50 degrees below) than the glass-transition temperature observed during the DSC measurements.[160,163,166] The conventional vehicle-type mechanism is based on the assumption that viscosity affects ionic transport, in agreement with the Walden rule (see Table 3 and dedicated section).[167]

Structural Relaxation: Structural relaxation stands out as the most commonly observed mechanism in polymer electrolytes. This is primarily because ion transport relies on segmental relaxation, making it a pivotal process in this context. Similarly to the vehicular mechanism, it results in a VTF-like behavior for the ionic conductivity in compliance with the Walden rule using the polymer segmental relaxation time τ_α in the place of macroscopic viscosity.[167]

Assuming a rate of ion motion equal to the segmental relaxation rate, it was estimated that reaching an ionic conductivity of 1 mS cm^{-1} (with an averaged length for a single jump ≈0.1–0.2 nm, and a concentration of ≈1–3 ions nm^{-3}) would require a very high frequency per single jump $1/\tau_\alpha$ ~10^9–10^{10} s^{-1}, which is hardly attainable for dry polymer electrolytes, considering that the segmental relaxation in amorphous PEO is in the range 10^{-7}–10^{-6} s at room temperature. The addition of a liquid plasticizer can increase the rate of structural relaxation in the polymer (easily exceeding 10^{10} s^{-1}) and enable ion transport through the liquid phase (see **Figure 5a**).[167]

In gel electrolytes, ions can be transported by exchanges in different solvation environments, depending on the interactions between the polymer host, the alkali metal salt, and the plasticizer. Strong interactions, typical of PEO-based gels, ensure high chemical stability (particularly in terms of limited phase separation and leakage over time). Poly(methylmethacrylate) – PMMA and, to a lower extent, poly(acrylonitrile) – PAN are also able to form stable gels due to the polymer-solvent interactions, particularly when inorganic fillers are added to the system. This is particularly important considering that these systems have generally poor mechanical properties. On the other hand, when weak interactions occur among the components, the mechanical properties are generally improved, because the polymer host basically acts as a porous separator loaded with a liquid electrolyte. In this latter case, the ion transport mechanism relies on the liquid phase (vehicular transport), which is typical for PVdF-HFP and PVdF-based gels, due to the poor coordination ability of fluorinated moieties.[168,169]

It is generally accepted that most crystalline phases (including salt-polymer crystalline complexes) in semi-crystalline polymers, such as PEO and polycaprolactone (PCL), are poor ionic conductors, and their presence causes a significant drop in ionic conductivities by discontinuing the conduction pathways in the amorphous phases. For this reason, several strategies have been adopted to reduce the degree of crystallinity and reach higher ionic conductivity in these systems. On the other hand, since macromolecules above the entanglement limit do not show sufficiently fast relaxation in the amorphous phase, strategies to lower the T_g have been pursued to increase the ionic conductivity, e.g., by lowering the average molecular weight of the polymer or by the addition of plasticizers.[169–171] Lowering the T_g and degree of crystallinity decreases the Young's modulus of the polymer electrolyte and its ability to act as a separator, therefore crosslinked systems, advanced polymer architectures and composite polymer-based electrolytes including inorganic phases have been developed to balance the physical and transport properties.[162]

Decoupled Transport: Structural motion (not to be confused with structural relaxation) represents the diffusion of ions through successive ion dissociation/association exchanges across different coordination environments. Superionic glasses and crystals exhibit this kind of ion transport mechanism, in which ion motion can be 10^{10}–10^{12} times faster than expected from the Walden rule, with ionic conductivities in the solid state

Table 3. The fundamental equations and definitionsfor discussing transport properties and conduction mechanisms in electrolytes.

	Measurement	Equations	Notes	References
Ionic conductivity (S cm^{-1})	EIS	$\sigma = \frac{l}{R_{bulk}A}$	R = bulk resistance[a] (Ω) l = sample thickness (cm) A = area (cm^2)	[156–158]
	eNMR	$\sigma = \sum_i z_i c_i F \mu_i$	z_i = charge of the i-th tracer F = Faraday's constant (C mol^{-1}) c_i = concentration of the i-th ion (mol cm^{-3}) μ_i = electrophoretic mobility of the i-th charged tracer (cm^2 V^{-1} s^{-1})	
	PFG-NMR[b]	$\sigma = \frac{F^2}{R_{gas}T}\sum_i z_i^2 c_i D_i$	D_i = apparent diffusion coefficient of the i-th tracer from PFG-NMR (cm^2 s^{-1}) R_{GAS} = universal gas constant (J K^{-1} mol^{-1}) T = temperature (°K)	
	H_R + PFG-NMR[b]	$\sigma = \frac{F^2}{R_{gas}T\,H_R}\sum_i z_i^2 c_i D_i$	H_R = Haven ratio	
Transference number[c]	eNMR	$TN_i = \frac{\sigma_i}{\sum_i \sigma_i}$	σ_i = ionic conductivity of the i-th charged tracer from eNMR	[157–159]
	PFG-NMR[b]	$TN_i = \frac{\lvert z_i\rvert c_i D_i}{\sum_i \lvert z_i\rvert c_i D_i}$		
	EIS + CA (Bruce-Vincent)[d]	$TN_+ = \frac{I_{ss}(\Delta V - I_0 R_0)}{I_0(\Delta V - I_{ss}R_{ss})}$	I_{ss} = steady state current from chronoamperometry (CA) I_0 = initial current from CA R_0 = initial SEI+charge transfer resistance from EIS R_{ss} = SEI+charge transfer resistance at steady state from EIS	
Haven ratio	EIS + PFG-NMR[b]	$\frac{\sigma_{PFG-NMR}}{\sigma_{EIS}}$	σ_{EIS} = ionic conductivity from EIS $\sigma_{PFG\text{-}NMR}$ = ionic conductivity from PFG-NMR	[157,158]
	eNMR + PFG-NMR[b]	$\frac{\sigma_{PFG-NMR}}{\sigma_{eNMR}}$	σ_{eNMR} = ionic conductivity from eNMR	
Walden rule	η (T) + σ (T)	$\Lambda\eta = c$	Λ = molar conductivity (S cm^2 mol^{-1}) η = viscosity (Poise) c = constant	[160,161]
		$\Lambda\eta^\alpha = c$	α = coefficient of the fractional Walden rule ($0 < \alpha < 1$)	
		$\Lambda\eta = c\left(\frac{1}{r_i^+} + \frac{1}{r_i^-}\right)$	r_i^+ = ionic radius of the cation r_i^- = ionic radius of the anion	
Activation energy	σ (T)	$\sigma = \sigma_0 e^{\left(-\frac{E_\sigma}{R_{gas}T}\right)}$	E_σ = Arrhenius activation energy (kJ mol^{-1}) σ_0 = pre-exponential factor (S cm^{-1})	[160,162,163]
		$\sigma = \sigma_{VTF} e^{\left(-\frac{E_{VTF}}{R_{gas}(T-T_0)}\right)}$	E_{VTF} = VTF activation energy (kJ mol^{-1}) σ_{vtf} = pre-exponential factor (S cm^{-1}) T_0 = ideal glass transition temperature (30-50 °K below T_g)	

[a] grain boundary resistance is added to the bulk one to compute the overall ionic conductivity; [b] Nominal charges (z) are used in all equations for PFG-NMR (the technique is not sensitive to the charge of the tracers); [c] Considering Na^+ transport, the transference numbers of all positively charged species containing sodium atoms should be added up together at the numerator. The term "transport number" is referred to to systems with free-charged species and no ion association, instead;[162] [d] similar methods are reported in[164] and.[165]

>1 mS cm^{-1}. This mechanism, often called hopping, demonstrates a strong decoupling of ion diffusion from structural relaxation and usually shows an Arrhenius-like temperature dependency.[167] The prefactor σ_0 depends on the ionic charge, hopping distance, activation entropy, dimensionality of the conducting channels, the charge of the mobile carrier, and ion vibrational attempt frequency. The activation energy E_σ depends on the energy barriers for defect formation and mobility.[162]

In polymers, ions follow the fastest route, being both the liquid-like and the solid-like mechanism possible in principle. The latter is controlled by the energy barrier due to electrostatic and elastic contributions.[167] Aiming at decoupling ion transport from the segmental relaxation of the polymer backbone, side-chain solvation approach has been proposed, which is challenging due to the absence of the secondary relaxation effect (e.g., the motion of side chains) before reaching sufficient relaxation time (e.g., 10^{-10} s). Other strategies include using polymers with weakly coordinating repeating units, such as poly(carbonates), and highly concentrated polymer-in-salt systems.[171] Poly(carbonate)-based electrolytes show decoupled ionic conductivity in terms of relatively high conductivity near the T_g, i.e., higher mobility than expected based on the polymer segmental relaxation, due to the weak coordination ability of the carbonyl oxygen in the backbone.[167] Polymer-in-salt

poly(carbonate)-based electrolytes having carbonyl to Na^+ molar ratio below 5 (e.g., 2–3) show relatively high ionic conductivity, ascribed to ion percolation through salt aggregates. In this respect, caution should be used due to the tendency of these systems to partially depolymerize (unzipping), particularly depending on the drying procedure and solvent casting procedure. Additionally, more depolymerization was observed at higher salt concentrations.[172]

Walden Plot: For dilute systems relying on vehicular ion transport, the ionic conductivity depends on the size of the charge carrier (including the solvation sheath) and the electrolyte viscosity.[144]

The original Walden rule established a direct proportionality relation (by a constant c) between the equivalent ionic conductivity Λ and viscosity η (see Figure 5b).[160] On a plot of log Λ versus log ϕ (ϕ is the fluidity, viz. the reciprocal of η), data for a 0.01 M KCl solution provide a straight line that passes through the origin used as the ideal reference (Walden plot).[161] Dilute aqueous KCl solutions are used because they are assumed to be fully dissociated and to have ions of equal mobility.[161] The use of data for higher concentrations (e.g., KCl 1 M) is controversial, because they significantly deviate from the ideal assumptions.[173]

In the Walden plot, systems for which the constant c differs significantly from the ideal one are offset from the reference line. The study of molten salts lead to the development of the "'fractional"' Walden rule including an exponent α ($0 < \alpha < 1$, $\alpha = 1$ for the ideal reference) affecting the slope of data in the Walden plot.[160] The fractional Walden rule implies that the activation energy for conductivity is lower than that for viscosity, which is the characteristic behaviour of "'superionic"' conductors (top left-hand corner of the diagram), combining high conductivities with low fluidities.

A modified version corrected for the ionic radii of the cation (r_i^+) and the anion (r_i^-) was proposed by extrapolating them from the Stokes-Einstein equation relating the viscosity to the self-diffusion coefficients of the ions, and using these latter to compute the ionic conductivity via the Nernst-Einstein equation.[161]

For ionic liquids, the most favorable systems combine high fluidities with high conductivities, with room-temperature values in the top right-hand corner of the diagram.[161] The lower right-hand half of the diagram represents "poor" ionic liquids approaching the behavior of molecular liquids.[174]

The behavior of poor ionic liquid, and in general of poor electrolyte solution in this description, is generally attributed to a low degree of dissociation, mostly due to non-conductive neutral ion pairs. An additional contribution is given by the polarization-induced internal field due to the counterions opposed to the external electric field and the movement of ions along it.[160,161] The apparent degree of dissociation, or "ionicity", i.e., the reciprocal of the Haven ratio, is often given as the ratio between the ionic conductivity measured under a (small) applied electric field (mostly measured by electrochemical impedance spectroscopy – EIS) and the ionic conductivity derived from the apparent self-diffusivity measured by PFG-NMR via the Nernst-Einstein relation. This latter tends to be overestimated, due to the contribution of all the species bearing the tracer, whereas EIS only accounts for mobile charge carriers.[136] It has been pointed out that the offset from the ideal KCl reference is not a reliable descriptor of the degree of dissociation.[173]

Correlation in Ion Transport: The correlations among ions have been taken into account in several computed models and simulations on Na-based battery electrolytes to describe the transport properties of highly concentrated-, ionic liquid-, and polymer-based electrolytes (e.g., drawing upon the theoretical treatments by Onsanger, Green-Kubo, Stefan-Maxwell, and Wheeler-Newman).[127,140,158,167,175]

In general, sub-ionicity and experimental evidences yielding a Haven ratio >1 are attributed to the presence of ion-pairs unable to transport charges. Besides neutral ion pairs, other types of ion-ion correlations can reduce the ionic conductivity. In the statistical-mechanical non-equilibrium treatment, if the total correlated mean-squared charge displacement related to the ionic conductivity (arising from the description of ionic conductivity in terms of velocity–velocity correlations of all the ions in the system) is smaller than expected for random jumps $\sim N\lambda^2$ related to the self-diffusion coefficient (N is the number of ions involved in correlated motion, and λ is the averaged jump length arising from velocity–velocity self-correlation function), then the reciprocal of the Haven ratio will be smaller than 1. This might lead to a significant (≈10 times) decrease in ionic conductivity relative to the conductivity expected when there are no ion–ion correlations. On the microscopic level, this may be explained by a sort of backflow mechanism involving concerted mobile ion rearrangements, which result in ion diffusion with minimal or no charge displacement.

Cation–anion correlation is due to the electrostatic attraction and involves the movement of ions with opposite charges in the same direction (i.e., neutral ion pairs). It is not very important in highly diluted systems, whereas it affects transport in systems showing aggregation (see the section dedicated to solvation), where ions move together in a correlated manner for the lifetime of the aggregate.[127] This kind of cation–anion correlation decreases the ionic conductivity. On the other hand, there is also the case of cation-anion anticorrelation (ions moving in opposite directions), which increases the ionic conductivity, but can negatively affect the transference number, also depending on the technique used to measure it. This was found to be the case in solvate ionic liquids with long-lived metal ion-glyme chelates, where cation-anion anticorrelation leads to an increase of the ionic conductivity and a decrease of the steady state current under anion-blocking conditions, resulting in a low transference number measured by the Bruce-Vincent method.[158]

Cation-cation and anion-anion correlations include the self-correlation related to diffusivity (e.g., captured by PFG-NMR) and the mutual correlation among distinct ions of the same type (in this respect it is particularly relevant if they move in the same or opposite directions)[158] (see Figure 5c). In dilute liquid electrolytes, ions bearing the same charge will either interact very little or move in an anticorrelated manner (i.e., in opposite directions) because of electrostatic repulsion.[167] The correlations among distinct ions of the same type are substantial in systems with a high degree of ion aggregation due to the use of poor solvents with low dielectric constant, as well as in highly concentrated systems, and in polymer electrolytes, particularly polyanions (i.e., polymeric single ion conductors) and polycations (here polyionic liquids).[127] For example, a major decrease in conductivity in ionic liquids may appear as a result of anion–anion and cation–cation anticorrelations (i.e., ions mov-

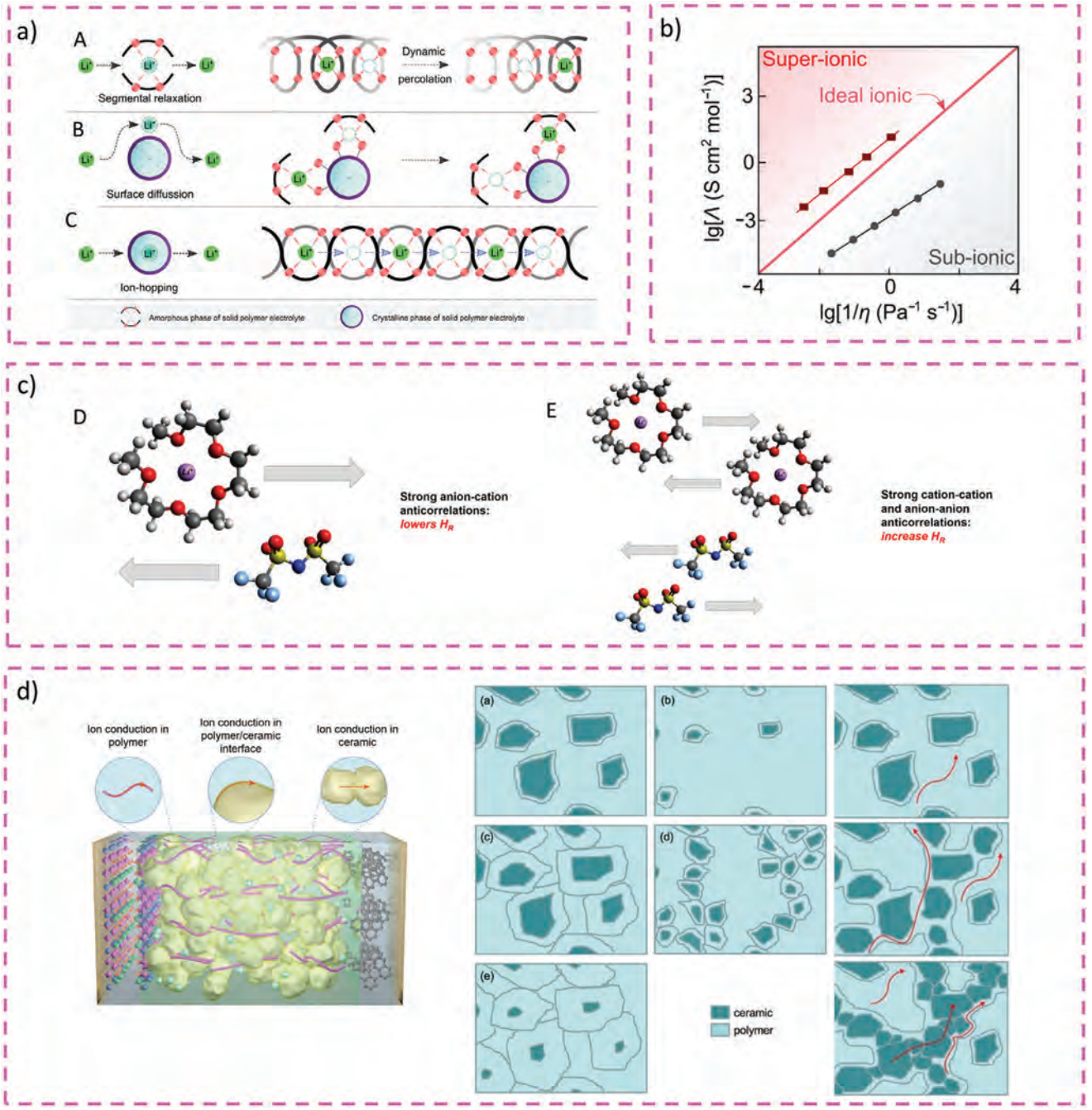

Figure 5. a) Graphical representation of the microscopic transport of Li^+ ions in fully amorphous phases, wherein Li^+-ion migration is closely correlated with the segmental dynamics of polymer backbones (A), Graphical representation of the microscopic transport of Li^+ ions in a mixture of amorphous and crystalline phases. In this scenario, the surface functional groups of crystalline phases facilitate the transport of ionic species (B), Graphical representation of the microscopic transport of Li^+ ions in crystalline phases, where cationic species migrate via the ion-hopping mechanism (C). Adapted under terms of the CC-BY license.[171] Copyright 2023, Song, Z. et al., published by Springer Nature. b) Walden–Angell plot for ionic materials. Adapted under terms of the CC-BY license.[171] Copyright 2023, Song, Z. et al., published by Springer Nature. c) Illustration of the phenomenon of anticorrelated ion movements in solvate ionic liquids based on the tetraglyme-LiTFSI system: cation-anion anticorrelations contribute to lowering the Haven ratio (HR) of solvate ionic liquids (D), this effect is overcompensated by strong cation–cation and anion–anion anticorrelations, resulting in an HR value greater than 1 (E). Adapted under terms of the CC-BY license.[158] Copyright 2019, Vargas-Barbosa, N. M., Roling John B., published by Wiley and Sons. d) Ion conduction mechanism in the solid-state, regions of enhanced Na-ion conductivities along with different microstructure scenarios Adapted with permission.[166] Copyright 2023, John Wiley and Sons.

ing in opposite direction) resulting in a Haven ratio > 1. This kind of anticorrelation can be responsible for measured ionic conductivities up to ten times lower than expected based on the apparent self-diffusivities in both polyanionic (i.e., polymeric single-ion conductors) and polycationic (i.e., polyionic liquids) systems, due to the covalent bonding of the ionic monomers.[158,167] In general, the most substantial contribution in polyionic systems is given by anion-anion correlations, particularly within the same chain, where anticorrelation is due to electrostatic repulsion, but positive correlation may also occur in aggregates including different charged chains with their counter ions.[127] Positive correlation among ions of the same type moving in the same direction results in a Haven ratio <1.[158] This is the case for many superionic glasses and crystals, where ionic conductivities can be 3–5 higher than expected based on the apparent self-diffusivity. In these systems, the charge diffusion is actually faster than ion diffusion, which is due to correlated cation-cation motion, drastically improving the conductivity.[167]

It deserves special mention the case of systems rich in charged aggregates showing fast exchange and rearrangement, e.g. highly concentrated ionic liquid-based sodium electrolytes. In these systems, the high measured transference number[163] and high-rate capability[137] were ascribed to decoupled ion pathways for Na ions, relying on short residence time and fast exchanges in the coordination environment. The high CN variance for Na^+ ions, evidenced in several MD simulations of highly concentrated systems,[132,137,140,144] has been ascribed to the flexible character of the coordination environment at high salt concentration, possibly resulting in a Grotthuss-like transport mechanism, via successive jumps across different coordination environments.[127,144]

Ion Transport in Composite Electrolytes: In general, composite electrolytes are classified depending on the amount of dispersed phase relative to matrix (which is low in ceramic-in-polymer systems, and high in polymer-in-ceramic ones) and the ability of the inorganic phase to transport the alkali metal ion (often called active filler), as opposed to the use of inert fillers (also called "inactive", or "passive").

With inert fillers, the ceramic-in-polymer approach is the most convenient because of its easier film processability. In general, ceramic-in-polymer electrolytes with low ceramic loading have room temperature conductivities higher by one order of magnitude compared to polymer electrolytes without filler.[176] Composite electrolytes with an inert ceramic phase dispersed in sodium-ion conductive polymer and components are mainly aimed at improving the mechanical properties while hindering polymer crystallization upon cooling from the amorphous state, similar to Li-based systems with PEO.[177] However, the decrease of the polymer host crystallinity, e.g., with semi-crystalline poly(caprolactone), is not always found to increase the ionic conductivity of ceramic-in-polymer systems with inert fillers.[162] On the other hand, an increase in conductivity has been reported for nanocomposite systems where the polymer matrix (e.g., with PAN) is completely amorphous regardless of the presence of particles). In this respect, many studies have stressed the importance of Lewis acid sites on the particles' surface, which are able to interact with the anions, thus helping the dissociation of ion pairs and improving the alkali metal ion transport properties.[162,176] Simulations have also shown that an interface area exists between the bulk polymer and the ceramic particles, in which the disorder of the polymer chains increases as well as salt dissociation, leading to the improvement of the ionic conductivity[166] (see Figure 5d). It is important to stress here that the use of the solvent casting method to obtain the composite films can lead to misleading results due to residual solvent traces, particularly regarding the effects on the polymer crystallinity and chain arrangement at the interface with the particles' surface.[178] Indeed, several studies (including quasi-elastic neutron scattering measurements) evidenced that the segmental dynamics of the PEO chains near the particle surface are hindered in both "salt-free" and "salt-doped" systems.[162,176] On the other hand, the improved retention of the liquid phase is largely exploited in hybrid gel-composite electrolytes.[166,179]

The effective medium theory and the percolation theory are commonly used to model the conductivity of composite electrolytes. The former expresses overall conductivity as a function of the conductivities of the constituent phases and their volume fractions. More recent models take into account three phases, i.e., the host, the disperse phase (including the particle size and geometry), and the conductivity and thickness of the interfacial region among them. Additionally, they take into account the percolation threshold, which affects the continuity of the conductive pathways.[180]

A percolation pathway parallel to that of the host may arise above a critical threshold for the ceramic content. The threshold depends on the conductivity of the components (conductor–superconductor versus conductor-insulator mixtures) and the conductivity along the interface among them. The influence of local interfacial regions with enhanced conductivity on the overall transport properties depends on their (radial) extension, the size, and the volume fraction of the ceramic particles (the interfacial regions will be more important for small particles with large surface area). Below the percolation threshold, the conductive pathways along highly conductive interfacial regions are discontinued. On the other hand, a reduced ionic conductivity can be observed at high ceramic phase content due to particle agglomeration.[166] In this respect, it is worth mentioning that high heterogeneity (e.g., due to agglomeration) may lead to non-uniform contact and uneven ionic flux at the interface with the electrodes.[162] In this respect, surface functionalization of the dispersed phase was demonstrated to improve the compatibility among the components and cycling ability with the metal anode in Li-based systems.[181] Composite materials including sodium ion conducting ceramic, are aimed at enhancing the Na-ion transport properties by exploiting the highly conductive inorganic phase. Several different composite systems including β''-Al_2O_3, NSZP, and Na_3SbS_4 have been investigated in this respect, particularly in combination with PEO. In these systems, the conductivity is affected by the interfacial regions, the resistance at the polymer/ceramic interface, and the resistance between ceramic particles.[166]

In the case of non-percolating systems, the resistance across the polymer/ceramic interface is the most important, because it could enable fast transport in the ceramic phase regardless of the discontinuous conduction pathway. In most cases, the interfacial properties were found to hinder ion exchange across the polymer/ceramic interface, in both polymer-in-ceramic and ceramic-in-polymer systems.[176]

Several factors affect ion transport across the polymer/ceramic interface, including the formation of insulating secondary interphases due to side reactions, and the space-charge effect. The former is likely due to impurities on the surface of ceramic particles, or the reactivity in contact with the polymer matrix (e.g., H_2O traces in hygroscopic PEO may react with sulfide ceramic conductors). The space charge effect is associated with charge depletion and enrichment at the interface between different conductive phases (e.g., grains with different orientations, and different materials), resulting in an internal electric field and a modified concentration of charge-carrying defects close to the interface. This latter affects the ionic conductivity. It is worth mentioning that such effect is ascribed to a confined portion of the sample near the interface and the electric field vanishes in the bulk interior, therefore the finite size of the conductive regions must be considered particularly in polymer-in-ceramic nanocomposite materials.[162,180]

The polymer-in-ceramic systems contain high concentrations of ceramics as the main ion-charge carriers, with minimal amounts of polymer. This approach aims at exploiting the properties of the polymer in terms of improved contact with the electrodes, ability to buffer the volume variations, and ease of processing. Fast ion transport is limited by the low ionic conductivity of the polymer matrix. In this respect, in the absence of efficient exchanges across the polymer/ceramic interface, the simple dispersion of the inorganic particles easily results in lower ionic conductivities with respect to the reference ceramic pellets, which usually undergo densification to eliminate voids and/or grain boundaries. The continuity of the ceramic phase is found to be fundamental to form a percolating ionic pathway. For example, aligned ceramic nanowires with high aspect ratio were found to improve the ionic conductivity over random particles dispersions, thanks to the long-range ionic pathways in the former. The ion transport properties would also benefit from such alignment in the presence of local interfacial regions with enhanced ionic conductivity. Finally, the geometry of the continuous ceramic scaffold can also affect the polarization overpotential and the mechanical properties.[166,176]

5. Separators

In all-liquid-electrolyte based batteries, the electrolyte solution is normally soaked in a separator, a porous membrane sandwiched between electrodes of opposite polarity, permeable to ionic flow but able to prevent the direct contact of the electrodes and related short-circuit.[182] A good separator has to meet some minimal requirements (**Figure 6a**):

a) it must be electronically insulating (the electron flow occurs in the external circuit);
b) it must be chemically and electrochemically stable towards the electrolyte and the electrode components;
c) it must be mechanically robust to withstand the solicitations occurring during battery assembly and operation;
d) it must effectively prevent the migration of particles or colloidal or soluble species between the two electrodes;
e) it should be thin with a sufficient and an interconnected porous structure for soaking as much as possible electrolyte solution, thus assuring high ionic conductivity and proper operation;
f) it should be uniform in thickness and, at the same time, lightweight. Quantitatively speaking, the MacMullin number (e.g., the ratio of the resistivity of the separator filled with the electrolyte divided by the resistivity of the electrolyte alone) should be as low as possible;[183]
g) it must be thermally stable: less than 5% shrinkage after 60 min at 90 °C under vacuum.[182] Moreover, it should be able to close the pores when the internal temperature in the battery dramatically increases. This phenomenon is called "shutdown";
h) it should be low-cost and easy to fabricate. In general, the price of a separator counts up to around 20% of the total cost of battery materials/components at the cell level[184] (mostly because of the expensive fabrication process).

Separators used in batteries can be grouped into three categories: micro-porous polymeric membranes, nonwoven materials, and composite membranes. Micro-porous polymeric membranes are semi-crystalline materials based on polyolefins, such as polyethylene (PE), polypropylene (PP), and their blends. They are the most commonly used separators in batteries due to sufficient porosity, good mechanical properties, high chemical stability, and low cost.[185] However, their low melting points compromise thermal stability, thereby impacting battery safety. Additionally, when exposed to temperatures exceeding their melting points, these polyolefin membranes experience a significant loss of mechanical integrity, leading to short circuits. Nonwoven materials, either oriented or randomly arranged, bonded together by chemical or physical methods, are promising alternatives due to their high porosity and excellent thermal stability. These materials can be bio-based (e.g., cellulose), or synthetic, such as polyamide (PA) or PVdF. However, their weak inter-fiber interactions result in subpar mechanical strength, making these membranes susceptible to dendrite penetration.

Thus, the separator preparation, including the modification process, is critical to enhance thermal stability by strictly controlling flame and dendrite growth. Recent years have yielded significant progress in creating high-performance separators by grafting, coating, or filling organic (polymers)/inorganic (ceramics) material on the surface of traditional polyolefin separators.[186] Recently, a novel PE-HEC-TiO_2 composite separator (where PE = polyethylene, HEC = hydroxyethyl cellulose) was developed by *Zhu* et al. by sequentially applying hydroxyethyl cellulose (HEC) coating and in situ self-growth of TiO_2 nanoparticles. This composite separator effectively improves electrolyte absorption by addressing the issues of low surface energy and poor wettability common in conventional PE separators. In a $Na|Na_3V_2(PO_4)_3$ battery cell using the PE-HEC-TiO_2 separator and 1.0 M $NaClO_4$ in EC/PC (1:1, weight ratio) with 5.0 wt% FEC additive as electrolyte, it demonstrates a reversible capacity of 99.0 mAh g^{-1} and maintains an excellent capacity retention of 94.8% even after 1000 cycles at 5C, while concurrently providing a stable Coulombic efficiency close to 100% (Figure 6b).[187] Mun et al. prepared composite separators based on PE by an impregnation method using SiO_2 ceramic nanoparticle filler, thus improving thermal stability, ionic conductivity, and cell performance. When utilizing a nano-SiO_2-impregnated PE separator

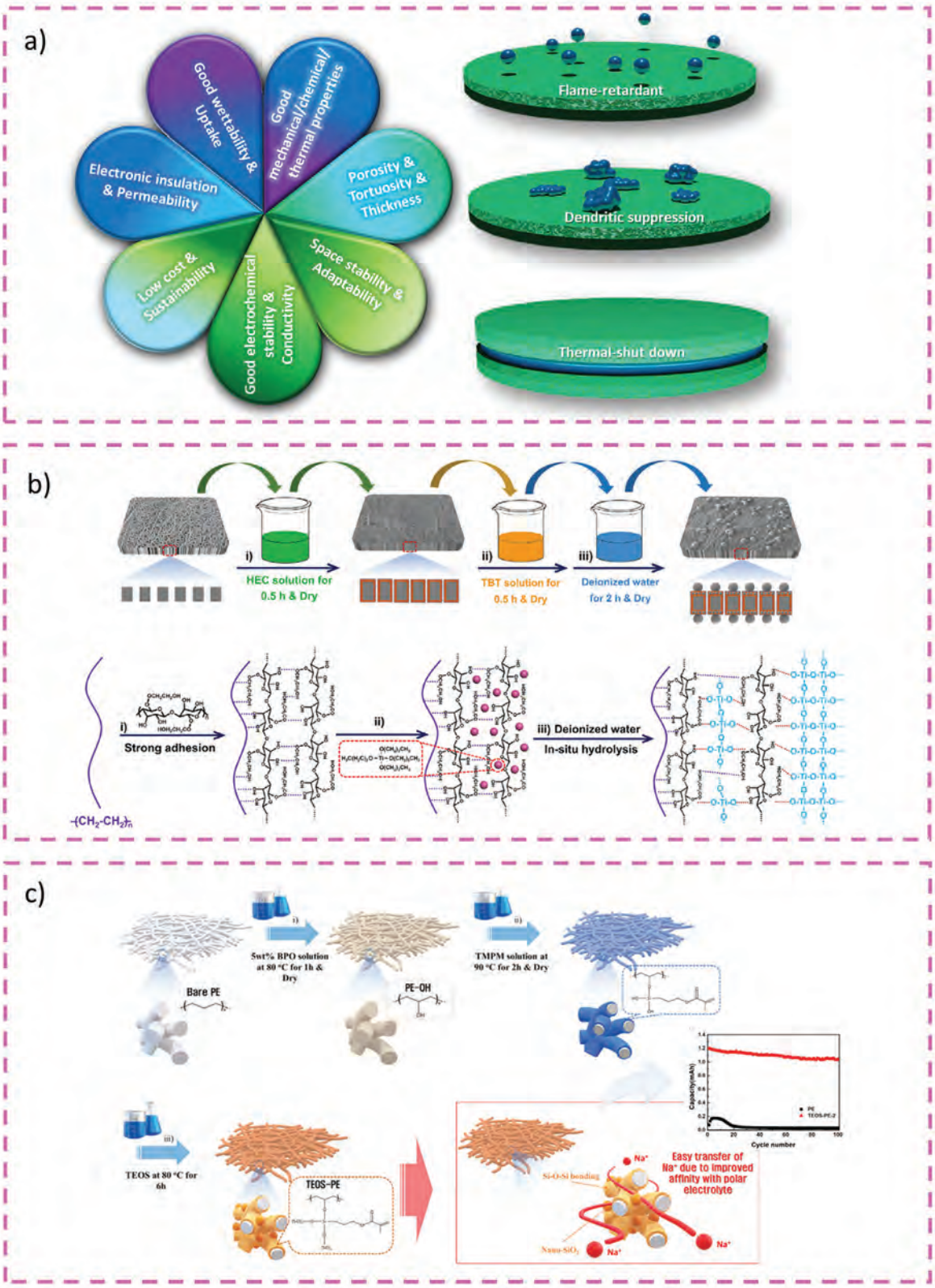

Figure 6. a) Requirements for the separator to tackle secondary battery challenges; b) Preparation procedure and proposed mechanism of the PE- HEC-TiO_2 composite separator. Adapted with permission.[187] Copyright 2023, John Wiley and Sons. c) Schematic of the fabrication of PE/SiO_2 separator. Adapted with permission.[188] Copyright 2020, Elsevier.

in Na full-cell systems with 1 M $NaPF_6$ in EC:PC (5:5, weight ratio) as electrolyte, which includes $Na_{0.9}Li_{0.05}Ni_{0.25}Fe_{0.25}Mn_{0.5}O_2$ and HC electrodes, a significant improvement in both cycle life and rate capabilities is demonstrated (Figure 6c).[188]

Electrolyte filling in commercial cells is one of the most time-consuming steps, and it needs to be overcome, as well as costly formation, for next-generation batteries.[189,190] Artificial intelligence will play a major role in making the process more efficient, hopefully adapting fast to new materials and requirements, depending on data availability.[191] Cell filling with conventional electrolytes is limited by the high vapor pressure of the organic solvents, limiting the evacuation (under)pressure and time, as well as the filling temperature.[192] All these parameters can be increased using IL-based electrolytes without any risk of evaporation or degradation. At present, benchmark commercial separators tailored for ILs are still not established, and most researchers use thick glass fiber separators (in the order of hundreds of microns) for material characterization at the laboratory scale, which is not compatible with large-scale production. Dedicated studies pointed out that most polyolefine-based commercial separators are not properly wet by ILs.[193] In particular, ILs having cations with long side chains and TFSI anions are more compatible with hydrophobic separators. For example, Celgard 2500 was found to be better wet by pyrrolidinium-based ILs with TFSI compared to those with BF_4^- and FSI anions.[194,195] With the exception of PC, the addition of organic diluents was found to be beneficial to decrease viscosity and improve wetting with Celgard 2500, regardless of the choice of the anion.[196] Dilution strategy was also demonstrated to improve wetting of tortuous pores in commercial LFP electrode tapes (≈10 mg cm^{-2}, ≈53% porosity), by reducing the time required to stabilize the impedance upon formation, with a threshold at which it was halved at 50% dilution. It is worth mentioning here that the negligible vapour pressure of ILs, coupled with their high thermal and chemical stability, allows including them directly in the electrode slurry or in mixtures for extrusion.[197] Additionally, polymeric ILs have been proposed as alternative electrode binders,[198] notably including fluorine-free systems for aqueous electrode slurries.[199]

In general, hydrophilic separators, such as polyamide and cellulose, have been shown to be more compatible with ILs in terms of wetting, compared to the hydrophobic ones. The hydrophilic commercial Al_2O_3/PET (Separion) separator is compatible with most ionic liquids,[193] but it was found to be detrimental for the cell performance in lithium metal cells due to dendrite formation, possibly in relation with its surface roughness and high porosity, also depending on the SEI-forming ability of the ionic liquid, mostly relying on the choice of the anion.[194] A comparative study evidenced that Celgard®3501 is more compatible than Separion® with both lithium metal and concentrated IL-based electrolytes with FSI anion.[200] IL-based electrolytes will be further discussed in the following section.

Overall, both the structural design of the separator and its interaction with the liquid electrolyte significantly impact the transport of Na^+ ions and contribute to cell overpotentials.[183] Despite progress in finding suitable separators, there remains a pressing need to enhance their performance further. This challenge stems from the requirement for separators to meet multiple performance criteria simultaneously, including thermal resistance, chemical compatibility, mechanical strength, dendritic suppression, as well as considerations like sustainability, flexibility, and thickness.[186] These attributes are crucial for the practical implementation of large-scale battery systems. Moreover, there exists a significant gap in our understanding of how the properties of separators directly influence NIB performance. Enhancing both the safety and the electrochemical efficiency of next-generation NIBs necessitates the advancement of innovative composite separators tailored for use with liquid electrolytes. It is imperative to reduce reliance on toxic solvents, costly nanomaterials, and binders, as these components are typically essential in coating processes aimed at functionalizing inorganic materials onto PE separators.[185]

This emphasis on sustainability and cost-effectiveness is essential for driving progress in battery technology while minimizing environmental impact. Additionally, the creation of smart separators featuring practical functionalities is going to be always more relevant in the coming future. These smart separators should be capable of responding to various conditions such as temperature, current, and voltage fluctuations, contributing to better battery management and safety.[201] Furthermore, efforts should focus on integrating separators into solid electrolytes, a promising approach that can enhance the stability and efficiency of next-generation batteries, including NIBs.

6. The Versatility of Ionic Liquids: Toward Gel and Composite Electrolytes

While conventional organic electrolytes offer the advantage of ease of handling and exhibit superior properties, particularly around room temperature, they also present significant safety challenges that must be addressed before their widespread use in large-scale devices. One major challenge is the volatile and flammable nature of organic solvents, which poses safety hazards.[202] In contrast, room temperature ionic liquids (RTILs) present an enticing alternative to standard liquid electrolytes due to their inherent safety characteristics.[203] RTILs are salts with melting points below 100 °C, generally constituted by organic cations and anions with a highly delocalized charge. In battery applications, the most used cations are based on organic species, such as imidazolium (Im), pyrrolidinium (Pyr), piperidinium (PP), phosphonium, and linear quaternary ammonium. The anions can be inorganic (i.e., BF_4^-, PF_6^-) or organic (usually, FSI^- or $TFSI^-$). Compared to organic carbonate solvents, RTILs have low vapor pressure, high boiling points, and high thermal stability, allowing battery operation at high temperatures, while reducing fire hazards. However, one of the main challenges of RTILs is their cost, generally elevated for relatively expensive synthesis and purification, which is a disadvantage in the framework of NIB technology, targeting to lower the cost compared to its LIB counterpart.[204]

The addition of metal salts to RTILs results in decreased ionic conductivity because of increased viscosity and ion clustering. Moreover, the transference number of the Na^+ ion in RTILs is generally below 0.2. The reduced conductivity and the limited transference number generally result in a limited rate capability in comparison with liquid electrolytes based on organic solvents at ambient temperature. When the temperature is increased, RTIL-based cells display improved specific capacity, rate capability, and cycle life. This trend is shown in **Table 4**,

Table 4. Electrochemical performance of different electrodes employing RTILs- or organic carbonates-based liquid electrolytes.

Electrolyte	σ [S cm^{-1}]		Cell	De-sodiation capacity [T, C-rate] [mAh g^{-1}]	Capacity retention [T, C-rate, cycle #] [%]	References
	@Low T [°C]	@High T [°C]				
$NaClO_4$ 1 M in EC/DEC	–	–	Na/NFP	120 (25 °C, 0.05C) 140 (50 °C, 0.05C)	≈73 (25 °C, 0.3C, 100) 62 (50 °C, 0.3C, 100)	[235]
NaTFSI 0.5 M in Pyr_{14}TFSI	1.2×10^{-3} (25)	3.8×10^{-3} (75)	Na/NFP	56 (25 °C, 0.05C) 125 (50 °C, 0.05C)	≈60 (25 °C, 0.3C, 100) ≈80 (50 °C, 0.3C, 100)	[235]
NaFSI 1 M in Pyr_{13}FSI			Na/FeF_3-CNFs	~95 (25 °C, 50 mA g^{-1})	Capacity decays ~0.030% per cycle (25 °C, 50 mA g^{-1}, 1000) Capacity decays ~0.25% per cycle (60 °C, 50 mA g^{-1}, 60)	[209]
NaFSI in Pyr_{13}FSI (2: 8 molar ratio)	–	–	Na/$Na_2Ni_2TeO_6$	~80 (25 °C, C/20) ~80 (50 °C, C/20)	–	[236]
$NaClO_4$ 1 M in EC/DEC	6.3×10^{-3} (25)		Na/NMO	108 (25 °C, 0.05C) 112 (50 °C, 0.05C)	84 (25 °C, 0.3C, 100) ≈60 (50 °C, 0.3C, 100)	[237]
$NaClO_4$ 1 M in Pyr_{14}TFSI	1×10^{-3} (25)	3.6×10^{-3} (75)	Na/NMO	97 (25 °C, 0.05C) 109 (50 °C, 0.05C)	65 (25 °C, 0.3C, 100) 80 (50 °C, 0.3C, 100)	[237]
NaFSI 0.5 M in Pyr_{14} TFSI	1.42×10^{-3} (25)	–	Na/NCO	147 (25 °C, 50 mA g^{-1}) 100 (25 °C, 200 mA g^{-1})	88 (25 °C, 50 mA g^{-1}, 500)	[238]
$NaClO_4$ 1 M in EC/PC	7.38×10^{-3} (25)	–	Na/NCO	172 (25 °C, 50 mA g^{-1}) 100 (25 °C, 40 mA g^{-1})	66 (25 °C, 50 mA g^{-1}, 100)	[238]
NaFSI 1 M in Pyr_{13}TFSI	3.2×10^{-3} (25)		Na/NVP	112 (25 °C, 0.5C) 100 (25 °C, 5C)	99 (25 °C, 0.5C, 100)	[239]
NaFSI 1 M in EC/PC	5.5×10^{-3} (25)		Na/NVP	112 (25 °C, 0.5C) 95 (25 °C, 5C)	87 (25 °C, 0.5C,100)	[239]
NaFSI 1 M in P_{1i444}FSI	–	–	Na/NVP	99 (60 °C, C/5) ≈60 (60 °C, 4C)	98 (60 °C, C/5,60)	[240]
NaFSI 1 M in EC/PC	–	–	Na/NVP	96 (60 °C, C/5) ≈45 (60 °C, 4C)	87 (60 °C, C/5,60)	[240]
$NaClO_4$ 1 M in EC/PC	–	–	Na/HC	97 (25 °C, 50 mA g^{-1}, 500)	72 (25 °C, 300 mA g^{-1}, 100)	[23]
NaFSI 1 M in Pyr_{13}FSI	2×10^{-3} (25)	7×10^{-3} (60)	Na/HC	280 (25 °C, 30 mA g^{-1}) 51 (25 °C, 8C)	90 (25 °C, 30 mA g^{-1}, 200)	[241]
0.1 NaTFSI-0.9[N_{1114}][FSI]	$1.8\pm 0.1 \times 10^{-3}$ (20)	$5.4\pm 0.3 \times 10^{-3}$ (50)	Na/HC	175 (25 °C, 30 mA g^{-1}) 109 (25 °C, 1C)	98 (25 °C, 60 mA g^{-1}, 1500)	[210]
NaTFSI 1 M in PC+3 wt.% FEC	–	–	Na/HC	153 (25 °C, 30 mA g^{-1}) 125 (25 °C, 1C)	–	[210]
NaPF6 1 M in EC:PC	–	–	Na/TiO_2	243.9 (25 °C, 0.1 mA g^{-1})	156.2 (25 °C, 0.1 mA g^{-1}, 10 000)	[242]
NaTFSI 10 mol% in Pyr_{13}FSI	5.6×10^{-3} (25)		Na/TiO_2	159 (25 °C, 0.1C)	96 (25 °C, 0.1C, 80)	[243]
$NaClO_4$ 1 M in PC/FEC	6×10^{-3} (25)	8.4×10^{-3} (60)	Na/SbSg	710 (25 °C, 50 mA g^{-1}) 285 (25 °C, 1.5 A g^{-1})	83 (25 °C, 100 mA g^{-1}, 100)	[244]
NaFSI 1 M in Pyr_{13}FSI	2×10^{-3} (25)	7×10^{-3} (60)	Na/SbSg	660 (25 °C, 50 mA g^{-1}) 240 (25 °C, 1.5 A g^{-1})	96 (25 °C, 100 mA g^{-1}, 100)	[244]
NaTFSI/PVDF-HFP/EMIMTFSI	1.9×10^{-3} (30)		Na-NMC || Na	~108 (30 °C, 0.1 C)	94 (30 °C, 0.2 C, 200)	[219]
NaFSI/PEO/Pyr_{14}FSI	1.2×10^{-3} (20)		P2-$Na_{2/3}Ni_{1/3}Mn_{2/3}O_2$|| Na	140 (20 °C, 1C)	99 (20 °C, 1C, 100)	[223]
NaTFSI/diglyme (G2)/PVDF-HFP/SIL	1.1×10^{-3} (25)		$NaCoO_2$ || Na	~ 91.76 (25 °C 0.05C)	68 (25 °C, 0.1 C, 100)	[220]
NaTFSI/PY_{13}FSI/PVDF-HFP/SBA-15	2.5×10^{-3} (30)		NVP || Na	110.7 (30 °C, 0.1 C)	92 (30 °C, 0.1 C, 300)	[245]

NFP = $NaFePO_4$; NMO = $Na_{0.44}MnO_2$; NVP = $Na_3V_2(PO_4)_3$; SbSg = Sb_2S_3-graphene; *considering one-electron theoretical capacity; **pre-sodiated anode.

which resumes the electrochemical performances of different electrodes with RTILs- or organic carbonates-based electrolytes from some recent literature reports. While the high reactivity of Na metal with organic solvents can be detrimental to the cycling ability of anode half-cells,[205] the significant resistance at the Na metal/electrolyte interface can affect the electrochemical performance in the presence of RTILs. As a result, in the Na-ion full cell configuration, where Na-metal is not present, the NaFSI 1 M in $Pyr_{13}FSI$ electrolyte outperforms $NaClO_4$ 1 M in EC/DEC in terms of both specific capacity and cycling ability, even at ambient conditions.[206]

Some RTILs can form a beneficial SEI layer on the aluminium current collector, thus preventing corrosion with NaFSI and NaTFSI salts. For instance, NaFSI salt in PC causes pitting corrosion of Al collectors upon cyclic voltammetry tests. Conversely, NaFSI in $Pyr_{13}FSI$ was found to stabilize the Al surface up to 5 V versus Na^+/Na, with no evidence of corrosion.[207] Similarly, NaTFSI 0.8 M in $Pyr_{13}TFSI$ electrolyte was found to shift the corrosion potential of Al from 3.5 to 4.0 V versus Na^+/Na. Interestingly, both $Pyr_{13}TFSI$ and N-butyl-N-methyl-ImTFSI (BMImTFSI) electrolytes containing NaTFSI were found to preclude Na deposition on Al during cyclic voltammetry experiments in the range −0.5/3 V versus Na^+/Na, even though the cycling ability of $Pyr_{13}TFSI$ and $Pyr_{14}TFSI$ has been demonstrated with different Na salts in half-cell configuration (Table 4).[208]

Recent works highlighted significant improvements in the performance of FeF_3-CNF cathodes when used in various RTIL-based electrolytes, namely, 1 M NaFSI in $Pyr_{1,3}FSI$, $Pyr_{1,4}FSI$, and EMIMFSI, at room temperature and above. In particular, the $Pyr_{1,4}FSI$ electrolyte displayed the best cycling stability, reaching more than 1000 cycles at room temperature. The authors linked the elevated stability of the CEI formed in $Pyr_{1,4}$, which guarantees a less resistive CEI at room temperature compared to $Pyr_{1,3}$ (the difference has been associated with the different alkyl chain length). However, at higher temperatures (i.e., 35 and 60 °C), the $Pyr_{1,3}FSI$ ionic liquid displayed a superior CEI and better performance stability (**Figure** 7a). These findings suggest the potential of RTILs in designing a protective CEI for stable SIBs. The CEI induced by EMIMFSI remained stable at room temperature, but it exhibited rapid degradation and cell decay when exposed to higher temperatures.[209] Some studies have been done with RTILs to investigate their applicability as HC in NIBs. Maresca et al. concentrated on unravelling the chemical and electrochemical factors contributing to the outstanding performance of HC anodes when employing [EMI][FSI] and [N1114][FSI] electrolytes. They exploited cyclic voltammetry, impedance spectroscopy, and Raman spectroscopy to delineate the influence of RTILs on the stability of the SEI, alterations in sodium ion (Na^+) transport properties, and surface modifications of the HC anodes during cycling.[210]

RTILs with polymerizable moieties, such as allyl or vinyl groups, have been shown to form protective coatings on the Na metal electrode.[211] The artificial SEI layers were obtained by electropolymerization of the RTIL monomer added into the PC/EC-based electrolyte. Electrolytes containing 1,3-diallyl imidazolium perchlorate (DAIM) exhibited improved Coulombic efficiency (95%) during a galvanostatic plating/stripping test at 1 mA cm^{-2} in a Na/stainless steel laboratory-scale cell. A protected sodium anode, formed after 10 h of DAIM electrodeposition, was tested in a $Na/Na_3V_2(PO_4)_3$ half-cell upon galvanostatic cycling. The cell could maintain a discharge capacity of 97 mAh g^{-1} after 160 cycles, with a Coulombic efficiency exceeding 96%. In contrast, with the pristine Na electrode, a sharp decrease of the discharge capacity to 20 mAh g^{-1} was observed in 30 cycles; this notwithstanding the known cathodic instability of imidazolium-based RTILs due to the reactive acidic proton in C-2 position.[212–214]

Although this review article aims to cover the use of RTILs as electrolytes in NIBs, it is worth mentioning that these compounds have also been introduced into the material structure during synthesis to reduce the nucleation rate and provide high-performing electrode materials. In this regard, Jiang et al.,[215] successfully synthesized a high-performance Prussian Blue (PB) material with elevated sodium content, minimal vacancies, and low water interaction through an ionic liquid-assisted approach. Specifically, 1-butyl-3-methylimidazolium chloride was found to interact with Fe^{2+} ions, facilitating the controlled release of Fe^{2+} ions over time. In the other research, a novel material, nitrogen-boron co-doped carbon-coated NVPF, was synthesized by Yu et al. using a straightforward sol–gel method. Notably, an ionic liquid, 1-vinyl-3-methyl imidazole tetrafluoroborate, was employed as a source of nitrogen and boron, marking the first instance of such utilization. The obtained material showed excellent capacity retention at a high C-rate upon long cycling. The authors also studied the stability of this material by in situ X-ray diffraction, evidencing the elevated structural stability of the material upon cycling.[216]

Polymer hosts encompassing RTIL-based electrolytes to yield gel-polymer electrolytes (GPEs) can further improve safety and cycle life, preventing electrolyte leakage while allowing for flexibility in configuration options. In section 7.2.2, we delve into the intricacies of GPEs with a more detailed analysis. Within this section, instead, we will specifically focus on GPEs incorporating RTILs, providing a comprehensive discussion of their characteristics, properties, and applications. In this regard, there are several reports of Im-based RTILs in poly(vinylidene fluoride)-hexafluoropropylene PVdF-HFP copolymer matrix with different sodium salts.[85,217,218] The resulting GPEs can achieve high room temperature ionic conductivity and thermal stability up to 150 °C, with good electrochemical stability window in the range of 1.5 V to 5.0 V versus Na/Na^+. Free-standing, translucent, and flexible GPEs have been produced by Mishra et al. by employing the polymer PVdF-HFP as a host matrix with varying weight percentages of a salt-ionic liquid (SIL) solution (Figure 7b). The GPE containing 70 wt% SIL exhibits outstanding characteristics. It demonstrates excellent thermal stability and a high ionic conductivity of 1.9×10^{-3} S cm^{-1} at 30 °C. The optimized electrolyte performance was evaluated using a Na-NMC cathode and a Na-metal anode to assemble Na-metal cells. The charge-discharge results revealed a specific discharge capacity of 108 mAh g^{-1} at 0.1 C. The cell maintained a capacity retention rate of 94% over 200 charge-discharge cycles at 0.2 C, showcasing both high capacity and excellent capacity retention for sodium batteries.[219] A GPE based on solvate ILs has been also developed by Parveen et al. using a solvate IL, where an equimolar complex of sodium salt NaTFSI and diglyme (G2) is immobilized within a PVdF-HFP copolymer matrix as the host. These GPEs are produced as free-standing, flexible, and transparent films, making them suitable

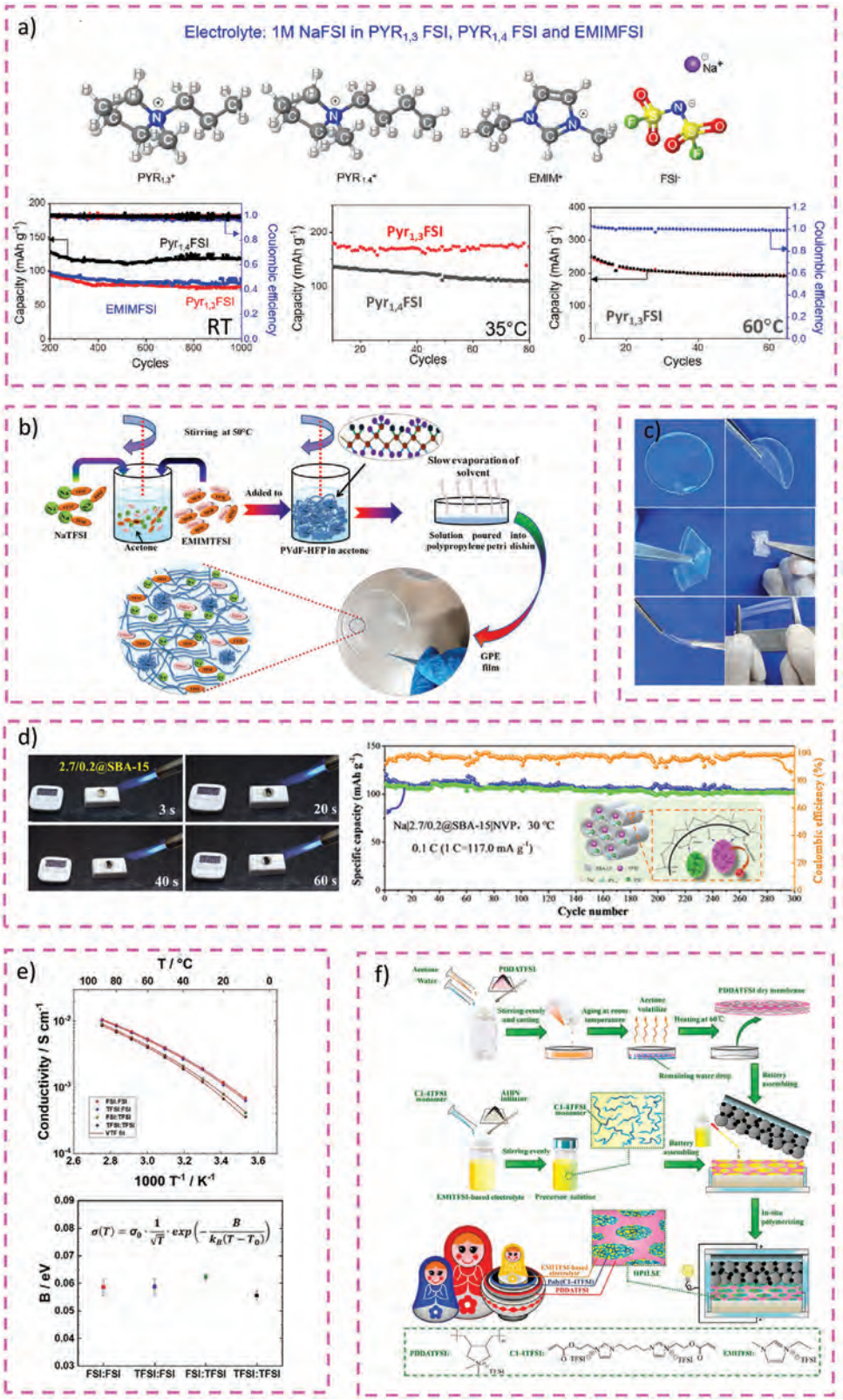

Figure 7. a) Cycling stability of FeF_3-CNF cathodes when used in various RTIL-based electrolytes, namely, 1 M NaFSI in $Pyr_{1,3}FSI$, $Pyr_{1,4}FSI$, and EMIMFSI, both at room temperature and elevated temperatures. Adapted with permission.[209] Copyright 2022, American Chemical Society. b) A sequential visual depiction outlining the synthesis method for the GPE. Adapted with permission.[219] Copyright 2021, American Chemical Society. c) Images of the solvate ionic liquid-incorporated GPE film subjected to various deformative forces, such as folding, twisting, and stretching. Adapted with permission.[220]

for integration into quasi-solid-state NIBs. Electrochemical investigations have shown that this GPE possesses notable characteristics, including high ionic conductivity (≈1.1×10^{-3} S cm^{-1}), a wide oxidative stability window (around 5.2 V versus Na^+/Na), a high sodium transference number (0.58), which contributes to elevated sodium-ion conductivity, stable sodium stripping/plating behavior, and thermal stability up to 100 °C. The GPE was evaluated with a $Na_{0.7}CoO_2$ cathode by galvanostatic charge–discharge cycling, exhibiting an initial discharge capacity of 91.76 mAh g^{-1} at a 0.05C rate (Figure 7c).[220] Gao and colleagues[221] combined SBA-15 with a sodium salt, $Pyr_{13}FSI$, and PVDF-HFP, aiming at the attainment of GPE with improved mechanical stability and enhanced ionic conductivity. Their protocol resulted in the formation of an iongel characterized by exceptional thermal stability, as shown in Figure 7d. Notably, the optimized version of this electrolyte can endure exposure to a flame gun with temperatures reaching ≈1500 °C. When paired with an NVP cathode and a metallic Na, it exhibited an initial specific discharge capacity of 110.7 mAh g^{-1} at room temperature, maintaining 92% of the initial capacity after 300 cycles (Figure 7d). The study evidenced that by controlled regulation of ionic electrolytes and their interactions, enhanced safety and electrochemical performance can be obtained, thereby promoting their practical applications in NIBs.

Over the past decade, persistent endeavors have been directed towards impeding the crystallization of PEO through the use of RTIL plasticizers. Chen et al. integrated $Pyr_{13}FSI$ into a PEO-$NaClO_4$ electrolyte to explore the plasticizing impact through infrared spectroscopy characterizations and DFT calculations. The findings suggest that FSI^- anions exhibit a propensity to adhere to the PEO backbone, thereby engendering enhanced coordination ability and a greater number of coordination sites.[222]

Recently, Passerini et al. created solvent-free ternary quasi-solid electrolytes using cross-linked PEO, NaFSI or NaTFSI, and RTILs. An elevated concentration of ILs plasticizer is anticipated to yield favorable room temperature ionic conductivity, while the cross-linking of polymer chains serves to uphold mechanical stability. The obtained electrolyte shows promise for use in sodium-based batteries. The synthesis process is entirely solvent-free, making it easily scalable. Extensive characterization revealed excellent thermal and electrochemical stability up to 3.8 V, along with high amorphicity and low glass transition temperatures, indicating high mobility within the polymer matrix. This high mobility leads to impressive ionic conductivities up to 1 mS cm^{-1} even at 20 °C (Figure 7e).[223]

Poly(ionic liquid)s (PILs), an innovative subclass of functional polymers, have garnered significant interest in recent years. These polymers feature ionic species covalently bonded to the polymer backbones. PILs have attracted attention due to their ability to retain the favorable properties of ILs, such as ionic conduction, non-flammability, and high electrochemical stability, while offering supplementary advantages over ILs, such as excellent mechanical performance and favorable processability. The first report of electrolytes based on PILs for NIB application included a free radical polymerisation step directly on the electrode surface (see Figure 7f).[224]

In the first stage, the electrolyte is fabricated by filling the pores of a PIL membrane made of poly(diallyldimethylammonium) (PDDA) TFSI with a solution containing a dicationic polymerizable RTIL based on ImTFSI (C1-4TFSI) and NaTFSI dissolved in N-ethyl-N- methyl-ImTFSI (EMImTFSI) together with a photoinitiator. The polymerizable RTIL contains two acryloyloxyethyl moieties available for the thermally activated free radical polymerization of the first membrane on top of the $Na_{0.9}[Cu_{0.22}Fe_{0.30}Mn_{0.48}]O_2$ (NCFMNO) cathode. In half-cell configuration at room temperature, the delivered specific capacity is 101.0 and 59.9 mAh g^{-1} at 0.05 and 1C, respectively, and the capacity retention is 85.5% after 100 cycles at 0.1 C, with Coulombic efficiency near 100%.

RTILs have also been used to decrease the interfacial resistance between cathode and ceramic ion-conductors. Zhang et al. reported a study of four different NASICON-derived ceramic syntheses used as sodium ion conductors.[225] In half-cell configuration with the pristine pellet and NVP as the cathode, the total resistance was found to be in the order of 1 kΩ, and the specific discharge capacity at room temperature decreased from 85 to 44 mAh g^{-1} in 10 cycles. The addition of ≈5 µL of either 0.8 M $NaPF_6$ in EC/DMC or with 1-mehyl-3-propyl-PPFSI ($PP_{13}FSI$) as a wetting agent decreased the cell resistance by one order of magnitude. An improved initial specific discharge capacity of 107 mAh g^{-1} at 0.2C was observed employing the carbonate-based electrolyte. However, a drop in the delivered capacity was observed after 250 cycles, attributed to the possible liquid electrolyte degradation/evaporation. Substituting the liquid electrolyte with the RTIL yielded specific discharge capacities as high as 113 mAh g^{-1} at 0.2 C and 86 mAh g^{-1} at 10C, with an outstanding cycling ability (10 000 cycles with negligible capacity fading). It is worth mentioning that the poor performance of the pristine ceramic electrolyte (without the wetting agent) was observed despite the cathode slurry having been spin-coated and directly sintered on top of the pellet, highlighting the challenges of obtaining an optimal electrode/electrolyte interface with ceramic pellets.

An attempt to circumvent the pelletization process of ceramic NASICON by preparing a composite hybrid electrolyte with a RTIL has been reported by de la Torre-Gamarra et al.,[226] $Pyr_{14}TFSI$ was mixed with NASICON powder (filler loading >90 wt%) with and without NaTFSI, and the resulting mixture was processed into a membrane by solvent casting in acetonitrile. The ionic conductivity values displayed by the hybrid electrolytes are lower as compared to the sintered NASICON pellet and to $Pyr_{14}TFSI$ or the $Pyr_{14}TFSI$-NaTFSI electrolyte, but they are higher with respect to a non-sintered NASICON pellet. Among the hybrids, those containing NaTFSI displayed higher

Copyright 2022, American Chemical Society. d) Flammability test of prepared 2.7/0.2@SBA-15 electrolyte membrane using a flame gun, and cycle stability of Na|2.7/0.2@SBA-15|NVP at 0.1 C. Adapted with permission.[221] Copyright 2020, American Chemical Society. e) Temperature-dependent ionic conductivity and VTF fit, and Pseudo activation energy (B) for ion conduction in the SPE bulk determined by the fit. Adapted under terms of the CC-BY license.[223] Copyright 2023, Roscher D., Kim Y., et al. published by John Wiley and Sons. f) Schematic illustration for the in situ synthesis route of nesting doll-like HPILSE. Adapted with permission.[224] Copyright 2017, Elsevier.

ionic conductivities despite the liquid $Pyr_{14}TFSI$-NaTFSI electrolyte being less conductive than $Pyr_{14}TFSI$. Significant grain boundary resistance and a high energy barrier for Na^+ ions transfer at the ceramic/RTIL interface have been proposed to explain the lack of a fast conduction mechanism. A similar approach was previously experimented for LIBs application by mixing 80 wt.% of garnet-type Li^+ ions conductor $Li_7La_3Zr_2O_{12}$ (LLZO) powder with $Pyr_{14}TFSI$-LiTFSI electrolyte.[227] Even in this case, the non-sintered ceramic pellet displayed an inferior room temperature ionic conductivity with respect to the hybrid and the $Pyr_{14}TFSI$-LiTFSI electrolytes, which was also nearly two orders of magnitude lower than that of sintered LLZO pellets reported in the literature.[228] Functionalization of the ceramic electrolyte or the RTIL has been proposed as a possible strategy to achieve a synergistic effect on ionic conductivity. Alternatively, sintered nanostructured ceramic conductor networks can enhance the contribution of the ceramic electrolyte to the composite transport properties, compared to the simple dispersion of the ion-conductive particles.[229–231] Martínez-Cisnero et al. successfully developed hybrid quasi-solid sodium conducting electrolytes by integrating porous NASICON layers with ionic liquids. Their primary goal was to create electrolytes with improved room temperature conductivity, utilizing porous ceramic electrolyte layers infused with ionic liquids. This approach resulted in various microstructures and porous morphologies, leading to a significant enhancement in conductivity (ranging from 0.45 to 0.96×10^{-3} S cm^{-1} at 30 °C) for the infiltrated samples compared to pore-free samples.[232] These findings suggest that the porous NASICON material can be used as a functional macroporous inorganic separator.

High cost is still one of the main drawbacks of RTILs, which could be overcome by new synthetic methods[233] and production at scale, similarly to the case of FSI-based alkali metal salts.[234] Employing lower energy consumption processes and implementing recycling methods for RTILs may emerge as viable alternatives essential for reducing the overall cost and mitigating environmental challenges associated with the synthesis of RTILs.

7. Polymer Electrolytes: the Current Challenge

Conventional NIBs, employing organic liquid electrolytes akin to commercial LIBs, likely encounter safety concerns stemming from the propensity for leakage and flammability inherent in the organic phase.[246] Polymer electrolytes (PEs) offer a prospective solution to alleviate these challenges and foster the development of high-energy-density electrical devices. Moreover, they afford ease of processing, flexibility, softness, and enhanced resilience to vibrational forces, stress, and mechanical deformation.[247] PEs can be prepared by introducing metal salts into a solid polymer host. Since the host polymer represents the matrix where ions move, it must be able to form complexes with salt Na^+ cations. Amongst others, the following key factors are chiefly required for the formation of these complexes: i) high concentration of sequential polar solvating groups (—O—, —NH—, —CN, etc.), ii) elevated donor number and polarizability of the solvating groups that should have a high dielectric constant to facilitate salt dissociation, iii) low lattice energy of the salt, and iv) low lattice energy of the polymer. The solvation ability of the polymer chains depends upon the number of repetitive units (e.g., the cation solvation in $CH_3O(CH_2CH_2O)_nCH_3$ is better with higher n values). A plenitude of polymers have been investigated for their prospective application as PEs. Examples include poly(ethylene oxide) (PEO), poly(acrylonitrile) (PAN), polyvinyl alcohol (PVA), poly(vinyl pyrrolidone) (PVP), poly(methylmethacrylate) (PMMA), poly(vinylchloride) (PVC), poly(vinylidene difluoride) (PVDF), poly(vinylidene fluoride hexafluoropropylene) (PVDF–HFP), along with several others. Here, we point at providing an overview of the latest advancements in PEs for NIBs. In the context provided, the PEs utilized in NIBs are classified into two main groups: the first category encompasses solid (dry) polymer electrolytes (SPEs) where only sodium salts are dissolved within polymer matrices, and the second category consists of hybrid polymer-based electrolytes, which includes composite polymer electrolytes (CPEs) and quasi-solid-state electrolytes or gel polymer electrolytes (GPEs).

7.1. Truly (Dry) Solid Polymer Electrolytes

SPEs offer several benefits over inorganic solid electrolytes, including elasticity, pliability, adaptability to promote intimate contact between the electrolyte and electrodes, thus enhanced materials utilization, and simplified manufacturing processes. Consequently, SPEs are considered highly promising candidates for next-generation solid-state battery applications.[100] In this section, the current advancements in SPE for NIBs are summarized in **Table 5**.

Based on NMR studies conducted above the T_g by Berthier et al.,[248] the transport mechanism was ascribed to the amorphous phase region in the polymer, where the local segmental motion of the polymer chains facilitates ionic conduction. In the elastomeric region, the polymer chains have fast internal modes in which bond rotations cause segmental motion. As a result, although the viscosity is very high at the macroscopic level, the local relaxation processes at the microscopic level can be seen as liquid-like, where the degrees of freedom are comparable to the molecular liquid situation. For these reasons, PEO has been one of the most studied polymer matrices in the battery field. In this respect, Souquet et al. suggested an elegant model for PEO in which ionic transport occurs along the ordered helix that this polymer forms upon the complexation of the salt.[249]

As ion transport was considered to occur only in the amorphous region, the research community investigated only polymers having a low T_g, to improve ionic conductivity at the standard cell operating temperature. However, Bruce et al.,[250] later demonstrated the ionic conductivity in a crystalline polymer, first with PEO_6:$LiXF_6$ (where X = As, P, Sb) and then for other alkali metals, such as Na and K. These studies revealed that ions transport could occur above the T_g as well, by ion hopping mechanism taking place along fixed pathways in the crystal lattice (**Figure 8a**). The crystalline polymer electrolyte PEO_8:$NaAsF_6$, containing methoxy-terminated PEO with an average molar mass of 1000 Da and a sodium salt, showed a conductivity of 5×10^{-6} S cm^{-1} at 25 °C. Remarkably, this value is 1.5 orders of magnitude higher than the corresponding electrolyte based on a lithium salt, i.e., PEO_6:$LiAsF_6$. This study also suggested that it was possible to raise the conductivity in the

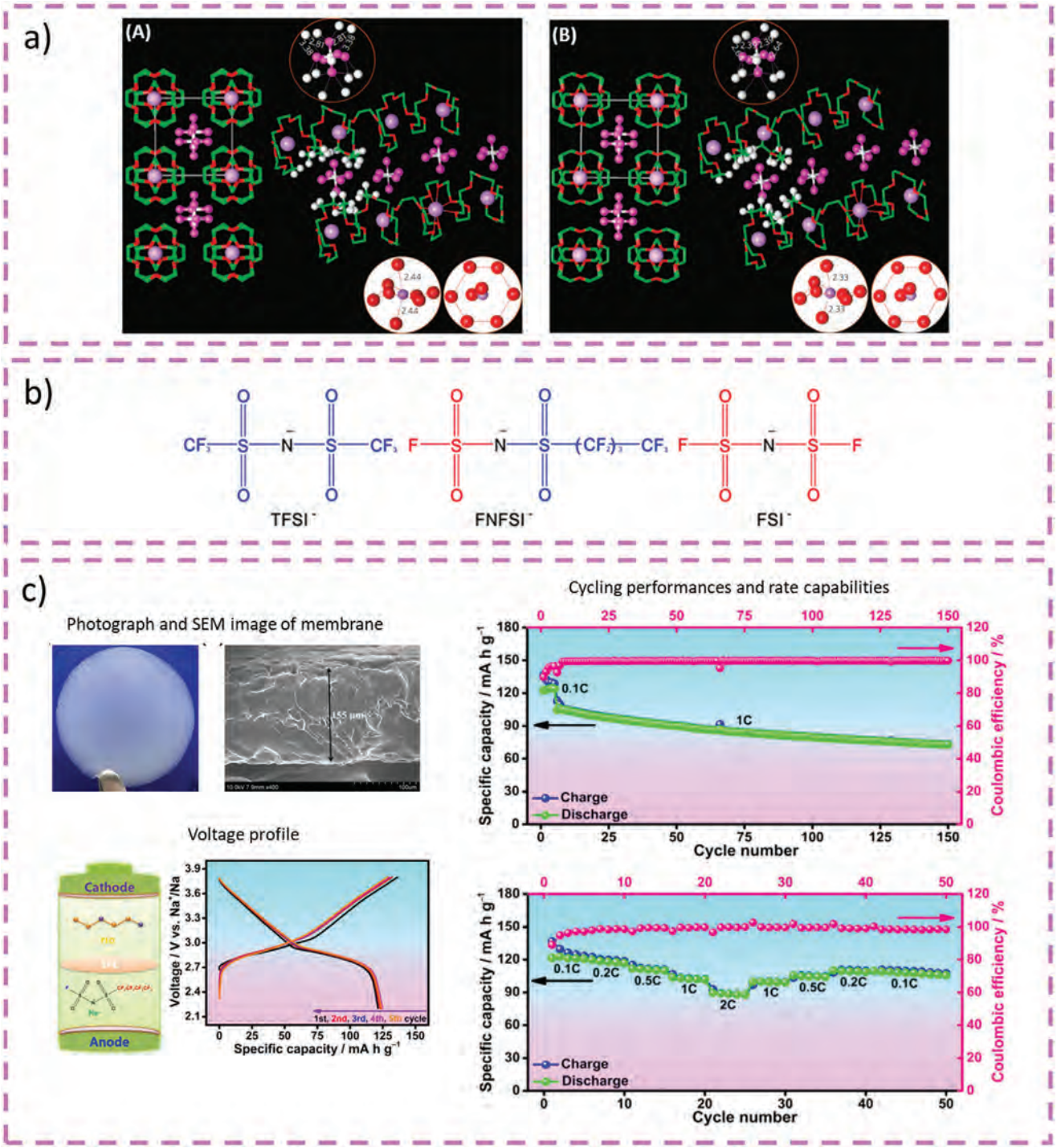

Figure 8. a) Structure of PEO8:$NaAsF_6$, from the single-crystal data collected at 25 °C (A) and −180 °C (B). Left: view of the complete structure (hydrogens are not shown). Right: fragment of the structure showing neighboring tunnels with dedicated anions (only hydrogens closest to the leftmost AsF_6^- anion are shown). The circular insets show the immediate environment of the anion and the cation, with the numbers indicating selected F–H and Na–O distances. Colors legend: purple = Na, red = O, green = C, magenta = F, white small circle = As, white large circle = H. Adapted with permission.[250] Copyright 2009, Springer Nature. **b)** Chemical structures of $TFSI^-$, $FNFSI^-$ and FSI^- anions used in Na-based SPEs. Adapted with permission.[266] Copyright 2017, American Chemical Society. **c)** The photograph and SEM image for the membrane of the NaFNFSI/PEO (EO/Na^+ = 15) blended polymer electrolyte, Electrochemical performances of the Na/SPE/$NaCu_{1/9}Ni_{2/9}Fe_{1/3}Mn_{1/3}O_2$ cell with NaFNFSI/PEO (EO/Na^+ = 15) blended polymer electrolyte at 80 °C. Adapted with permission.[265] Copyright 2017, The Royal Society of Chemistry.

Table 5. The electrochemical performance of laboratory-scale sodium-ion battery cells assembled with SPE and CPE.

Composition	Na salt	Cell system	Ionic conductivity [S cm^{-1}]	De-sodiation capacity [C-rate, T] [mAh g^{-1}]	Capacity retention [C-rate, cycle #, T] [%]	References
PEO	NaFSI	NNM || Na	4.1×10^{-4} at 80 °C	≈70 (0.2C, 80 °C)	≈95 (0.2C, 50, 80 °C)	[262]
PEO	NaFNFSI	$NaCu_{1/9}Ni_{2/9}Fe_{1/3}Mn_{1/3}O_2$ || Na	3.36×10^{-4} at 80 °C	122.4 (0.1C, 80 °C) 89.7 (2C, 80 °C)	≈70 (1C, 150, 80 °C)	[265]
PEO/Na-CMC)	$NaClO_4$	$NaFePO_4$ || Na	1×10^{-3} at 60 °C	≈90 (0.2C, 60 °C)	≈90 (0.2C, 20, 60 °C)	[270]
PTMC	NaTFSI	PB || Na	10^{-6} at 60 °C	≈120 (0.1C, 60 °C)	≈81 (0.1C, 8, 60 °C)	[276]
PCL–PTMC	NaFSI	PB || HC	2.23×10^{-5} at 40 °C	≈80 (10 μAcm^{-2}, 22 °C)	≈44 (10 μAcm^{-2}, 125, 22 °C)	[277]
PEO/NZSP	NaTFSI	NVP || Na	2.8×10^{-3} at 80 °C	115.9 (0.1C, 80 °C)	≈100 (0.2C, 80, 80 °C)	[293]
PEO/NZSP	$NaClO_4$	$Na_2MnFe(CN)_6$ || Na	2.1×10^{-5} at 30 °C	109.3 (0.5C, 60 °C)	83 (0.5C, 300, 60 °C)	[294]
PEO/NZSP	NaTFSI	NVP || NVP	1.4×10^{-4} at 23 °C	41.2 (0.1C, 23 °C)	83.7 (0.1C, 100, 23 °C)	[299]
PEO/TiO_2	$NaClO_4$	$Na_{2/3}Co_{2/3}Mn_{1/3}O_2$ || Na	2.62×10^{-4} at 60 °C	≈49.2 (0.1C, 60 °C)	≈91.4 (0.1C, 25, 60 °C)	[300]
PEO-SN-/PAN- NZSP	$NaClO_4$	PB || Na	1.36×10^{-4} at 25 °C	124 (0.05C, 25 °C) 59 (1C, 25 °C)	83.3 (0.2C, 200, 25 °C)	[297]
PEO/PAN/NZSP		NVPF || Na	4.13×10^{-4} at 30 °C	116 (0.2C, 25 °C) 88 (5C, 25 °C)	81 (0.2C, 460, 25 °C)	[298]
PMA/PEG/α-Al_2O_3	$NaClO_4$	NVP || Na	1.46×10^{-4} at 70 °C	110 (0.1C, 70 °C) 85 (1C, 70 °C)	94.1 (0.5C, 350, 70 °C)	[301]
β-CD/PMMA-*b*-PPEGMA	$NaSO_3CF_3$	$NaNi_{1/3}Fe_{1/3}Mn_{1/3}O_2$ || Na	1.3×10^{-4} at 60 °C	102.4 (0.1C, 60 °C)	87.8 (0.1C, 80, 60 °C)	[302]

$Na_{0.67}Ni_{0.33}Mn_{0.67}O_2$ (NNM); NASICON-type $Na_3Zr_2Si_2PO_{12}$ (NZSP); $Na_3V_2(PO_4)_2F_3$ (NVPF).

crystalline phase by doping, modifying chain ends and EO/salt ratio.

As previously stated, PEO is one of the most popular polymer electrolytes for LIBs, which was already demonstrated in "real application" by Blue Solutions, part of the Bolloré Group, with its LMP technology, viz. a lithium metal polymer battery based on a LFP catholyte coupled with a Li metal anode and a dual solid polymer electrolyte chiefly based on PEO with dissolved lithium salt. Due to the crystalline nature of the polymer, a common salt-in-PEO electrolyte does not allow sufficient lithium ion conductivity at room temperature; indeed, the LMP cells are generally operated up to 80 °C. PEO is also widely studied for application in NIBs, thanks to its ability to make complexes and solvate ions. PEO is a solid, semi-crystalline polymer at room temperature, with ethylene oxide (C_2H_4O) as a repeating unit and with a molecular weight higher than 20 000 g mol^{-1}, as opposed to liquid poly(ethylene glycol) (PEG) the molecular weight of which is lower. The most common approach to prepare PEO-based electrolytes is by solvent casting in acetonitrile or methanol solvents.[251–255] As detailed in the following paragraphs, several sodium salts were used for electrolytes formulation, depending on the specific characteristics required.

The first reports on sodium-based SPEs date back to 1985 by West et al., who fabricated an all solid-state Na/PEO-NaI (10:1)/MoS_3 cell.[256] Later on, the use of $NaClO_4$ led to improved electrochemical performance.[257] PEO:$NaClO_4$ electrolytes displayed a conductivity that could reach 6.5×10^{-4} S cm^{-1} at 80 °C with a EO:Na^+ molar ratio of 12:1. This concentration was also tested in a Na/PEO:$NaClO_4$/α-V_2O_5 configuration, that showed a reasonably high cycling stability. However, the study revealed the formation of a corrosion layer on the sodium electrode during open circuit and cycling conditions.

In 1993, Doeff et al. overcame the corrosion problem mentioned above by using a $P(EO)_8$:$NaCF_3SO_3$ blend as both the electrolyte and the "active" electrode binder in full and half cells with $Na_{0.6}CoO_2$/$P(EO)_8$:$NaCF_3SO_3$/$Na_{15}Pb_4$ and Na configurations, respectively.[258,259] In fact, monitoring internal resistances with a four-probe electrode demonstrated that the PEO/Na interfacial resistance was stable and not affected by corrosion or other side-reactions. The cell displayed a reversible electrochemical insertion of Na^+ ions and was cycled for over 200 cycles at 90 °C with 50% capacity retention.

A few years later, Chandra et al. prepared PEO:$NaPF_6$ films with different EO/Na^+ ratios.[260] The highest room-temperature conductivity (i.e., 5×10^{-6} S cm^{-1} at room temperature and 1×10^{-3} S cm^{-1} at 80 °C) was reported for EO:Na^+ molar ratio of 15:1 (EO/Na^+ = 0.065). This study investigated the formation of polymer:salt complexes by optical microscopy, IR and XRD studies. Indeed, the addition of sodium salt decreased the amount of the PEO crystalline phase, also affecting transport properties. The sodium transport number in these electrolytes was around 0.45, which is relatively high compared to that of lithium salt $LiPF_6$ in PEO, usually comprised between 0.2 and 0.4. Zhang et al. synthesized PEO_n-$NaPF_6$ (where n = 10, 12, 14, 16, 18) SPEs using a traditional solution casting method, where "n" represents the molar ratio of EO to Na^+. The resulting SPEs exhibited a relatively high ionic conductivity of 6.3×10^{-4} S cm^{-1} at 80 °C, along with a sizeable Na^+ transference number of 0.58. Moreover, these electrolytes demonstrated adequate thermal stability up to 200 °C, making them suitable for use in solid-state NIBs.[261]

Research has been also focused on sodium bis(trifluoromethylsulfonyl)imide (NaTFSI or $NaNTf_2$) and sodium bis(fluorosulfonyl)imide (NaFSI) based SPEs.[262,263] These salts are promising because they guarantee good ionic

conductivity at low temperatures with a wide electrochemical stability window, up to 4.7 V vs Na^+/Na. In particular, Boschin et al. extensively studied ionic transport and inter-molecular interactions in PEO with different concentrations and found that NaTFSI salt leads to better ionic conductivity;[263] indeed, PEO_9:NaTFSI conductivity values were 1×10^{-5} and 2×10^{-4} S cm^{-1} at 25 and 80 °C, respectively. As observed in LIBs with LiX (X = TFSI or FSI) salts,[264] $TFSI^-$ anion tends to reduce PEO crystallinity and dissociate better from Na^+ cations, thus improving ionic transport. Despite these attributes, NaTFSI exhibited a relatively low corrosion potential (i.e., voltage < 4 V versus Na^+/Na) of the Al current collector, while NaFSI displayed lower interfacial resistances when tested in NIBs.[262] PEO_{20}:NaFSI cycled with good stability in cells employing $Na_{0.67}Ni_{0.33}Mn_{0.67}O_2$ (NNM) and NASICON $Na_3V_2(PO_4)_3$@C (NVP@C) cathode materials.

Corrosion and thermal stability were improved by using a combination of the latter two anions, $TFSI^-$ and FSI^-, that is $[(FSO_2)(n\text{-}C_4F_9SO_2)N]^-$ (abbreviated as $FNFSI^-$), for applications in LIBs and NIBs (see the chemical structures in Figure 8b).[265] The decomposition of these salts is assumed to form stable SEI films and thus improve their stability when in contact with metals.[266] Despite exhibiting no improvement in ionic conductivity, PEO_{15}:NaFNFSI SPEs had excellent anodic electrochemical stability (≈4.87 V versus Na^+/Na) and displayed good cycling and current-rate performances for the Na/SPE/$NaCu_{1/9}Ni_{2/9}Fe_{1/3}Mn_{1/3}O_2$ cell (Figure 8c).

Since fluorinated salts may negatively affect electrolyte safety, cost, and environmental friendliness, alternative fluorine-free options have also been considered. Sodium 4,5-dicyano-2-trifluoromethylimidazolate (NaTDI), sodium 4,5-dicyano-2 pentafluoroethylimidazolate (NaPDI), sodium pentacyanopropenide (NaPCPI), sodium 2,3,4,5-tetracyanopyrrolate (NaTCP), and sodium 2,4,5-tricyanoimidazolate (NaTIM) exhibited promising characteristics from an application standpoint, including good thermal stability, high electrolyte conductivities, and electrochemical stability higher than 4.5 V versus Na^+/Na.[267,268] Bitner-Michalska et al. in 2017[269] reported all-solid-state electrolytes with percyano-substituted organic salts NaPCPI, NaTCP, NaTIM and PEO. Liquid-like ionic conductivity of over 1 mS cm^{-1} for PEO_{16}:NaTCP above 70 °C and a wide electrochemical stability window (up to 5 V) were found. The remarkably high ionic conductivity was attributed to low cation-anion (Na^+-TCP^-) interaction energy, thus facilitating a more efficient charge transport. Additionally, anions (TCP^-) form larger tetrameric units through π–π stacking, effectively softening PEO and enhancing charge mobility.

Carboxymethyl cellulose (CMC) is an ionic ether derivative of cellulose synthesized from alkaline cellulose and chloroacetic acid through etherification. Typically utilized in its sodium salt form (Na-CMC), it finds widespread use across various industrial sectors. Na-CMC is preferred for its ability to enhance the mechanical stability of resultant films while preserving ionic mobility and the interfacial characteristics of electrodes/electrolytes. Furthermore, it exhibits favorable water solubility, cost-effectiveness, biodegradability, biocompatibility, and non-toxicity. To improve the mechanical properties of PEO-based electrolytes, Colò et al. firstly demonstrated the possibility of using sodium carboxymethyl cellulose (Na-CMC) without hampering the ionic conductivity and thermal stability.[270] The optimal PEO:$NaClO_4$:Na-CMC blend composition was 82:9:9 by weight. At the same time, Na-CMC as a binder improved the interface between the electrode and electrolyte and displayed a lower charge transfer resistance than bare PEO electrolyte. The obtained SPE showed an ionic conductivity of 4×10^{-7} S cm^{-1} at 25 °C, but values above PEO melting temperature at 60 °C, around 10^{-3} S cm^{-1}, proved to be sufficient for good operation in Na/SPE/TiO_2 and Na/SPE/$NaFePO_4$ laboratory-scale cells.

SPE with controlled network structure were designed by Zheng et al., who polymerized octakis(3-glycidyloxypropyldimethylsiloxy) octasilsesquioxane (octa-POSS) and amine-terminated PEG in the presence of $NaClO_4$.[271] The goal of this recipe was to inhibit Na dendrites growth, and plating/stripping experiments demonstrated excellent stability of the SPEs (the symmetrical Na/Na cell was stably cycled for at 5150 h at 0.1 mA cm^{-2}). After having optimized the formulation to achieve a conductivity of 2.56×10^{-4} S cm^{-1} at 80 °C, SPEs were sandwiched between metallic Na and δ-$Na_xV_2O_5$ nanobelts: the initial capacity was over 300 mAh g^{-1} at 15 mA g^{-1} current and 80 °C.

Despite all the research efforts described in the previous paragraphs, polyether-based polymer electrolytes are still limited in performance for NIBs. Their low oxidation potential (generally ≤ 4.0 V) restricts the choice of positive electrode materials. Different polymeric host matrices have been investigated to overcome some of these limitations.

PAN is a polymer commonly used with liquid solvents in gel-polymer electrolytes. Osman et al. obtained an excellent ionic conductivity at room temperature of 7.1×10^{-4} S cm^{-1} for the solid PAN:$NaCF_3SO_3$ (containing 24 wt% of the salt), however, without reporting information on the electrochemical behavior of the proposed system in Na cells.[272]

Mindemark et al. developed different polycarbonate-based SPEs, such as the aliphatic polycarbonate poly(trimethylene carbonate) (PTMC), and also copolymers of trimethylene carbonate (TMC) and ε-caprolactone (CL), as polymer electrolytes for LIBs.[273–275] Subsequently, these matrices were employed for NIBs. Compared to PEO, they present a higher T_g, negatively affecting the cell performance for high-power applications. However, by properly combining plasticizing and cross-linkable moieties, the ionic conductivity can be significantly enhanced by lowering T_g values.

A fundamental choice in the preparation of PEs is the sodium salt. Brandell's group investigated the use of NaTFSI and $NaClO_4$ in combination with a PTMC polymeric host.[276] PE membranes were prepared by solvent casting, and the ionic conductivity was similar to the Li-based counterparts (10^{-6} and 10^{-8} S cm^{-1} at 60 and 25 °C, respectively). Since the best ionic conductivity was found for the sample based on $PTMC_3$:NaTFSI, this electrolyte was used for assembly a Na-metal cell with Prussian blue as the working electrode, granting a high specific capacity of about 120 mAh g^{-1}, with limited polarization at C/10 and 60 °C. Later, the same research group investigated an innovative electrolyte system combining polyester-polycarbonate (PCL-PTMC) copolymers with NaFSI, which resulted in room temperature conductivity of 10^{-5} S cm^{-1} for 35 wt.% salt content and a cationic transference number of ca. 0.5 at 80 °C.[277]

PVP, a water-soluble polymer well known for its use as a binder in pharmaceutical tablets and as an adhesive in glue sticks and hot-melt adhesives, was proposed more than ten years ago in combination with sodium salts. Subba Reddy et al. studied 100 µm-thick polymer electrolytes based on PVP complexed with $NaClO_4$ (10-30 wt%) prepared by solution-cast technique.[278] DMF was chosen as the solvent, the preparation process took 10–12 h, and samples were vacuum-dried at 353 K. The activation energy values for the sodium ion transport in PVP, PVP:$NaClO_4$ (90:10), PVP:$NaClO_4$ (80:20) and PVP:$NaClO_4$ (70:30) were 0.72, 0.54, 0.38 and 0.26 eV, respectively. The observed lowering of activation energy values was correlated with the increased amorphous nature of the SPEs for elevated salt concentration, thus facilitating the Na^+ ions motion in the polymer network. The transference number of Na^+ was evaluated to be around 0.27, implying a higher mobility of the anions (ClO_4^-). Electrochemical cells Na/(PVP:$NaClO_4$)/V_2O_5, with a V_2O_5 xerogel electrode modified with PVP, were fabricated, and their discharge profiles were studied. The discharge capacity of the modified xerogel film is lower than that of the unmodified counterpart, i.e., 186 versus 125 mAh g^{-1}, respectively.

A new solid polymer electrolyte has been created by combining the polymers PEO and PVP with $NaNO_3$ through the conventional solution-casting method. The authors assessed changes in the mobility, viscosity, and diffusion coefficient of charge carriers with varying salt concentrations (**Figure 9**a,b). The blend polymer matrix with salt ratio O/Na = 14 showed the highest ionic conductivity of 2.92×10^{-5} S cm^{-1} at RT.[279] To delve deeper into the current system, they investigated ion-ion interactions by examining the infrared (IR) active anion vibration mode (NO_3^-), whereas the cation (Na^+) remains IR inactive (Figure 9c).

PVA, a polymer with a carbon chain backbone with hydroxyl groups attached to methane carbons, is another possible choice for SPEs. Hydroxyl groups characterize PVA as a source of hydrogen bonding, able to assist the formation of polymer blends and high tensile strength: these features justify its wide use for supercapacitors, solar cells and batteries.[280–287] Duraikkan and colleagues fabricated blend electrolytes utilizing PVA and PVP mixed with $NaNO_3$ via the solution casting technique. Remarkably, the blend containing 50% PVA, 50% PVP, and 2 wt% $NaNO_3$ exhibited the highest conductivity, reaching 1.25×10^{-5} S cm^{-1} at room temperature.[288] As a general analysis, SPEs show several advantages over inorganic counterparts, such as lightweight, low cost, improved mechanical flexibility, ease of fabrication process, and tolerance towards electrode volume changes during charge/discharge. Thus, various polymer frameworks have been explored in the development of SPEs. Despite these efforts, none have demonstrated ionic conductivity at a practical level exceeding 10^{-4} S cm^{-1}.

7.2. Hybrid Polymer-Based Electrolytes

Truly solid PEs maintain rather limited ionic conductivity, while inorganic ones exhibit limited mechanical properties and processability, and are difficult to integrate into large-scale battery production processes.[289] Most of the existing research aimed at enhancing the ionic conductivity of SPEs focuses on maximizing their amorphous nature. However, despite these efforts, their ionic conductivity remains below 10^{-4} S cm^{-1} at room temperature, the sodium transference number hardly approaches 0.5, and their mechanical stability is poor above the melting temperature.[290] For addressing these shortcomings of SPEs, numerous strategies have been investigated. One strategy involves the utilization of inorganic fillers, which prove advantageous by promoting enhanced amorphous characteristics within the polymer chains. Additionally, ion-conductive inorganic materials may be employed as substitutes for inorganic fillers aiming at further enhancing ionic conductivity. Furthermore, supplementary components such as metal–organic frameworks (MOFs) have been integrated into PEs. Collectively, these variations are referred to as composite polymer electrolytes (CPEs). Another approach entails the adoption of organic liquid electrolytes, which can be introduced to generate quasi-solid-state electrolytes or gel polymer electrolytes (GPEs).[291]

7.2.1. Composite Polymer Electrolytes

Among the strategies mentioned in the previous paragraph, considerable research efforts aimed at demonstrating that incorporating inorganic fillers into SPEs to form CPEs is an effective approach for comprehensively enhancing various electrolyte properties. Typically, these inorganic fillers are classified into two main groups: active and passive fillers, contingent upon their possession of intrinsic ion conductivity. Active fillers include diverse types of inorganic solid electrolytes, such as NASICON (sodium super ionic conductor)-type. On the other hand, passive fillers typically lack inherent ion conductivity and commonly comprise oxide ceramics, including Al_2O_3, SiO_2, and TiO_2, etc.

Active fillers denote ceramics containing Na^+ ions, which possess the capability to enhance both the physical and electrochemical properties of the host polymer. $Na_3Zr_2Si_2PO_{12}$, $Na_3Zr_{1.8}Mg_{0.2}Si_2PO_{12}$, and $Na_2Zn_2TeO_6$ are commonly utilized as active inorganic fillers due to their high ionic conductivity, rigidity, and wide electrochemical stability window. The intrinsic bulk ionic conductivity arises from continuous defects, resulting in low activation energy for multiple ions hopping rather than single ion movement. These active fillers play a vital role in facilitating ion migration and conductivity in CPEs, offering numerous pathways for ion transport.[292] In this section, the current advancements in CPE for NIBs are summarized in Table **5**.

Zhang et al. introduced a flexible CPE comprising NASICON-structured $Na_{3.4}Zr_{1.8}Mg_{0.2}Si_2PO_{12}$ (50 wt %) and NaTFSI-PEO through a solution cast method. Remarkably, this electrolyte demonstrated a high ionic conductivity of 2.8×10^{-3} S cm^{-1} at 80 °C, while additionally exhibiting favorable thermal and electrochemical stabilities. Furthermore, when incorporated into NVP/CPE/Na solid-state cells, this CPE exhibited high reversible capacity and maintained excellent capacity retention at 80 °C.[293] Yu et al. presented the fabrication of a CPE comprising a PEO matrix, $NaClO_4$ salt, and a ceramic Na^+-ion conductor ($Na_3Zr_2Si_2PO_{12}$, 25 wt %) dispersed within, using a straightforward slurry-casting method. The resulting CPE exhibited enhanced Na^+-ion conductivity (2.1×10^{-5} S cm^{-1} at 30 °C), improved dendrite suppression, reduced interfacial issues, and good elasticity. Utilizing the CPE, all-solid-state batteries

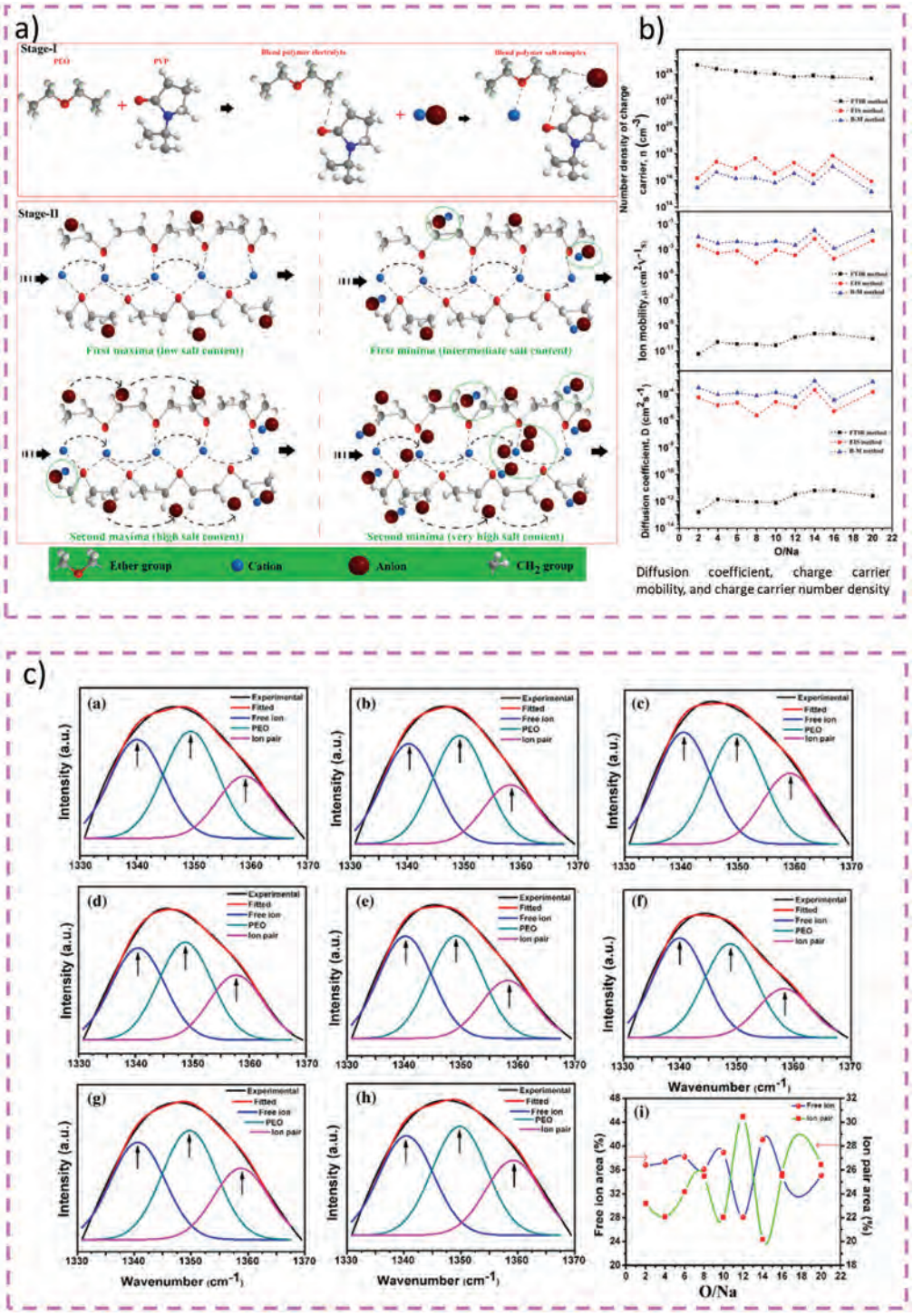

Figure 9. a) Schematic representation of proposed ion-transport mechanism in the solid polymer electrolyte. b) the diffusion coefficient, charge carrier mobility, and charge carrier number density at different $NaNO_3$ salt concentrations (O/Na) within the PEO/PVP/$NaNO_3$ electrolyte system using three distinct methods: FTIR, EIS, and B-M techniques. **c)** Deconvolution of the NO_3^- vibration mode for PEO/PVP/$NaNO_3$ (O = Na^+) a) 2, b) 4, c) 6, d) 8, e) 10, f) 14, g) 16, h) 20, and f) variation of fraction of free anion and fraction of ion pair against salt content. Adapted with permission.[279] Copyright 2019, Springer Nature.

featuring a sodium-metal anode and a $Na_2MnFe(CN)_6$ cathode demonstrated stable long-term cycling performance.[294] Hiraoka et al. developed a flexible and self-supporting polyether-based CPE with a 30 wt% $Na_3Zr_2Si_2PO_{12}$, which achieved an ionic conductivity of 1.03×10^{-5} S cm^{-1} at 25 °C.[295]

CPEs comprising more than 50 vol% of inorganic particles are categorized as inorganic-rich CPEs. The likelihood of these inorganic particles forming a three-dimensional percolation network is considerably high, contingent upon various factors including particle size and distribution. Should such a percolation network be established, an additional pathway for Na^+ ions through interconnections within the inorganic conductor becomes available. Conversely, for polymer-rich CPEs where the inorganic content is less than 50 vol%, the probability of pathways through inorganic particles is notably low. In a broader context, the movement of Na^+ ions within these CPEs can occur through multiple avenues, including: i) pathways formed by a combination of polymer electrolyte and inorganic particles, ii) migration along the boundaries between polymer and inorganic particles, iii) exclusively through the polymer electrolyte phase in polymer-rich hybrids, and iv) solely through the inorganic electrolyte phase in inorganic-rich hybrids.[292] Lim et al. presented a study employing a methodology for fabricating a polymer-in-ceramic electrolyte. Initially, a NASICON solid electrolyte was sintered to establish ion transport channels. Subsequently, the as-sintered electrolyte was impregnated with epoxy polymer, resulting in the development of epoxy-NASICON CPE. This hybrid material exhibited a doubling of physical strength while maintaining consistent thermal and electrochemical performance (**Figure 10a**).[296]

A laminated by-layer composite electrolyte was created by Yu et al., consisting of an anodic-friendly PEO-SN-$NaClO_4$ layer and a cathodic-friendly PAN-$Na_3Zr_2Si_2PO_{12}$-$NaClO_4$ layer. This composite provided a Na^+-ion conductivity of 1.36×10^{-4} S cm^{-1} at RT, and it had an electrochemical window spanning from 0 to 4.8 V versus Na^+/Na. The laminated solid electrolyte, together with a Na-metal negative electrode and a $Na_2MnFe(CN)_6$ positive electrode, demonstrated remarkable cycling stability at RT (Figure 10b).[297] In a similar fashion, a sandwiched NASICON framework comprising a PAN layer, designed to be stable in oxidation, and a PEO layer designed to be stable in reduction, was proposed by Ran et al. The PEO layer on the negative side helps in preventing decomposition, allowing the realization of a CPE with a wide electrochemical window of up to 5.0 V. This solid composite electrolyte with $Na_3V_2(PO_4)_2F_3$ demonstrated an excellent rate performance with a long cycle life (Figure 10c).[298] Wang et al. developed a CPE by combining PEO and NaTFSI, along with a nanostructured framework of NASICON-type $Na_3Zr_2Si_2PO_{12}$ (NZSP). This innovative approach provided enhanced ionic conductivity (1.4×10^{-4} S cm^{-1} at 25 °C) and improved mechanical strength, particularly by employing filler particles.[299]

Passive fillers, referred to the Na^+ free ceramics, have been also widely utilized in NIBs to modify the chemical and physical properties of SPEs, albeit at the expense of their reduced crystallinity and glass transition temperature. The conductivity of PEO:$NaClO_4$-based PEs was improved by Ni'Mah et al., who introduced nanosized TiO_2 fillers (3-4 nm, 5 wt%) and achieved 2.62×10^{-4} S cm^{-1} at 60 °C.[300] The Na/SPE/$Na_{2/3}Co_{2/3}Mn_{1/3}O_2$ half-cell showed a discharge capacity of 49.2 mAh g^{-1}, half compared to that of the liquid counterpart; mainly ascribed to the elevated thickness (≈0.18 mm) of the solid electrolyte.

Poly(methacrylate) -PMA is another suitable matrix for PEs, as demonstrated by Zhang et al.,[301] Their CPE consisted of PMA, PEG, α-Al_2O_3 with acidic surface sites and $NaClO_4$, and exhibited reasonably high conductivity (1.46×10^{-4} S cm^{-1} at 70 °C), wide ESW (4.5 V versus Na^+/Na) and good mechanical strength. The TGA results indicated no mass loss before 250 °C, highlighting outstanding thermal stability. When tested with a $Na_3V_2(PO_4)_3$ cathode, the all-solid-state sodium ion cells showed good cycling performance, with a reversible capacity of 85 mAh g^{-1} when operated at 0.5C and 94.1% capacity retention after 350 cycles at 70 °C.

Natural macrocyclic compounds can represent a possible alternative to PEO-based polymer networks. For example, Chen et al. synthesized a star-like hyperbranched polymer by grafting β-cyclodextrin (β-CD) with multiple oligo(methyl methacrylate)-*block*-oligo(ethylene glycol) methyl ether methacrylate (PMMA-b-PPEGMA) short chains via atom transfer radical polymerization (ATRP).[302] This architecture presented several advantages: i) as a star-like hyperbranched polymer, it had many short oligomeric chains radiating from the core and an amorphous phase structure, favouring the ionic conduction; ii) it had 7 glucose units head-to-end linked into a ring through oxygen atoms; iii) β-CD had an inner cavity structure providing additional free-volume for the movement of the polymeric segments. A conductivity of 1.3×10^{-4} S cm^{-1} at 60 °C and a ESW of 5.2 V versus Na^+/Na were obtained. Moreover, the hybrid SPE formed a stable, protective interfacial layer on the surface of the Na metal electrode. Na/SPE/$NaNi_{1/3}Fe_{1/3}Mn_{1/3}O_2$ half-cells were cycled at 60 °C for over 80 cycles, exhibiting a capacity retention of 87.8% (88.9 mAh g^{-1}).

Despite the considerable research efforts invested, scientists continue to encounter practical limitations in the utilization of CPEs in NIBs. New paradigms and endeavors are imperative to bridge the disparity between experimental findings and commercial viability. One of the primary challenges that persist is the low ionic conductivity, which impedes achieving performance levels comparable to highly conductive liquid electrolytes.

7.2.2. Quasi-Solid-State Electrolytes (Gel) -Polymer Electrolytes: A Compromise Between Performances and Processability

Compared to SPEs, GPEs are generally characterized by a higher ionic conductivity due to the enhanced ionic mobility guaranteed by the liquid electrolyte solution trapped in (usually) a polymer matrix. The salt and organic solvent can be selected from the common Na salts and solvents used in liquid electrolytes. The solvent acts as a plasticizer, and its addition results in the swelling of the polymer matrix, the physical aspect of which changes from a solid to a gel. The gelling of the membrane facilitates the interfacial interaction with the solid electrodes, generally guaranteeing better performance than SPEs. The most common polymers used to prepare GPEs are PAN,[303–305] PMMA,[306–308] PVC,[309] and PVDF.[310] The current advancements in GPE for NIBs are summarized in **Table 6**.

The room temperature ionic conductivity of GPEs generally ranges from 10^{-4} to 10^{-3} S cm^{-1}. Polymers with an amorphous

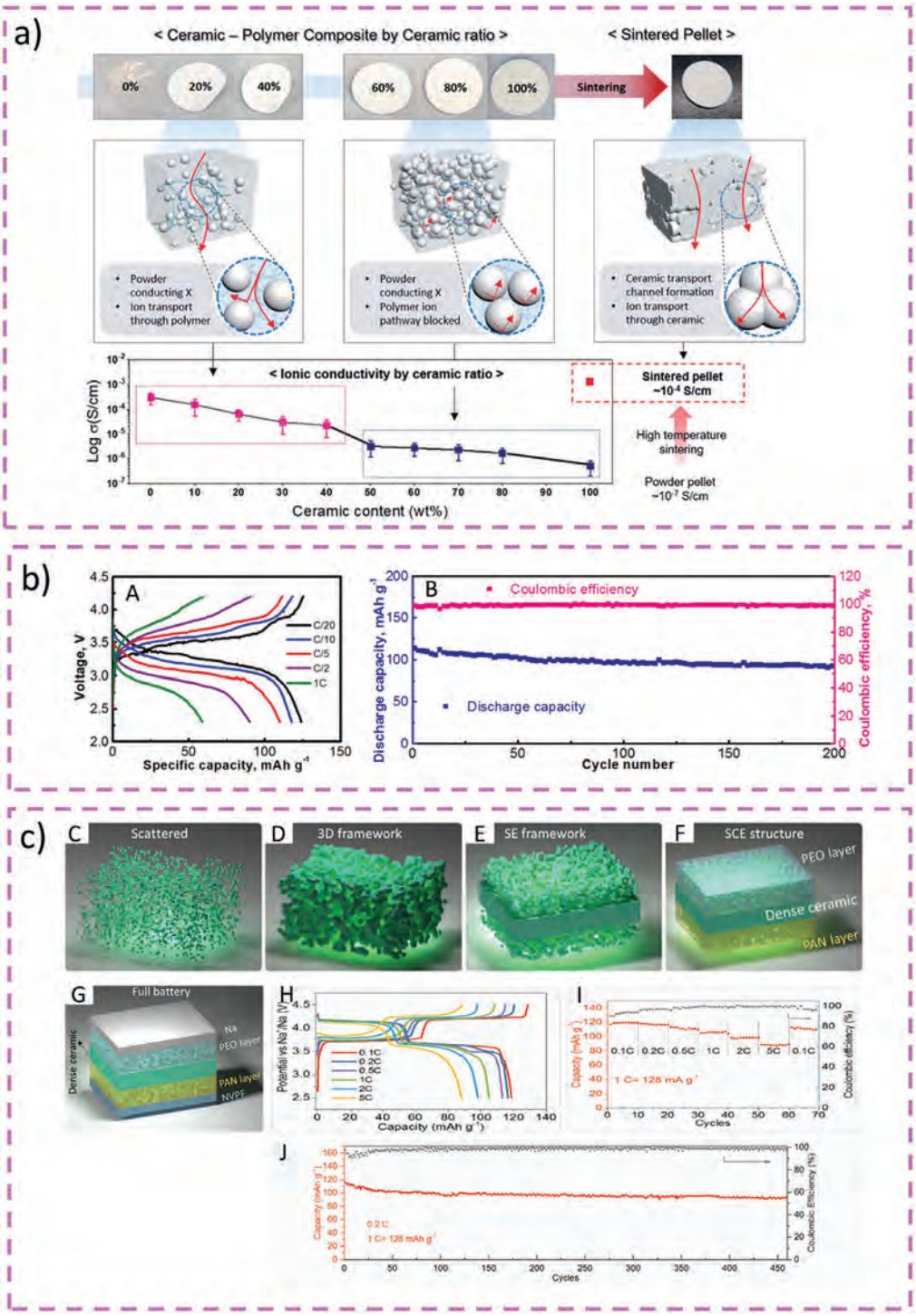

Figure 10. a) Assessing the impact of varying ceramic ratios on ionic conductivity within a ceramic-polymer composite state. Adapted with permission.[296] Copyright 2020, The Royal Society of Chemistry. b) E versus Q galvanostatic profiles at various C-rates (A) and cycling performance (B) of Na || PEO-SN-$NaClO_4$/PAN-$Na_3Zr_2Si_2PO_{12}$-$NaClO_4$ || PB cells at RT. Adapted with permission.[297] Copyright 2020, John Wiley and Sons. c) Schematic representation of scattered fillers, 3D framework, solid electrolyte framework, and CPE structure; Schematic representation of the solid-state NIB combining NVPF with PAN/PEO/NASICON CPE (C-G), E versus Q galvanostatic profiles at various C-rates (H), rate capability (I), cycling performance (J). Adapted with permission.[298] Copyright 2021, Elsevier.

Table 6. The electrochemical performance of laboratory-scale sodium-ion battery cells assembled with GPEs.

GPE Composition	Plasticizers	Cell system	Ionic conductivity [S cm^{-1}]	De-sodiation capacity [mAh g^{-1}] @C-rate/current density	Capacity retention [%] (C-rate, cycle #)	References
PVDF-HFP	$NaClO_4$/PC/FEC	NVPOF@FCC||FCC	–	111 (@1C) 74.1 (@10C)	~89.7 (1C, 1000) 78.14 (10C, 1000)	[336]
PVDF-HFP/Al_2O_3	$NaPF_6$/EC-DMC-EMC	graphite || Sn	1.3×10^{-3} at 25 °C	96.8 (@5C)	97.5 (5C, 600)	[337]
PVDF-HFP/GF	$NaClO_4$/PC	$Na_2MnFe(CN)_6$ || Na	4.6×10^{-3} at 25 °C	~120 (@1C)	84.1 (1C, 100)	[320]
PVDF-HFP/GO	$NaClO_4$/EC+PC	NVP || Na	2.3×10^{-3} at 25 °C	107 (@1C) 87 (@5C)	93.5 (1C, 1100)	[338]
PVDF-HFP/NASICON	$NaClO_4$/(EC+DMC)	NVP/C || Na	2.2×10^{-3} at 25 °C	98 (@0.2C)	85 (0.5 C, 175)	[323]
PVDF-HFP/PBMA/hydroxyapatite	$NaClO_4$/EC+PC	NVP/C || Na	1.1×10^{-3} at 25 °C	136 (@0.1 C) 117 (@1C)	71.7 (1 C, 500)	[327]
PVDF-HFP/PEO/PMMA/SiO_2	$NaPF_6$/PC	NVP || Na	0.88×10^{-3} at 25 °C	106.7 (@0.1 $mAcm^{-2}$) 101.5 (@1 $mAcm^{-2}$)	93 (0.1 $mAcm^{-2}$, 100)	[324]
PVDF-HFP/PMMA/β-alumina nanoparticles	$NaClO_4$/EC+DMC	NVP || Na	2.4×10^{-3} at 25 °C	94.1 (@0.5 C)	85 (0.5 C, 300)	[325]
PVDF	$NaPF_6$/EC+ PC	$Na_{0.66}Fe_{0.5}Mn_{0.5}O_2$ || Na	1.1×10^{-3} at 25 °C	118.49 (@0.1 C)	~85 (0.1 C, 30)	[329]
PEO/PMMA/phosphonate	$NaClO_4$/EC+PC+FEC	NVP || Na	6.3×10^{-3} at 25 °C	110.7 (@1C)	81.8 (5C, 4500) 69.2 (5C, 10 000)	[326]
PAN	$NaClO_4$/EC+PC+DME	PI/MWCNT || Na	3.0×10^{-3} at 25 °C	~100 (@5C) 98.3 (@10C)	84 (5C, 3000)	[330]
PEO (XPE)	$NaClO_4$+PC	TiO_2 || Na	1×10^{-3} at 25 °C	≈250 (0.04C, 25 °C) ≈100 (0.2C, 25 °C)	≈60 (0.2C, 1000, 25 °C)	[334]

$[Ni_{0.60}Mn_{0.35}Co_{0.05}]O_2$ (Na-NMC); Glass fiber (GF); Graphene oxide (GO); $Na_3V_2(PO_4)_3$ (NVP); solvate ionic liquid (SIL); polyimide/multiwalled carbon nanotube nanocomposite (PIMWCNT); PEO-based crosslinked polymer electrolyte (XPE).

character like PMMA provide high ionic conductivities, but their mechanical properties are usually poor due to the lack of rigidity in their matrix. PAN and PVDF provide good mechanical properties due to a high degree of crystallinity, but this also implies reduced ionic mobility. The development of copolymers, such as poly(vinylidene fluoride hexafluoropropylene) (PVDF–HFP),[311,312] can help in overcoming the loss of mechanical properties while keeping a sufficient ionic conductivity.[313–317] The presence of CF_3 groups in the HFP monomer increases the amorphocity of the copolymer compared to PVDF, which is more prone to crystallization. Thus, PVDF–HFP is one of the most popular and widely used polymer hosts in GPE systems. The higher ratio of the amorphous phase enhances the ionic conductivity of the pure PVDF-based GPE up to 7.5×10^{-3} S cm^{-1}, while the crystallinity provided by PVDF eases film cohesion and its processability.[318] However, PVDF-HFP suffers from poor interfacial characteristics when paired with Li or Na metal anodes, often forming undesirable side products. Researchers have undertaken various approaches to enhance electrolyte conduction and electrochemical properties, including the cross-linking of the polymer network and the inclusion of ceramic additives (**Figure 11**).

The strong interest in GPEs is reflected by the increasing number of research articles published in recent years, with the number of manuscripts having sodium-ion and GPEs in their keywords almost doubled. An original approach was designed by Kim et al., who developed structural GPEs in order to overcome the most typical issues of the conventional Glass Fiber (GF)/PVdF-HFP systems, i.e., the poor pathways for ion transfer because of unsuitable pore size.[319] Controllable pore generation and positioning were achieved via a nonsolvent-induced phase separation (NIPS) method (**Figure 12a**), leading to micropores generation ordered in a uniform pathway for Na^+ ions transfer. This structure was preserved even after liquid electrolyte injection for the formation of the GPE, and NIPS technique allowed the positioning of the porous polymeric film on the top of the GF surface, thus further strengthening the separator/electrode interfacial adhesion. In the first 100 cycles, pristine GF exhibited a 27.9% retention of discharge capacity, whereas the GF/GPE separator exhibited a 91.0% retention, with specific capacity decreasing from 296.2 to 269.4 mAh g^{-1}, also thanks to the decreased interfacial resistance associated with the SEI layer and charge transfer. In this research area, Goodenough and co-workers presented a hybrid GPE prepared by integrating PVDF-HFP with glass fiber paper, which acts as reinforcement.[320] The glass fiber tuned the mechanical and surface properties of the PVDF-HFP. The hybrid polymer matrix so conceived exhibited good mechanical strength and thermal stability up to 200 °C. The GPE was tested in a laboratory-scale sodium half-cell using $Na_2MnFe(CN)_6$ as cathode, obtaining an improvement of the rate capability, cycling performance, and Coulombic efficiency compared with a conventional glass fiber soaked in a liquid electrolyte. The strategy of using a fiber reinforcement on the classical PVDF-HFP copolymer was also used by Zhu et al.,[321] which employed polypropylene nonwoven (NW) as reinforcement. The NW/P(VDF-HFP) GPE gellified with $NaClO_4$ organic liquid electrolyte showed very

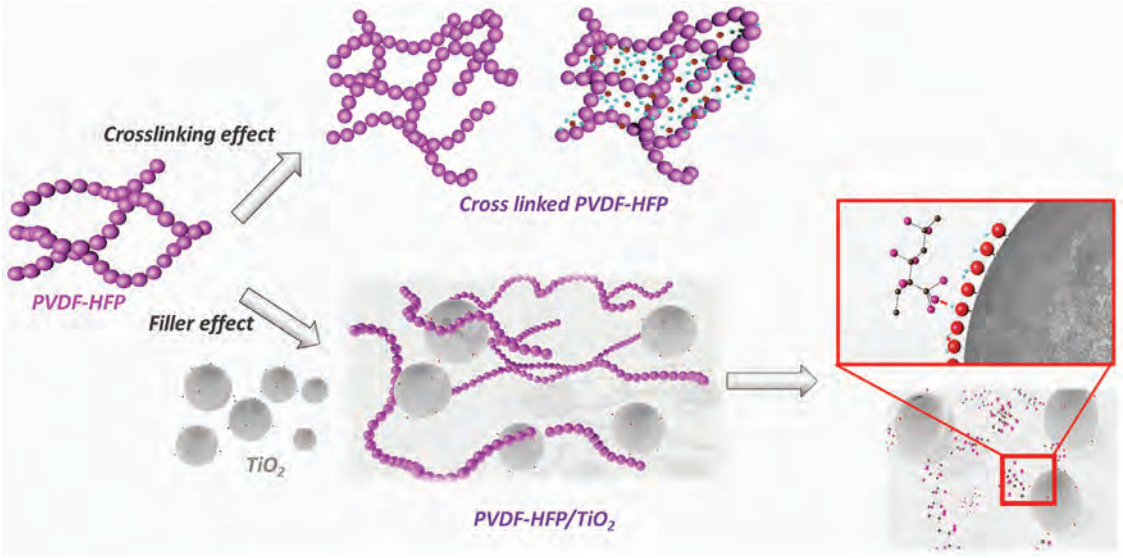

Figure 11. Schematic illustration of the polymer cross-linking and the inclusion of ceramic additives.

interesting Na^+ ion conduction at room temperature, actually four times higher compared to the conductivity of the commercial separator saturated with the same electrolyte. Electrochemical tests performed using coin cell configuration with $Na_4Mn_9O_{18}$ as cathode, Na as both the counter and the reference electrodes and NW/P(VDF-HFP) GPE as electrolyte gave promising insights on using this GPE in NIBs.

Moreover, in developing GPEs, researchers have used passive fillers such as SiO_2, TiO_2, ZrO_2, and $BaTiO_3$, but have also incorporated active fillers like, amongst others, NASICON-type ceramics and ionic liquids.[322] This approach combines the strengths of both inorganic ceramic electrolytes and organic polymer electrolytes, resulting in a composite GPE with simultaneously improved ionic conductivity, good mechanical properties, and high chemical/thermal stability. Incorporating ceramic particles or plasticizers can enhance the transference number; however, a substantial amount of ceramic filler may compromise the mechanical properties of the GPE.[102] Cheng et al. reported a straightforward solution casting method for PVDF-HFP polymer matrix combined with $Na_3Zr_2Si_2PO_{12}$ (NASICON) ceramic particles, then activated using a liquid electrolyte. The resulting hybrid polymer electrolyte demonstrates several positive characteristics, including good flexibility, a high ionic conductivity of 2.25×10^{-3} S cm^{-1} at room temperature, and excellent interface stability. The authors propose that the NASICON particles serve a dual role: they act as a physical barrier, inhibiting the growth of sodium dendrites, and simultaneously function as pathways facilitating the transfer of sodium ions.[323]

Shi et al. proposed a GPE based on a porous composite polymer membrane formed by blending of PEO, PMMA, PVDF-HFP (Figure 12b) and different nanosized oxide fillers (Al_2O_3, TiO_2, SiO_2).[324] Ceramic fillers promoted pore formation and the polymer chain's segmental motion, enhancing electrochemical properties. Liu et al. reported the synthesis of a GPE membrane using a blend of PVDF-HFP/PMMA, enriched with sodium-conductive β-alumina nanoparticles. The incorporation of these nanoparticles notably enhances the performance of the electrolyte membrane. This improvement is attributed to the reduction in crystallinity degree and the enhancement of Na-ion transference number, ultimately leading to increased ion mobility.[325]

A different polymeric matrix was proposed by Zheng et al., who designed a novel phosphonate-based porous cross-linked GPE (PEO/PMMA/phosphonate) by in situ thermal polymerization on a GF separator used to guarantee mechanical integrity.[326] The system showed a high conductivity of 6.29×10^{-3} S cm^{-1} and an excellent ESW of 4.9 V versus Na^+/Na. When cycled in half-cells with a $Na_3V_2(PO_4)_3$ cathode, it provided a capacity of 110.7 mAh g^{-1} at 1C. Moreover, the long-term cycling at 5C showed that the GPE retained 81.8 and 69.2% capacity after 4500 and 10 000 cycles, respectively, even outperforming the liquid electrolyte when measured at 60 °C. Vijaya Kumar Saroja et al. have focused on creating a gel polymer by incorporating hydroxyapatite, a calcium phosphate-based compound, into a blend membrane composed of PVDF-HFP and poly(butyl methacrylate) (PBMA). The resulting membrane exhibits a suitable ionic conductivity approaching 1.1×10^{-3} S cm^{-1}, ascribed to its good porosity and electrolyte uptake, and an electrochemical stability up to 4.9 V versus Na^+/Na.[327]

Another approach was published by Janakiraman et al., who prepared an electrospun fibrous membrane consisting of PVDF-HFP swelled by a solution of $NaClO_4$ 1 M in EC/DEC.[328] A high ionic conductivity of 1.13×10^{-3} S cm^{-1} was obtained at ambient temperature, outperforming the commercial Celgard membrane, with an ESW above 4.8 V versus Na^+/Na. The Na-metal/$NaNi_{0.5}Mn_{0.5}O_2$ cell tested employing the prepared electrolyte retained 97% of the initial capacity after 50 cycles at 0.1C rate. Successively, they reported an electrospun electroactive PVDF-based fibrous polymer electrolyte with a high ionic conductivity of 1.08×10^{-3} S cm^{-1} at room temperature and an electrochemical stability window of 5.0 V versus Na^+/Na.[329] Electrospinning was also employed by Manuel et al., who prepared a 3D fiber network PAN membrane demonstrating a high electrolyte uptake.[330] This electrolyte was used in combination

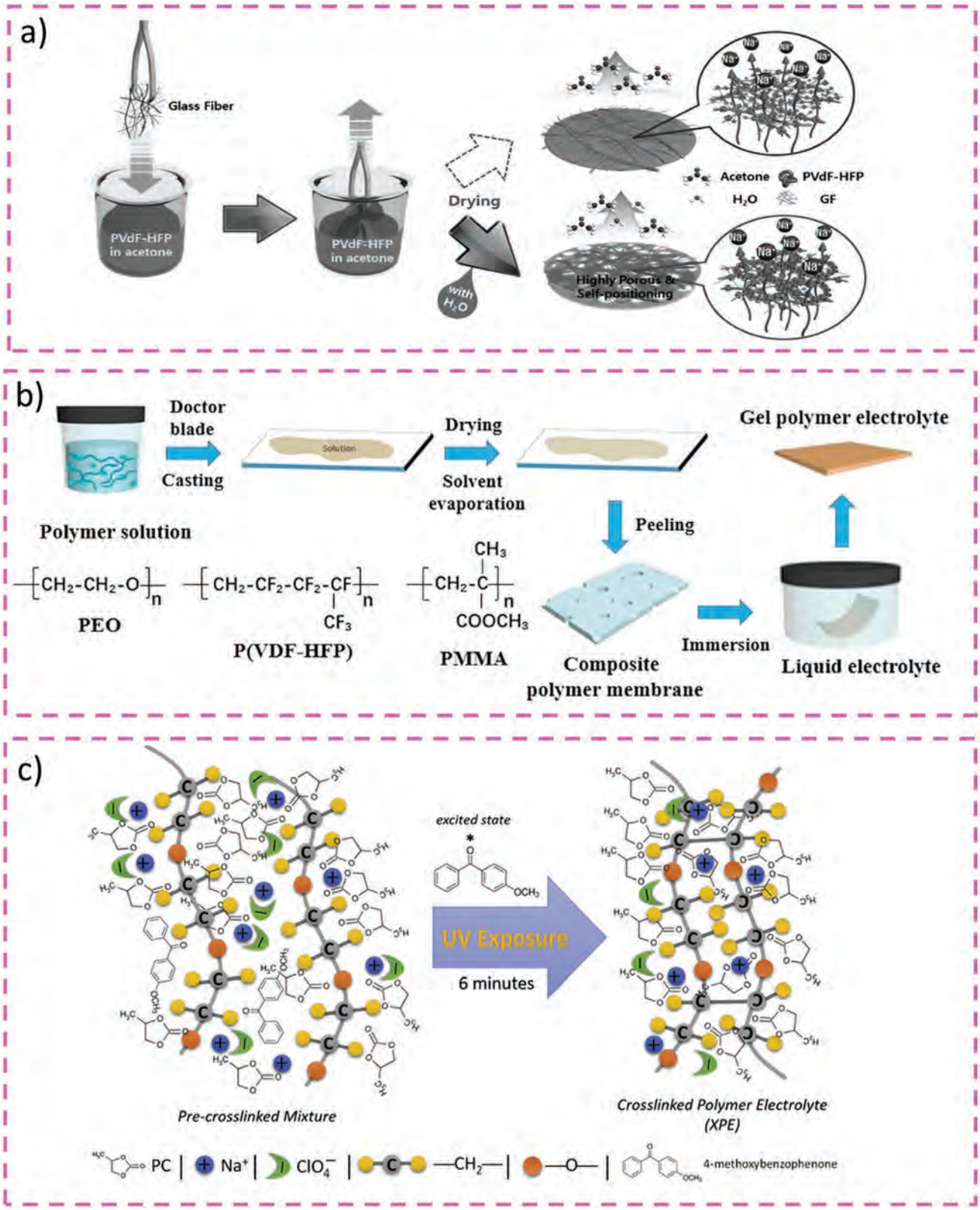

Figure 12. a) Schematic diagram of the NIPS-based fabrication method for a GF-based separator with a PVDF-HFP matrix. Adapted with permission.[319] Copyright 2017, John Wiley and Sons. b) Schematic illustration of the procedure for the preparation of the composite membrane. Adapted with permission.[324] Copyright 2018, Elsevier. **c)** Schematic representation of an expected reaction mechanism of light-induced crosslinking starting from $NaClO_4$:PC:PEO and a photoinitiator. Adapted with permission.[334] Copyright 2017, Elsevier.

with a polyimide/multiwalled carbon nanotube (PI/MWCNT) nanocomposite cathode material and employed in organic NIBs, leading to an ultralong life span of 3000 cycles and stable cycle performance at 5C rate. PAN was also used by Vignarooban et al. to fabricate a GPE including $NaClO_4$, EC and PC in the formulation (11PAN-12$NaClO_4$-40EC-37 PC, wt.%), obtaining a room temperature conductivity of 4.5×10^{-3} S cm^{-1}.[331] Thermo-gravimetric analysis revealed that the electrolyte was thermally stable up to 100 °C, which is sufficient for standard operating temperatures in battery cells. Gabryelczyk et al. presented a study on optimising sodium-ion conductive GPE composition by testing different polymer matrix-plasticizer combinations, and evaluating the compatibility of the selected GPEs with hard carbons, commonly used as anodes in sodium-ion batteries. The polymer matrix was composed of PAN and PMMA in different mass ratios, and the plasticizer was a blend of sulfolane and an imidazolium-based ionic liquid with either BF_4^- or NTf_2^- anions. They reported that, when utilizing this system in combination with a HC anode, the activation energy for the charge transfer process closely resembles that of Li-based chemistries.[332]

Gao et al. fabricated a NIB consisting of an antimony anode, a $Na_3V_2(PO_4)_3$ cathode and a GPE made of methyl methacrylate (MMA) and tetraethylene glycol dimethacrylate (TEGDMA) crosslinked by 2,2′-azobis(2-methylpropionitrile) (AIBN).[333] Two relatively hydrophilic monomers were used to be easily dissolved in a $NaClO_4$/PC/FEC solution; the mixture was then heated and drop-casted onto a porous cellulose membrane (0.1 mm thick). A transparent GPE was obtained, and the authors linked the transparency to the chemical compatibility between the GPE and the cellulose polysaccharide chains, causing the segregation of their bundles. The authors evaluated the electrochemical behaviour of the prepared membrane using an antimony-based anode, revealing limited interfacial and charge transfer resistances, enabling a reduced polarization, outperforming the liquid counterpart at 60 °C (95 vs 70 mAh g^{-1} after 100 cycles at 1C).

Colò et al. proposed a UV light-induced free-radical polymerization (UV curing) process to transform a starting liquid reactive mixture ($NaClO_4$:PC:PEO = 5:50:45 by wt%) into a crosslinked quasi-solid polymer electrolyte in just 3 min,[334] highlighting the simplicity and scalability of the proposed methodology, being solvent and catalyst free, in view of the upscaling of PEO-based solid systems for NIBs. Their approach (Figure 12c) led to excellent thermal properties ($T_g = -63$ °C, first TGA peak > 100 °C) and electrochemical behavior (ionic conductivity exceeding 1 mS cm^{-1} at 25 °C, ESW up to 4.7 V vs Na^+/Na). When assembled in TiO_2-based half-cells, the UV-cured electrolyte delivered a stable specific capacity of about 250 mAh g^{-1} at ambient temperature upon constant current cycling at 0.1 mA cm^{-2} (0.04C). Later on, a crosslinked PEO polymer electrolyte was reported by Lehmann et al., demonstrating impressive ionic conductivities of 7.1×10^{-4} and 2.0×10^{-4} S cm^{-1} at 70 and 20 °C, respectively, and robust mechanical properties across a broad temperature range.[335]

8. Single Ion Conductors

In theory, perfect Na^+ single ion conductors are characterized by an immobile anionic framework resulting in a unity cationic transport number. Consequently, in the case of ceramic Na^+ single ion conductors, the transport number is given as the ratio of the Na^+ ionic conductivity and the electronic conductivity, which is negligible in battery electrolytes. In polymeric Na^+ single ion conductors, the motion of anions attached to the polymer backbone is restricted so that the cation transference number approaches unity (see section 4 for more details).

In these systems, bulk polarization should be negligible, potentially enabling improved power capability and mitigating dendrite propagation (see **Figure 13**). As highlighted in several recent excellent studies and reviews,[125,339–344] metal dendrite formation in polymer-based electrolytes with dissolved salts is mostly attributed to the ineffective passivation of the anode similarly to liquid electrolytes (e.g., porous, resistive, inhomogeneous, thick, soluble, unstable layers), low lithium ion diffusivity, and insufficient Young's modulus. Nevertheless, dendrite growth has been observed with ceramic electrolytes with single-ion alkali metal ionic conductivity up 1–10 mS cm^{-1}, and Young's modulus in the order of 100 GPa. This phenomenon can be traced back to multiple factors, including polarization at the electrode/electrolyte interface, the presence of insulating phases at this latter, and grain arrangement and boundaries. Insulating phases include voids and side products with low ionic conductivity, which arise from the synthesis/densification procedure or operation below the cathodic stability window of the electrolyte. In this respect, mixed ionic-electronic conducting phases can also segregate at the metal/electrolyte interface, possibly causing the propagation of detrimental side reactions towards the electrolyte bulk.

All these aspects contribute to generating inhomogeneities at the metal/electrolyte interface-interphases, resulting in high local current densities upon cycling, well above the critical threshold above which metal dendrites can form and propagate. In most cases, propagation occurs at the boundaries between crystallites with different orientations, where secondary insulating phases often segregate. This phenomenon is more frequent with polycrystalline ceramic oxide-type electrolytes due to the high temperature required for their synthesis and densification.

The prospect of dendrite-free cycling is particularly important in connection to the gain in energy density, which would result from the use of a metal anode (estimated to be 70% when using a metal anode in the place of graphite.[190] The operative temperature range of solid state cells with Na metal may be somewhat limited by its relatively low melting point (≈98 °C),[345] yet the solid state technology can offer several advantages towards improved energy density regardless of using a metal anode. Notably, high-voltage bipolar stacks (coating the anode and the cathode of adjacent cells on the same current collector) could be implemented without internal short circuits in the absence of external separators, thus reducing the packaging volume and weight. Similarly, all the countermeasures used to keep the temperature below 60 °C, prevent leakages, and contain fire/explosion hazards in conventional batteries could be eliminated in solid-state batteries.[125,190,339,342,346]

Finally, finding effective materials and processes to build solid-state batteries could effectively mitigate the impact of safety issues during transport, storage, and dismantling of battery packs at the end-of-life prior to recycling or second-use, while possibly leading to a simplification of the design and packaging.[347]

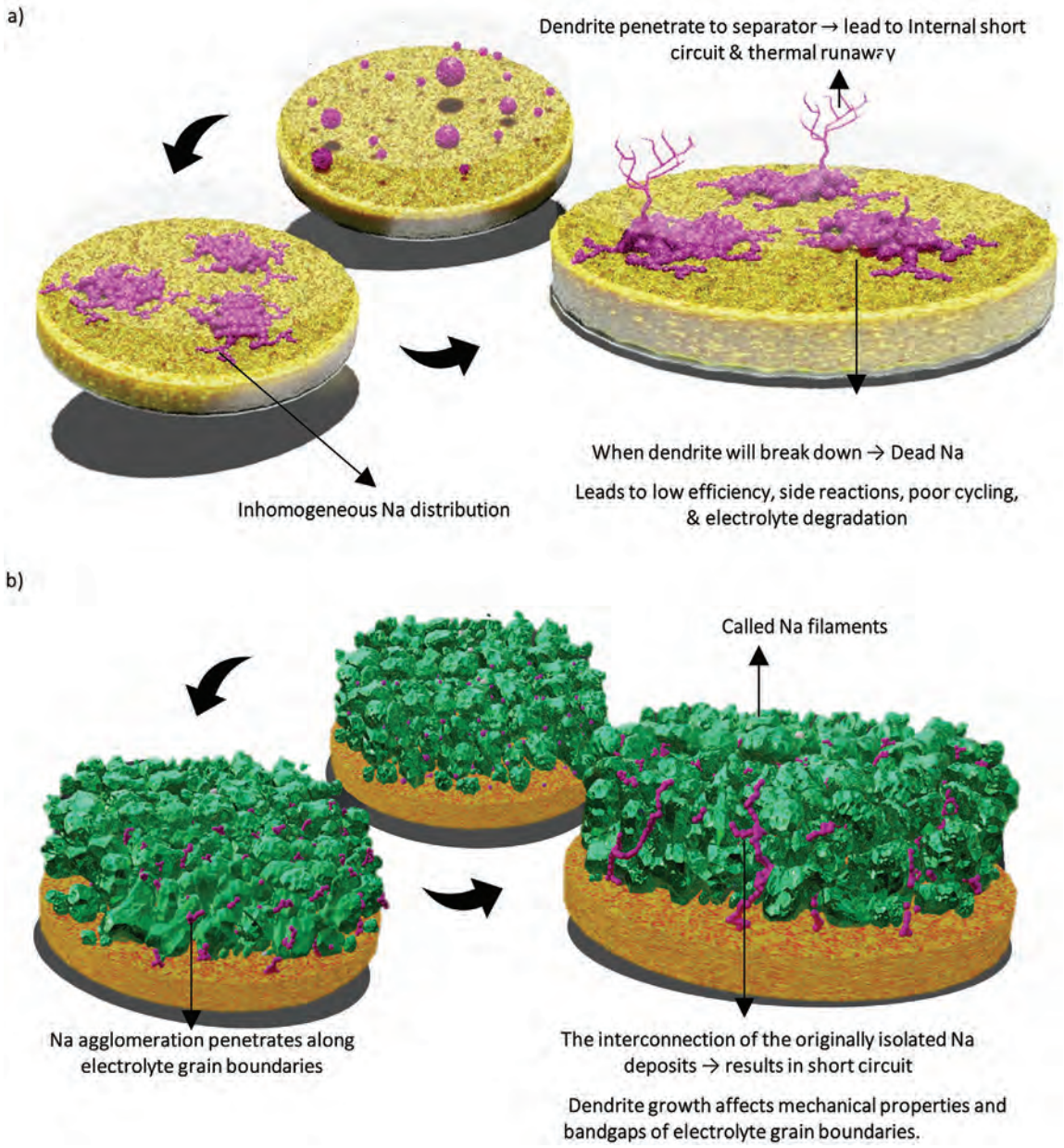

Figure 13. Schematic illustrating the dendrite growth mechanism in conventional batteries with liquid electrolyte (a) and in solid-state batteries with polycrystalline electrolyte (b).

8.1. Inorganic Single Ion Conductors

The first prototype of a sodium-based solid-state cell dates back to 1972. The cell featured sodium metal as the negative electrode, Na-β-alumina as the solid electrolyte, and an intercalation chromium oxide/graphite positive electrode. Several inorganic Li-ion conductors were known by then, as well as the main challenges related to their use in secondary battery cells, namely the poor physical contact at the electrode/electrolyte interface, and the inability to accommodate the mechanical stresses resulting from volume changes upon cycling, due to their high (in the order of 100 GPa) Young's modulus.[340]

Despite the electrolyte flammability/leakage, as well as sources of capacity fading such as transition metal dissolution, are negated with ceramic ion-conductors, gas evolution, side reactions, and dendrite formation have been observed with these latter, posing safety issues, and limiting the rate capability and cycle-life.[190,339,344,348] These issues, together with the difficulties and current high costs of production at scale,[190] are still major obstacles preventing from "leapfrogging" the current technology,[189] even though this latter is affected by manufacturing problems as well, such as impractical electrolyte filling and costly formation.[190]

Here follows an overview of the systems most relevant for secondary solid-state Na-based battery technology based on intercalation chemistry, and the strategies adopted towards their future practical application.

8.1.1. Chalcogenides

Many recent reports of Na^+ single ion conductors from this family have been developed based on metastable cubic Na_3PS_4 (2012),[349] showing an ionic conductivity of ≈0.1 mS cm^{-1}. The mechanochemical synthesis route led to high ionic conductivity due to the particle size reduction, favoring the densification and the introduction of mobile sodium defects enhancing ion transport in the metastable cubic phase. This latter could also be obtained by the application of high (>2 GPa) external pressure on the material in the low-conductivity tetragonal phase synthesized by conventional solid-state synthesis.[350]

This material, as most members of the chalcogenide family, has high compressibility, allowing densification by cold pressing, which is particularly attractive for battery cell manufacturing.

On the other hand, Na_3PS_4 is air and moisture-sensitive, releasing toxic and corrosive H_2S.[351] Additionally, the reductive decomposition of Na_3PS_4 resulted in the formation of Na_2S and Na_3P, which cannot passivate the interface with the negative electrodes; in addition, the latter is a mixed ionic electronic conductor.[352]

Chlorine doping of Na_3PS_4 was found to improve the ionic conductivity of the tetragonal phase, while resulting in the formation of Cl-based decomposition products at the interface with the anode able to slightly delay the severe capacity fading due to the high impedance increase (see **Table 7**).[353,354] On the other hand, oxygen doping to yield $Na_3PS_{4-x}O_x$ oxysulfide glass by mechanochemical milling demonstrated improved compatibility with Na metal anode and cycling performance in Na/S cells at 60 °C.[355] Reversible cycling in sodium-sulfur cells was also demonstrated at room temperature.[356]

Tetragonal Na_3SbS_4 (2016)[357] is another important reference of the Na^+ conducting chalcogenide family. It shows an ionic conductivity > 1mS cm^{-1}, thanks to the presence of multiple channels orthogonal to each other for Na^+ diffusion arranged in a 3D pathway. This material undergoes reversible hydration in contact with moisture, and is compatible with the solution synthesis route. Similarly to Na_3PS_4, it has a narrow electrochemical stability window (see **Figure 14a**) resulting in the formation of secondary phases upon reduction, unable to form a stable and functional passivation layer.[354] Subsequently, the sodium counterpart of highly conductive lithium-ion conducting LGPS, i.e., $Li_{10}MP_2S_{12}$ (M = Ge, Si, Sn) was developed. Differently from Na_3PS_4, $Na_{10}SnSb_2S_{12}$ shows an improved chemical and electrochemical stability attributed to the absence of P. $Na_{10}SnSb_2S_{12}$ shows a room temperature ionic conductivity of 0.5 mS cm^{-1}; it is compatible with the solution synthesis route, and densification by cold-pressing. Small $Na_{10}SnSb_2S_{12}$ particles with an even size distribution, derived from a liquid phase synthesis, improved densification upon cold pressing, resulting in a conformal interface with electrodes.[358]

8.1.2. Hydroborate

Similarly to chalcogenides, Na-hydroborates (in particular closoborate compounds) show high ionic conductivity and attractive mechanical properties associated with high compressibility, which allows for buffering the volume changes upon battery cycling and densification by simple cold-pressing. These compounds are also compatible with the solution synthesis route and stable in contact with Na metal, yet their soft character facilitates dendrite propagation, requiring high applied pressure to contrast it.[359]

Anion mixing in closo-borates and related compounds was found to stabilize the highly conductive high-temperature face-centered cubic phase observed with $Na_2B_{10}H_{10}$ above 100 °C. For example, the equimolar mixture of $Na_2B_{10}H_{10}$ and $Na_2B_{12}H_{12}$ results in a highly conductive (1mS cm^{-1} at 20 °C) face-centered cubic $Na_2(B_{12}H_{12})_x(B_{10}H_{10})_{1-x}$ stable from −170 to 450 °C.

Among the different $B_nH_n^{2-}$ species with n = 6–12, $(B_{10}H_{10})^{2-}$ and $(B_{12}H_{12})^{2-}$ with increased aromaticity show the highest oxidative stability, which can be further improved upon C and halogen doping. Careful electrochemical evaluation of $Na_{2-x}(CB_{11}H_{12})_x(B_{12}H_{12})_{1-x}$ oxidative stability using electrolyte/carbon mixtures to increase the surface area at the working electrode allowed the detection of an oxidation current at ≈4.1 V.[359]

An all-solid-state sodium battery cell, using a sodium metal anode and $NaCrO_2$ as the cathode, was first demonstrated using $Na_4(B_{12}H_{12})(B_{10}H_{10})$ as solid electrolyte. The cathode particles were coated in situ using an electrolyte solution in methanol, which enabled intimate and stable contact at the electrode/electrolyte interface; it allowed for stable cycling at 60 °C, with an upper cutoff voltage of 3.25 V (capacity retention of 85% after hundreds of cycles at C/5) (see Table 7).[360] Room temperature cycling was also demonstrated, yet dendrite formation compromised long-term cycling.

By applying 3.2 MPa to inhibit dendrite formation, excellent room temperature cycling was demonstrated using $Na_4(CB_{11}H_{12})_2(B_{12}H_{12})$ in a 4 V Na//NVP cell at relatively high (8 mg cm^{-2}) active material loading (see Figure 14b). This compound includes $[CB_{11}H_{12}]^-$ anions with high oxidative stability and has a high ionic conductivity (≥1 mS cm^{-1} at RT), thermal (>350 °C) and chemical stability (see Table 7).[361]

The main drawback of these systems consists in the high cost and low availability of pure precursors, as well as hazards related to hydrogen release following thermal decomposition at high temperatures.[359]

8.1.3. Oxides

Oxide-type ceramic electrolytes, notably Na-$\beta''Al_2O_3$ and NASICON-type Na-conductors, are more stable than sulfides (in terms of chemical stability in ambient atmosphere, and electrochemical stability window), but generally show significantly lower ionic conductivity.[125,339,341,344,362,363]

Na-$\beta''Al_2O_3$ has traditionally been employed in high-temperature battery systems,[364] yet operation at room temperature has been demonstrated, particularly in virtue of its excellent compatibility with Na metal. Indeed, it has also been exploited

Table 7. The electrochemical performance of laboratory-scale sodium-ion battery cells assembled with single-ion conducting solid electrolytes.

Electrolyte	Cathode (AM/SE/C)	Anode	Loading (tot).	Capacity (rate)	Capacity retention (cycles); rate	Temperature	References
L-$Na_{10}SnSb_2S_{12}$	TiS_2 (40/50/10)	Na	2.5 mg cm^{-2}	163.4 mAh g^{-1} (100 mAg^{-1}) 134 $mAhg^{-1}$ (200 mAg^{-1})	73% (100); 100 mAg^{-1}	25 °C	[358]
$Na_{3-x}PS_{4-x}Cl_x$, (x = 6.25%)	TiS_2 (33/67/0)	Na-Sn	7.5 mg cm^{-2}	80 $mAhg^{-1}$ (C/10)	100% (10); C/10	25 °C	[353]
$Na_4(B_{12}H_{12})_2(B_{10}H_{10})$	$NaCrO_2$ (70/20/10)	Na	1.8 mg cm^{-2}	88 $mAhg^{-1}$ (C/20)	85% (250); C/5	60 °C	[360]
$Na_4(CB_{11}H_{12})_2(B_{12}H_{12})$	NVPF (70/20/10)	Na	8.0 mg cm^{-2}	117 mAh g^{-1} (C/10) 40 $mAhg^{-1}$ (2C)	94% (150); C/5	25 °C	[361]
$Pip_{13}FSI$[a] | $Na_{3.3}Zr_{1.7}La_{0.3}Si_2PO_{12}$	NVP[a] (65/15/10)	Na	1.7 mg cm^{-2}	113 $mAhg^{-1}$ (C/5) 86 mAh g^{-1} (10C)	100% (10 000); 10C	25 °C	[379]
Liq[b] |$Na_5YSi_4O_{12}$	NVP	Na	0.8-1.2 mg cm^{-2}	115 mAh g^{-1} (C/2) 98 $mAhg^{-1}$ (1C)	95% (300); C/2	25 °C	[378]
$Na_{3.2}Ca_{0.1}Zr_{1.9}PSi_2O_{12}$	NVP[c] (60/30/10)	Na-SnO_2	8.9 mg cm^{-2}	103 $mAhg^{-1}$ (C/5) 95 mAh g^{-1} (1C) 81 $mAhg^{-1}$ (4C)	98% (500); 1C	25 °C	[376]
Na-$\beta''Al_2O_3$	NNM[d] (40/13.3/46.7)	Na	2.0 mg cm^{-2}	80 $mAhg^{-1}$ (C/10) 51 $mAhg^{-1}$ (8C)	90% (10 000); 6C	70 °C	[380]
Na-$\beta''Al_2O_3$	NFP[e] (83.4/12.4/4.2)	Na	4.4 mg cm^{-2} 0.8 mg cm^{-2}	95 $mAhg^{-1}$ (C/50) 56 $mAhg^{-1}$ (1C) 15 $mAhg^{-1}$ (10C)	87% (600); C/10 Loading 0.8 mg cm^{-2}	30 °C	[372,373]
PEO/Na(FSI-ethylcellulose)	HC (61/35/4)	Na	n.d.	178 $mAhg^{-1}$ (C/10)	56% (17); C/10	70 °C	[386]
PVdF/NaPA + EC/DMC[f]	NVP (50/20/30)	Na	n.d.	81 $mAhg^{-1}$ (C/5) 48 $mAhg^{-1}$ (1C)	≈90% (35); C/2	20 °C	[387]
Sodiated Nafion + EC/PC[g]	a-$NaMnO_2$[g] (76/12/12)	Na	n.d.	≈100 $mAhg^{-1}$ (10mAg^{-1}) ≈30 $mAhg^{-1}$ (20mAg^{-1})	≈50% (100); 10 mAg^{-1}	30 °C	[388]
PSP10 + EC/PC[h]	NVP[h] (80/10/10)	Na	n.d.	89 $mAhg^{-1}$ (C/5) 72 $mAhg^{-1}$ (4C)	99 (200); C/2	25 °C	[389]
NaPTAB-SGPE[i]	NVP[i] (80/10/10)	Na	1.56 mg cm^{-2}	90 $mAhg^{-1}$ (C/20) 49 $mAhg^{-1}$ (C/2)	≈92% (500); C/2	25 °C	[390]

[a] $Pip_{13}FSI$ = 5 µLcm^{-2} of N-methyl-N-propyl piperidium bis(fluorosulfonyl)imide; SE = $Na_{3.3}Zr_{1.7}La_{0.3}Si_2PO_{12}$/PVdF (15/10) treated at 700 °C to remove PVdF; [b] Liq = 20 µL $NaClO_4$ 1 M in PC/EC (1/1 v/v) + FEC 5 wt% at the interface with the cathode; [c] SE = PEO/succinonitrile/$NaClO_4$ (5/15/10); [d] NNM = $Na_{0.66}Ni_{0.33}Mn_{0.67}O_2$; SE = $Pyr_{14}FSI$; [e] NFP = $Na_2FeP_2O_7$; 4.4 mg cm^{-2} rate capability test. 0.8 mg cm^{-2} long term cycling test; [f] NaPA = Sodiated poly(bis(4-carbonyl benzene sulfonyl)imide-co-2,4-diamino benzenesulfonic acid); PVdF/NaPA blend 2/1 w/w. EC/DMC 1/1 v/v; [g] Membrane swelled in EC/PC (71.4/28.6) (64 wt.% uptake); SE = PVdF without any Na^+ ion source; [h] PSP10 = SEMI-IPN consisting of polymeric sodium tartaric acid borate (10 wt.%) and poly(VC) (90 wt.%) supported on nonwoven PET and swelled in EC/PC (1/1 w/w); SE = unspecified "LA-133"; [i] NaPTAB-SGPE = PVdF-HFP/sodium salt of poly(tartaric acid)borate blend (1/1 w/w) swelled in PC (polymer/solvent > 1/2 w/w); SE = PVdF without any Na^+ ion source.

as an interlayer between compressible $Na_4(B_{12}H_{12})(B_{10}H_{10})$ and Na metal, to allow cycling in Na//$NaCrO_2$ cells,[365] which would otherwise need higher temperature to avoid Na metal dendrite formation[360] (see Table 7), or the use of Na-Sn alloy.[366] The removal of surface impurities was found to further improve its cyclability against Na metal.[352] The X-ray tomography study of the Na/Na-$\beta''Al_2O_3$ interface upon plating/stripping revealed that the number and size of interfacial voids increase on stripping, decrease during the subsequent plating, but ultimately accumulate upon cycling as a function of cycle number and the current density applied on stripping. Severe contact losses resulting from this latter above a critical value cause dendrite growth when the current is reversed, due to high local plating currents. The critical stripping current density was found to be a function of the applied external pressure, which contrasts voids formation (e.g., it increased to 2.5 mA cm^{-2} under >9 MPa).[367]

NASICON-type $Na_{1+x}Zr_2P_{3-x}Si_xO_{12}$ (NZPS, typically x = 2-3) commonly shows a room temperature ionic conductivity in the order of 0.1-1 mS cm^{-1}, and high grain boundary resistance in the order of kΩ. This latter arises from voids, poor cohesion among grains, along with segregated insulating phases at the grain boundaries. The large interfacial impedance at the anode side can cause metal dendrites to form and rapidly propagate

through grain boundaries. The calculated thermodynamic electrochemical stability window of NZPS is in the range from 1.1 to 3.6 V vs Na^+/Na (see Figure 14a), meaning that passivation layers consisting of secondary phases form at the interfaces with most electrode materials upon cycling. Insulating NaO_x is formed at the interface with Na-metal, particularly at high temperature. Besides the use of Na-Sn alloy as the anode in the place of Na metal, the use of coatings and interlayers has been experimented, to avoid side reactions and improve the interfacial contact with the electrodes at the same time.[341,344,362,363]

Differently from chalcogenides and hydroborate Na-conductors, oxide-type ceramic electrolytes require high temperatures for densification (e.g., 1200–1500 °C for Na-β''-Al_2O_3 and 1250 °C for NZPS),[364,368] and insulating secondary phases detrimental for the electrochemical performance can segregate in the system, particularly in mixtures with carbon as the active material used to prepare the composite electrodes.[362,363]

All-ceramic monolithic systems have recently demonstrated stable cycling in Na metal cells for ≈100 cycles at relatively low current densities and room temperature, enabled by the use of sintering aids to decrease the synthesis/densification temperature, while improving the conductivity of the grain boundaries.[368–370] In situ synthesis of the electrode active material from liquid precursors on top of the ceramic pellet has also been adopted as a strategy to improve contact while minimizing possible side reactions.[371] Direct synthesis of crystalline $Na_2FeP_2O_7$ (NFP) was carried out via a glass-ceramic route from a melt-quenched precursor glass at 550 °C on the surface of Na-$\beta''Al_2O_3$ roughened by the use of a pore forming agent to increase the contact area. The sintering step did not require external pressure application, and allowed building pouch cells with a 25 cm^2 area. Na//NFP cells with an NFP areal loading up to ≈4.5 mg cm^{-2} demonstrated reversible cycling up to 5 C at 30 °C.[372] Long term cycling was demonstrated at much lower NFP loading (0.6 mg cm^{-2})[373] (see Table 7).

Monolithic ceramic assembly may require thick composite electrode layer with relatively high amounts of solid electrolyte to ensure ionic percolation, external pressure control to contrast volume variations upon cycling, and ultimately undergo capacity fading due to the induced mechanical stress.[339,374,375] Alternatively, hybrid strategies have been experimented to build battery cells with improved contact and compatibility among the components. Polymer-based electrolytes are often used as the ionically conductive binder in the composite electrode to build cells with oxide-type ceramic pellets as the electrolyte. Notably, the polymer-based electrolyte improves the contact among the components, and buffers the volume changes of the active electrode material upon cycling. Polymeric interlayers have also been experimented.[339,341,344,362,363]

The impregnation with SnO_2 particles into a tailored porous structure (≈100 µm thick) on the surface of a dense Ca-doped NZPS pellet (≈300 µm thick) was experimented to form a sodiophilic layer, allowing for the direct infiltration of melt Na metal. Calcium doping in NZSP was found to improve the bulk ionic conductivity and decrease the required densification temperature, thereby limiting the formation of insulating ZrO_2 secondary phases at grain boundaries. This strategy enabled stable cycling in Na//NVP cells at room temperature, using a composite cathode encompassing a polymer electrolyte as the binder[376] (see Table 7 and Figure 14c). For example, a polyether-based crosslinked polymer electrolyte doped with NaTFSI was used as both the binder to prepare a composite $NaTi_2(PO_4)_3$ electrode, and the interlayer at the NZPS/Na metal interface. Reversible cycling at C/5 with a delivered capacity 100 mAh g^{-1} and Coulombic efficiency of 99.7 ± 0.3% was demonstrated at 60 °C.[377]

Among the sodium rare-earth silicates with 3D structure framework similar to NASICON, lots of studies were conducted on $Na_5YSi_4O_{12}$ since the discovery of its high ionic conductivity. Stable room temperature cycling in a Na//NVP cell was recently demonstrated, using 20 µL of liquid electrolyte ($NaClO_4$ in a mixture of flammable PC, EC, and FEC) to wet the surface of the positive electrode (see Table 7).[378]

Ionic liquids have also been implemented in ceramic solid state cells. For example, a rapid capacity decay (from 85 to 44 mAh g^{-1} in 10 cycles) was observed cycling Na//NVP cells at room temperature, built with an electrode/electrolyte assembly obtained by spin-coating and annealing an NVP-based slurry onto a La-doped NZPS pellet. The use of a relatively small amount (5 ml cm^{-2}) of liquid electrolyte to wet the positive electrode side decreased the polarization improving the cycling performance. With $NaPF_6$/EC-DMC, after more than 200 cycles, a rapid capacity fade (from 100 to ≈0 mAh g^{-1} in about 20 cycles) was observed, attributed to the volatilization/decomposition of the liquid electrolyte. On the other hand, the use of a piperidinium-based ionic liquid resulted in an improved rate performance (up to 10C, see Table 7), and stable operation (≈100% of capacity retention over thousands of cycles), even when the areal loading of the positive electrode was doubled from ≈1.7 to 3.3 mg cm^{-2}.[379] Similarly, a toothpaste-like $Na_{0.66}Ni_{0.33}Mn_{0.67}O_2$ (NNM) electrode was designed, including carbon particles as the electronically conductive additive, and $Pyr_{14}FSI$ ionic liquid. The electrode paste could adhere onto the β''-Al_2O_3 pellet and keep the interface wet upon cycling. Na//NNM cells demonstrated stable (capacity decay of 0.04% per cycle) reversible operation at room temperature for 100 cycles (> 60 $mAhg^{-1}$ at C/2) and good cycling performance (74% capacity retention after 650 cycles at 2C) at 70 °C at the relatively high areal loading of 6 mg cm^{-2}[380] (see also Table 7).

8.2. Polymeric Single Ion Conductors

As stated in the previous section, the use of polymer-based ion conductors tackles several key-issues for the solid state battery technology, namely the interfacial contact optimization, the ability to buffer volume variations, and the possibility to fabricate thin film under mild condition. The advantages brought about by unity transport number in ceramic electrolytes in terms of improved rate capability and mitigation of dendritic growth are targeted by the research in the field of polymeric Na^+ single ion conductors.

Polymeric single-ion conductors often display lower ionic conductivity compared to their dual-ion counterparts. By now, this issue has mostly been addressed by adding organic carbonate ester solvents in a bid to increase Na^+ ion mobility, which is otherwise affected by strong ion-ion and ion-polymer correlation. This approach limits the potential to build battery cells with high safety and energy density. Alternative strategies have been

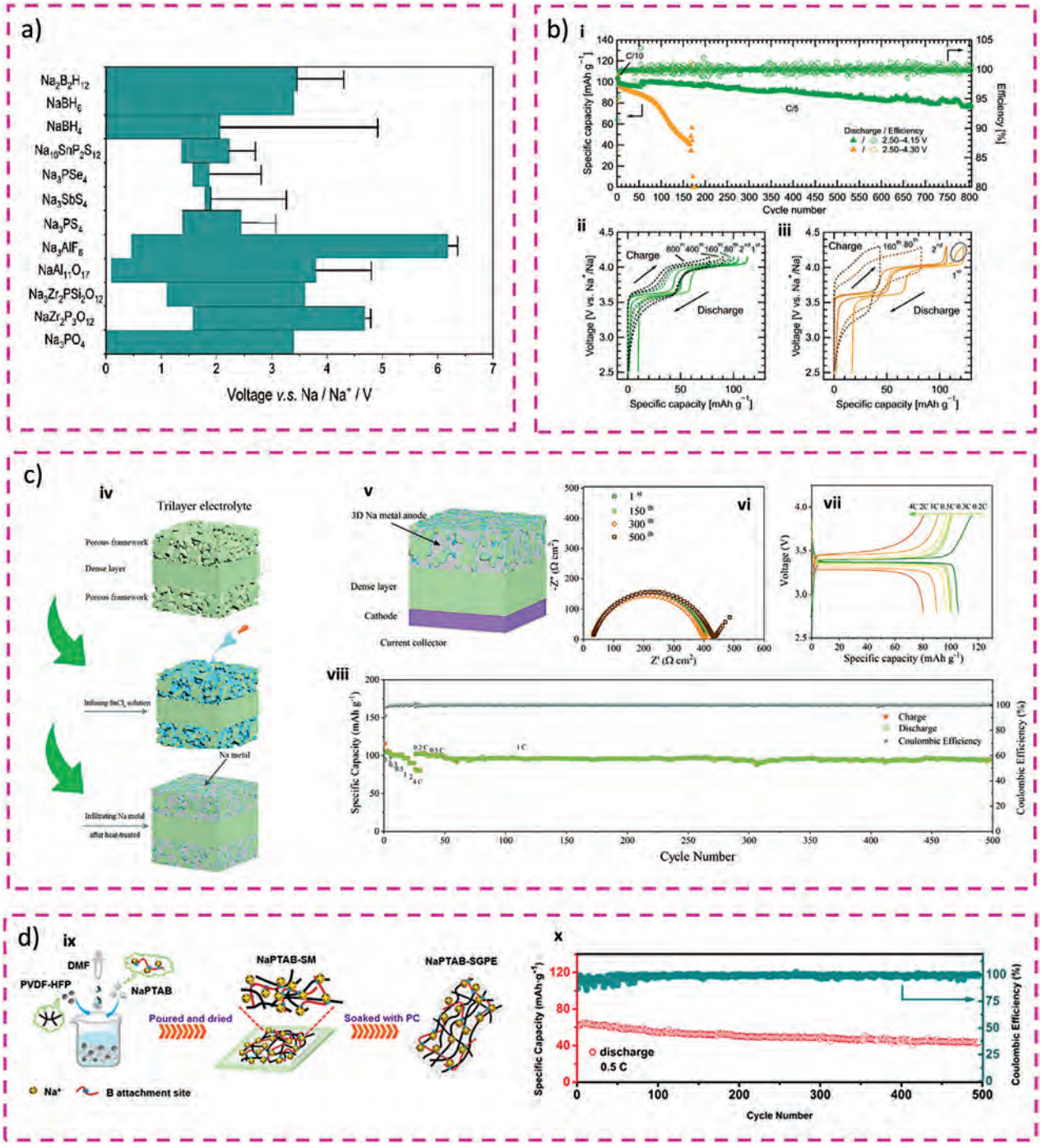

Figure 14. a) Thermodynamically calculated electrochemical stability windows of Na-ion conducting solid-state electrolytes, error bars on the right of the stability regions (thick bars) represent their calculated kinetic upper limit for oxidation. Adapted under terms of the CC-BY license.[343] Copyright 2020, Tietz, F. Ma, Q., published by John Wiley and Sons. b) Cycling performance of $Na_3(VOPO_4)_2F|Na_4(CB_{11}H_{12})_2(B_{12}H_{12})|Na$ all-solid-state cells at two different potential windows, 2.50 V and 4.15 V (green) or 4.30 V (yellow) at C/5 following two formation cycles at C/10 at room temperature (i), corresponding voltage profiles at C/10 (solid) and at C/5 (dashed) with the upper cutoff voltage of (ii) 4.15 V and (iii) 4.30 V. Adapted under terms of the Creative Commons Attribution 3.0 Unported Licence.[361] Copyright 2020, Asakura R. et. al., published by The Royal Society of Chemistry. c) Schematic of the trilayer NZSP solid-state electrolyte (iv), Full schematic of the SSSB (v), EIS plots showing the solid-state battery's performance after various cycles (vi), Voltage profiles recorded at different current densities (vii), Cycling profile illustrating the behavior of the solid-state battery under varying current densities (viii). Adapted with permission.[376] Copyright 2019, John Wiley and Sons. d) Synthetic route of NaPTAB gel polymer electrolyte (ix), cycling performance of NVP/Na cell using NaPTAB gel polymer electrolyte at current densities of 0.5C at 60 °C (x). Adapted with permission.[390] Copyright 2020, American Chemical Society.

proposed to improve the ionic conductivity. The first one involves the design of systems with a low T_g and increased polymer segmental mobility, e.g. by copolymerization. The second "mixed" co-cation approach decouples the ionic conductivity from the dynamics of the polymer backbone, e.g. by introducing bulky quaternary ammonium cations in the system.[346] Significant advances in the understanding of these single-ion conducting systems, and possible viable approaches to increase their ionic conductivity have been proposed in the field of lithium-based batteries, and will probably be mirrored by their sodium counterparts soon. Here below follows an overview of polymer-based systems proposed as Na^+ single ion conductors, with particular attention to the ones that enabled operation in sodium battery cells.

Organic–inorganic composite materials consisting in SiO_2 nanoparticles functionalized with sodium salt-terminated chains dispersed in a polymer matrix have been investigated as single Na-ion conducting films. Systems with phosphonate[381] and tri(fluoromethanesulfonyl)imide anionic[382] moieties in a poly(ether)-based polymer matrix were characterized, demonstrating room temperature ionic conductivities > 0.01 mS cm^{-1} and transference number of 0.9, determined by the Bruce-Vincent method. Standard PFG-NMR measurements could not be performed for ^{23}Na, due to the short spin–lattice relaxation times (typically less than 1 ms) characteristic of strong nuclear quadrupole coupling in the presence of a dynamic environment.

Blends of PEO and poly(sodium 1-[3-(methacryloyloxy)propylsulfonyl]−1-(trifluoromethanesulfonyl) imide) (PNaMTFSI) with different ratios were investigated as single-ion conducting polymer electrolytes for sodium batteries. NaMTFSI methacrylate monomer[383] was polymerized by reversible addition-fragmentation chain-transfer (RAFT). The blends with PEO were obtained by casting from an aqueous solution followed by hot-pressing at 70 °C. PNaMTFSI and PEO were found to be miscible (single T_g) in the whole range of compositions. The highest ionic conductivity values observed at 85 °C were ≈0.06 and 0.08 mScm^{-1} with 15 and 30 wt % PNaMTFSI, respectively. Higher amounts of PNaMTFSI resulted in amorphous systems with lower ionic conductivity. PNaMTFSI was found to reduce the crystal growth rate and dimension of PEO crystalline spherulites, while increasing their nucleation. The blends demonstrated high sodium-ion transference numbers in the range 0.8-0.9 and electrochemical stability window up to 4.5 V versus Na^+/Na, depending on the composition.[384]

Kuray et al. investigated the effect of several organic plasticizers on the conductivity and polymer dynamics of single-ion Na^+ conducting films obtained by photopolymerization of different oligomers, i.e., poly(ether)-based diacrylate and diurethane-based dimethacrylate, the sodium salt of 2-acrylamido-2-methyl-1-propanesulfonic acid sodium salt as the Na^+ ion source, and pentaerythritol-based crosslinker with 5–6 acrylate units per monomer. The highest ionic conductivity ($2{\cdot}10^{-8}$ S cm^{-1}) was observed at 100 °C using glycerol as plasticizer, possibly too low for practical operation in NIB cells.[385]

A cost-effective and simple strategy to synthesize single-ion conducting polymer electrolytes has been recently proposed by M. Armand's group. Sodiated ethylcellulose was functionalized with NaFSI upon reacting with fluorosulfonyl isocyanate. The former was previously synthesized by reacting the residual ethoxyl group in commercial ethylcellulose with an excess of NaOH in an aqueous solution. The PEO/Na(FSI ethylcellulose) blend (65/35 by weight, EO:Na ≈15 mol/mol) demonstrated a sodium ion transference number of 0.6 (by the Bruce-Vincent method) and ionic conductivity of 0.1 mScm^{-1} at 70 °C. A large increase of the ionic conductivity was observed above the melting temperature of PEO. The addition of Na(FSI ethylcellulose) increases the film stiffness, possibly contributing to contrast dendrite growth. The polymer electrolyte demonstrated reversible operation in laboratory-scale Na-metal cells with a HC (see Table 7).[386]

Sodiated poly(bis(4-carbonyl benzene sulfonyl)imide-co-2,4-diamino benzenesulfonic acid) (NaPA) single-ion conductor was blended with PVdF and used as the electrolyte and electrode (NVP) binder for NIB. The blend (wet with a mixture of EC/DEC) demonstrated an ionic conductivity of 0.09 mS cm^{-1} at 20 °C, and a sodium ion transference number of 0.83 (by the Bruce-Vincent method). Reversible cycling in Na//NVP cells was demonstrated at 20 and 80 °C, showing a performance similar to that observed using a standard binder and a separator drenched in 1 M $NaClO_4$ in EC/DEC (see Table 7).[387]

A NAFION membrane, sodiated by ion exchange in an aqueous NaOH solution, was investigated as Na^+ single ion-conducting polymer. The film (swelled in mixture of EC/PC up to 64 wt.% uptake) demonstrated an ionic conductivity of 0.5 mS cm^{-1} at 20 °C, and a sodium ion transference number of ≈0.8 (by PFG-NMR) or 0.5-0.6 (by the Bruce-Vincent method). Such difference was attributed to the large resistance at the Na metal/electrolyte interface. Reversible cycling was demonstrated in Na//a-$NaMnO_2$ cells built with the Na^+ single ion conducting film. (see Table 7) Na//a-$NaMnO_2$ cells built using a standard separator drenched in 1 M NaTFSI in PC showed better rate-capability performance and similar capacity fading upon long-term cycling[388] (see Table 7).

The sodium salt of poly(tartaric acid)borate from a synthesis in aqueous medium was used to prepare single Na-ion conducting gels, which demonstrated improved room temperature long-term cycling performances in Na//NVP cells compared to a standard liquid electrolyte (1 M $NaClO_4$ in EC/DEC). The synthesis of a SEMI-IPN (PSP10) including poly(VC) supported on nonwoven poly(ethylene terephtalate) (PET),[389] and the preparation of blends with PVdF-HFP (NaPTAB)[390] were investigated. PSP10 and NaPTAB were swelled in EC/PC and PC, respectively. These gels demonstrated an ionic conductivity in the order of ≈0.1 mS cm^{-1} at 30 °C, transference number of ≈0.9 (by the Bruce-Vincent method), and reversible cycling in Na//NVP cells at 25 and 60 °C (see Table 7 and Figure 14d).

9. General Overview and Future Perspectives

The continuous advancement in terms of high energy/power density and the widespread practical applications of NIBs bring about an escalating importance and challenges in ensuring battery sustainable development and production. Enhancing the competitiveness of NIBs is at the forefront, and a key frontier in this pursuit involves substituting liquid electrolytes with polymer electrolytes.[391] These alternatives, devoid of free-flowing solvents, aim at improving safety and greenness while concurrently enhancing the overall energy density and reduce

operating/capital costs. The European SET-Plan Action 7 for 2030 outlines a targeted objective to advance the development of solid-state batteries. The primary goal is to achieve a specific energy density surpassing 400 Wh kg^{-1} while maintaining durability for a substantial 2000 cycles. This initiative reflects a commitment to enhancing energy storage technologies for a more sustainable and efficient future society. In this context, we have provided detailed insights into the fundamental aspects and progress in the development of NIB electrolytes. Despite the considerable progress achieved thus far, there remains a significant distance to traverse in the successful realization of industrially viable solid-state system that boast competitive energy density and inherent safety. Consequently, we summarise here the prevailing challenges related to advanced electrolytes, focusing on several key aspects:

1) Regarding the imperative of achieving high energy density, it is crucial to note that the energy density of solid-state batteries is directly impacted by the mass-loadings of cathodes. However, many reported works on solid-state batteries have demonstrated relatively low areal mass loadings.[392] This is primarily due to the challenges associated with increased resistance in cathodes and the interface resistance between solid-state electrolytes and cathodes, and the challenges associated with the engineering of high loading electrodes granting good ion percolation. Future research endeavours should prioritize the enhancement of cathode mass-loadings without jeopardizing the electrochemical performance of batteries. This strategic focus is essential for propelling the overall effectiveness and viability of solid-state batteries in the forthcoming future.
2) Advancing the development of polymer-based solid electrolytes by achieving sufficiently high ionic conductivity for practical room temperature operation. Currently, the conductivity of most solid electrolytes is limited to around 10^{-4} S cm^{-1} at room temperature, creating a disparity with the 10^{-2}–10^{-3} S cm^{-1} ionic conductivity typical of conventional liquid electrolytes. The research should focus more on creating advanced polymer networks, through crosslinking for instance, or novel polymer matrices. The T_g can be reduced by either utilizing new polymers and/or polymer blends having low crystallinity, high segmental mobility, and reduced chain entanglement or by incorporating flexible chain segments through grafting onto the backbone. Additionally, emphasis has to be placed on obtaining highly conducting composite polymers, including active or inactive fillers, by finely adjusting the filler–polymer interface without filler aggregation. This strategy aims to establish a well-connected ion transportation network, addressing the current gap and ultimately improving room temperature conductivity in polymer-based solid electrolytes. In general, ion doping and substitution have the potential to improve the ionic conductivity of solid electrolytes by altering the bonding energy between mobile ions and their neighbouring atoms.
3) Significant initiatives are currently in progress to boost sustainability by substituting synthetic polymers with natural polymers.[322] This shift not only streamlines the utilization of less hazardous solvents and processing techniques but also harmonizes with the overarching objective of creating environmentally friendly energy storage solutions. In addition, there's a growing awareness in the market that value can be derived from reusing and recycling products in a closed loop. This approach transforms materials and products into valuable resources rather than letting them become waste to be just disposed. However, the existing literature in this field is still in the early stages of development and lacks comprehensive results pertaining to battery performance under these sustainable and low-cost solid-state configurations.
4) In-depth exploration of interfacial behaviour and compatibility between polymer electrolytes and electrodes is essential and can be accomplished through advanced characterization techniques, including in situ/operando analyses, as well as modelling studies both ab initio on the materials as well as multiscale on both materials and complex structures/devices. The establishment of stable electrolyte/electrode interphases is crucial to ensuring the long-term cycling stability of electrochemical energy storage devices, including NIB. Thus, investigating and understanding these interphase dynamics is pivotal for addressing and enhancing the overall performance and durability of next-generation battery system to intrude the market.

10. Summary

After a decade of dedicated endeavors, NIBs have emerged as the most promising battery technology following LIBs in terms of commercial viability. Yet, akin to other batteries utilizing alkali metal ions, the principle of electrolyte compatibility in NIBs remains a puzzle yet to be completely unraveled. This complexity arises from the intricate interactions among the diverse components within the electrolyte. In this overview of electrolyte transition towards solid-state NIBs, we highlighted how the selection of salts, solvents, polymeric matrices, and electrolyte additives strongly govern the electrochemical behavior of NIBs. As the resurgence of the "solvation theory" offers valuable insights, it directs our attention towards examining the solvation structure and inherent characteristics in various electrolyte systems for NIBs. These encompass conventional liquid electrolytes, ionic liquids, polymer electrolytes, superconcentrated electrolytes, and localized high-concentration electrolytes. Drawing from literature, we delve into the solvation within different Na-based electrolyte systems, illuminating their impact on critical properties like ion transport and the formation of SEI. Furthermore, essential fundamental equations and definitions crucial for delineating transport properties and elucidating conduction mechanisms across diverse Na-based battery electrolyte types are also thoroughly discussed. A particular focus is dedicated to the use of solid electrolytes. The main driving force pushing the replacement of the flammable and explosive liquid electrolyte with a solid one is the expected improvement in the safety and stability of the battery. However, one of the main challenges in using solid electrolytes is obtaining an efficient solid-to-solid interaction at the electrode/electrolyte interphase. Implementing systems based on ionic liquids or hybrid polymer electrolytes can guarantee an increased safety level of the system, decreasing the problem associated with solid/solid elevated interfacial resistances and, consequently, poor battery performances. The design of novel solid polymeric systems can guarantee an improvement

in the performance of NIB in terms of energy density, cycle life, and safety. In particular, PEO and alternative polymeric matrices can guarantee conductivity values exceeding 10^{-4} S cm^{-1} at room temperature and, with proper formulation engineering, lead to systems characterized by long cycle life and relatively good metrics in terms of energy and power density. The obtainment of a good electrode/electrolyte interface is fundamental to guarantee good performance. Processes involving the direct cast onto the electrode surface and in situ cross-linking allow an increase in the quality of electrochemical interfaces. Most of the report analyzed in the review reports cell evaluation at lab scale level, with coin cell or similar. If the scientific community aims to make these batteries available on a large scale in a few years (and not decades), greater efforts in the technology transfer from academia to industry and the validation of the system in large-scale devices (pouch cell or similar) will be pivotal to achieving stable, cheap, solid-state and efficient EES systems.

Acknowledgements

This study was carried out under the National Recovery and Resilience Plan (NRRP), within the NEST – Network 4 Energy Sustainable Transition (Mission 4, Component 2, Investment 1.3 – D.D. 1561 11.10.2022 of the Ministero dell'Università e della Ricerca (MUR), PE0000021), and the MOST – Sustainable Mobility Center and received funding from the European Union Next-GenerationEU (PIANO NAZIONALE DI RIPRESA E RESILIENZA – PNRR e Mission 4, Component 2, Investment 1.4 and D.D. 1033 17/06/2022 of the Ministero dell'Università e della Ricerca (MUR), CN00000023). This manuscript reflects only the authors' views and opinions, neither the European Union nor the European Commission can be considered responsible for them. Part of this work was carried out within the activities "Ricerca Sistema Elettrico" funded through contributions to research and development by the Italian Ministry of Economic Development.

Conflict of Interest

The authors declare no conflict of interest.

Keywords

composite electrolyte, electrolyte, gel polymer, ionic liquid, single-ion conductor, sodium battery, solid electrolyte

Received: December 12, 2023
Revised: May 14, 2024
Published online:

[1] X. Wu, Y. Dai, N. W. Li, X. C. Chen, L. Yu, *eScience* **2023**, 100173.
[2] A. Eftekhari, D. Kim, *J. Power Sources* **2018**, *395*, 336.
[3] T. Xiong, J. Li, J. Chandra, M. Koroma, Z. Zhu, H. Yang, L. Zhang, T. Ouyang, M. Balogun, M. Al-mamun, *J. Energy Chem.* **2023**, *81*, 71.
[4] X. Zhang, C. Xu, Y. Bai, J. Zhao, *Chem. Eng. J.* **2024**, *194*, 114304.
[5] B. Pandit, M. Johansen, B. P. Andersen, C. S. Martínez-Cisneros, B. Levenfeld, D. B. Ravnsbæk, A. Varez, *Chemic2023al Engineering Journal* **2023**, *472*, 144509.
[6] K. Chayambuka, G. Mulder, D. L. Danilov, P. H. L. Notten, **2018**, *1800079*, 1.
[7] X. Bai, N. Wu, G. Yu, T. Li, *Inorganics* **2023**, *11*, 289.
[8] C. Delmas, *Adv. Energy Mater.* **2018**, *8*, 1.
[9] Y. You, A. Manthiram, *Adv. Energy Mater.* **2018**, *8*, 1.
[10] P. K. Nayak, L. Yang, W. Brehm, P. Adelhelm, *Angew. Chem., Int. Ed.* **2018**, *57*, 102.
[11] M. Nowak, W. Zając, E. Hanc, J. Molenda, *Composites, Part B* **2021**, *213*, 108729.
[12] J. Deng, W. Luo, S. Chou, H. Liu, S. Dou, *Adv. Energy Mater.* **2018**, *8*, 1.
[13] M. Nowak, W. Zając, J. Molenda, *Energy* **2022**, *239*, 122388.
[14] M. Lao, Y. Zhang, W. Luo, Q. Yan, W. Sun, S. X. Dou, *Adv. Mater.* **2017**, *29*, 1.
[15] Q. Wang, C. Zhao, Y. Lu, Y. Li, Y. Zheng, Y. Qi, X. Rong, L. Jiang, X. Qi, Y. Shao, D. Pan, B. Li, Y. Hu, L. Chen, *Small* **2017**, *13*.
[16] C. Santamaría, E. Morales, C. del Rio, B. Herradón, J. M. Amarilla, *Electrochim. Acta* **2023**, *439*, 141654.
[17] P. Zhang, X. Wang, Y. Zhang, Y. Wei, N. Shen, S. Chen, B. Xu, *Adv. Funct. Mater.* **2024**, 2402307.
[18] European Commission, Study on the Critical Raw Materials for the EU 2023 Final Report, **2023**.
[19] H. S. Hirsh, Y. Li, D. H. S. Tan, M. Zhang, E. Zhao, Y. S. Meng, *Adv. Energy Mater.* **2020**, *10*, 1.
[20] S. Guo, C. Wei, L. Wang, B. Gao, K. Paul, *Cell Reports Physical Science* **2023**, *4*, 101463.
[21] E. Gabriel, C. Ma, K. Graff, A. Conrado, D. Hou, H. Xiong, *eScience* **2023**, 100139.
[22] H. Darjazi, A. Staffolani, L. Sbrascini, L. Bottoni, R. Tossici, F. Nobili, *Energies* **2020**, *13*, 6216.
[23] H. Darjazi, L. Bottoni, H. R. Moazami, S. J. Rezvani, L. Balducci, L. Sbrascini, A. Staffolani, A. Tombesi, F. Nobili, *Materials Today Sustainability* **2023**, *21*, 100313.
[24] S. Yang, Z. Zhang, X. Qiu, L. Zhong, J. Huang, H. Zhang, J. Ma, Q. Meng, X. Zu, W. Zhang, *Resources Chemicals and Materials* **2023**, *2*, 245.
[25] Y. Liu, Z. Yao, X. Zhu, Y. Liu, Z. Yao, P. Vanaphuti, X. Yang, L. Mei, X. Zhu, *Cell Reports Physical Science* **2023**, *4*, 101240.
[26] Y. Li, Y. Guo, K. You, C. Guo, C. Li, X. Zeng, W. Wang, Q. Tang, Y. Yuan, *Prog. Nat. Sci.: Mater. Int.* **2023**, *33*, 92.
[27] J. Tarascon, *Joule* **2020**, *4*, 1616.
[28] I. Hasa, J. Barker, G. A. Elia, S. Passerini, *Elsevier B.V.* **2023**, 1.
[29] W. Tang, Z. Chen, F. Xiong, F. Chen, C. Huang, Q. Gao, T. Wang, Z. Yang, W. Zhang, *J. Power Sources* **2019**, *412*, 246.
[30] J. Chen, H. Yang, T. Li, C. Liu, H. Tong, J. Chen, Z. Liu, L. Xia, Z. Chen, J. Duan, L. Li, *Frontiers in Chemistry* **2019**, *7*, 1.
[31] P. Desai, J. Huang, D. Foix, J.-M. Tarascon, S. Mariyappan, *J. Power Sources* **2022**, *551*, 232177.
[32] L. S. Domingues, H. G. de Melo, V. L. Martins, *Phys. Chem. Chem. Phys.* **2023**, *25*, 12650.
[33] J. Y. Hwang, S. T. Myung, Y. K. Sun, *Chem. Soc. Rev.* **2017**, *46*, 3529.
[34] J. Chen, G. Adit, L. Li, Y. Zhang, D. H. C. Chua, P. S. Lee, *Energy & Environmental Materials* **2023**, *6*, 1.
[35] D. Chao, C. Zhu, P. Yang, X. Xia, J. Liu, J. Wang, X. Fan, S. V. Savilov, J. Lin, H. J. Fan, Z. X. Shen, *Nat. Commun.* **2016**, *7*, 12122.
[36] B. Chen, M. Liang, Q. Wu, S. Zhu, N. Zhao, C. He, *Transactions of Tianjin University* **2022**, *28*, 6.
[37] M. Aizaz, U. Din, C. Li, L. Zhang, C. Han, B. Li, *Materials Today Physics* **2021**, *21*, 100486.
[38] Z. Hou, Y. Gao, Y. Zhang, J. Wang, *New Carbon Materials* **2023**, *38*, 230.
[39] Z. Qiu, F. Cao, G. Pan, C. Li, M. Chen, Y. Zhang, X. He, Y. Xia, X. Xia, W. Zhang, *ChemPhysMater* **2023**, *2*, 267.
[40] S. Chang, S. Qiu, S. Katiyar, J. F. Florez Gomez, Z. Feng, X. Wu, *Batteries* **2023**, *9*, 349.

[41] E. Gonzalo, M. Zarrabeitia, N. E. Drewett, J. Miguel, T. Rojo, *Energy Storage Mater.* **2021**, *34*, 682.
[42] Y. Wang, P. Niu, J. Li, S. Wang, L. Li, *Energy Storage Mater.* **2021**, *34*, 436.
[43] X. Wu, X. Lan, R. Hu, Y. Yao, Y. Yu, M. Zhu, *Adv. Mater.* **2022**, *34*, 1.
[44] S. Liang, X. Wang, R. Qi, Y. Cheng, Y. Xia, P. Müller-Buschbaum, X. Hu, *Adv. Funct. Mater.* **2022**, *32*.
[45] S. Dong, N. Lv, Y. Wu, Y. Zhang, G. Zhu, X. Dong, *Nano Today* **2022**, *42*, 101349.
[46] S. D. Shraer, N. D. Luchinin, I. A. Trussov, D. A. Aksyonov, A. V. Morozov, S. V. Ryazantsev, A. R. Iarchuk, P. A. Morozova, V. A. Nikitina, K. J. Stevenson, E. V. Antipov, A. M. Abakumov, S. S. Fedotov, *Nat. Commun.* **2022**, *13*, 4097.
[47] A. S. Samarin, A. V. Ivanov, S. S. Fedotov, *Clean Technologies* **2023**, *5*, 881.
[48] L. Qin, S. Xu, Z. Lu, L. Wang, L. Chen, D. Zhang, J. Tian, T. Wei, J. Chen, C. Guo, *Diamond & Related Materials* **2023**, *136*, 110065.
[49] H. Kim, D. I. Kim, W. Yoon, *J. Electrochem. Sci. Technol.* **2022**, *13*, 32.
[50] L. Wang, J. Światowska, S. Dai, M. Cao, Z. Zhong, Y. Shen, M. Wang, *Materials Today Energy* **2019**, *11*, 46.
[51] Y. Zhou, Q. Han, Y. Liu, Y. Wang, F. Jiang, N. Wang, Z. Bai, S. Dou, *Energy Storage Mater.* **2022**, *50*, 308.
[52] P. Wang, Y. You, Y. Yin, Y. Guo, *Adv. Energy Mater.* **2018**, *8*, 1.
[53] L. Wang, Z. Wei, M. Mao, H. Wang, Y. Li, J. Ma, *Energy Storage Mater.* **2019**, *16*, 434.
[54] Y. Zhao, L. P. Wang, M. T. Sougrati, Z. Feng, Y. Leconte, A. Fisher, M. Srinivasan, Z. Xu, *Adv. Energy Mater.* **2017**, *7*.
[55] X. Wang, G. Tan, Y. Bai, F. Wu, C. Wu, *Electrochem. Energy Rev.* **2021**, *4*, 35.
[56] C. N. Gannett, L. Melecio-Zambrano, M. J. Theibault, B. M. Peterson, B. P. Fors, H. D. Abruña, *Materials Reports: Energy* **2021**, *1*, 100008.
[57] L. Zhu, G. Ding, L. Xie, X. Cao, J. Liu, X. Lei, J. Ma, *Chem. Mater.* **2019**, *31*, 8582.
[58] P. Barpanda, L. Lander, S. Nishimura, A. Yamada, *Adv. Energy Mater.* **2018**, *8*, 1.
[59] N. V. Kosova, A. A. Shindrov, *Energy Storage Mater.* **2021**, *42*, 570.
[60] X. Cao, J. Liu, L. Zhu, L. Xie, *Energy Technol.* **2019**, *7*.
[61] J. Peng, W. Zhang, Q. Liu, J. Wang, S. Chou, H. Liu, S. Dou, *Adv. Mater.* **2022**, *34*, 1.
[62] M. Luo, H. Yu, F. Hu, T. Liu, X. Cheng, R. Zheng, *Chem. Eng. J.* **2020**, *380*, 122557.
[63] G. M. Tomboc, Y. Wang, H. Wang, J. Li, K. Lee, *Energy Storage Mater.* **2021**, *39*, 21.
[64] Q. Zhou, L. Wang, W. Li, K. Zhao, M. Liu, Q. Wu, Y. Yang, G. He, I. P. Parkin, P. R. Shearing, D. J. L. Brett, J. Zhang, X. Sun, *Electrochem. Energy Rev.* **2021**, *4*, 793.
[65] L. S. Batteries, W. Zhu, Y. Wang, D. Liu, V. Gari, C. Gagnon, A. Vijh, M. L. Trudeau, K. Zaghib, **2018**, *2*, 1.
[66] W. Zhu, D. Liu, A. Paolella, C. Gagnon, V. Gariépy, A. Vijh, K. Zaghib, *Front. Energy Res.* **2018**, *6*, 1.
[67] A. Brennhagen, C. Cavallo, D. S. Wragg, J. Sottmann, A. Y. Koposov, H. Fjellvåg, *Batteries Supercaps* **2021**, *4*, 1039.
[68] G. Li, X. Lou, C. Peng, C. Liu, W. Chen, *Chemical Synthesis* **2022**, *2*, 16.
[69] W. Zhang, C. Zhao, X. Wu, *Adv. Mater. Interfaces* **2020**, *7*, 1.
[70] J. Zhang, J. Gai, K. Song, W. Chen, *Cell Reports Physical Science* **2022**, *3*, 100868.
[71] K. Chayambuka, G. Mulder, D. L. Danilov, P. H. L. Notten, *Electrochim. Acta* **2022**, *404*, 139764.
[72] G. Åvall, J. Mindemark, D. Brandell, P. Johansson, *Adv. Energy Mater.* **2018**, *8*, 1.
[73] M. Roy, B. Domalanta, M. T. Castro, J. Anne, D. Rosario, J. D. Ocon, **2022**, *94*, 139.
[74] Z. Guo, G. Qian, C. Wang, G. Zhang, R. Yin, W. Liu, R. Liu, Y. Chen, *Prog. Nat. Sci.: Mater. Int.* **2023**, *33*, 1.
[75] L. Zhao, T. Zhang, W. Li, T. Li, L. Zhang, X. Zhang, Z. Wang, *Engineering* **2023**, *24*, 172.
[76] P. Yadav, A. Patrike, K. Wasnik, V. Shelke, M. Shelke, *Materials Today Sustainability* **2023**, *22*, 100385.
[77] Y. Wang, Z. Cao, W. Wahyudi, Z. Ma, Y. Liang, L. Cavallo, Q. Li, J. Ming, *Adv. Energy Mater.* **2023**, *13*, 1.
[78] L. Zhou, Z. Cao, J. Zhang, Q. Sun, Y. Wu, W. Wahyudi, J. Y. Hwang, L. Wang, L. Cavallo, Y. K. Sun, H. N. Alshareef, J. Ming, *Nano Lett.* **2020**, *20*, 3247.
[79] Y. Zou, Z. Cao, J. Zhang, W. Wahyudi, Y. Wu, G. Liu, Q. Li, H. Cheng, D. Zhang, G. T. Park, L. Cavallo, T. D. Anthopoulos, L. Wang, Y. K. Sun, J. Ming, *Adv. Mater.* **2021**, *33*, 1.
[80] H. Cheng, Q. Sun, L. Li, Y. Zou, Y. Wang, T. Cai, F. Zhao, G. Liu, Z. Ma, W. Wahyudi, Q. Li, J. Ming, *ACS Energy Lett.* **2022**, *7*, 490.
[81] Q. Li, Z. Cao, H. Cheng, J. Zhang, Z. Ma, W. Wahyudi, L. Cavallo, Q. Sun, J. Ming, *ACS Materials Letters* **2022**, *4*, 2469.
[82] S. Saffirio, H. Darjazi, M. E. Coller Pascuzzi, F. Smeacetto, C. Gerbaldi, *Heliyon* **2024**, *10*, e24493.
[83] A. Patriarchi, H. Darjazi, L. Minnetti, L. Sbrascini, G. A. Elia, V. Castorani, M. Á. Muñoz-Márquez, F. Nobili, *Batteries* **2024**, *10*, 11.
[84] L. Qiao, X. Judez, T. Rojo, M. Armand, H. Zhang, *J. Electrochem. Soc.* **2020**, *167*, 070534.
[85] H. Che, S. Chen, Y. Xie, H. Wang, K. Amine, X. Liao, Z. Ma, **2017**, 1075.
[86] Z. Tian, Y. Zou, G. Liu, Y. Wang, J. Yin, J. Ming, H. N. Alshareef, *Adv. Sci.* **2022**, *9*, 1.
[87] N. Aslfattahi, L. Samylingam, M. S. Kiai, K. Kadirgama, V. Kulish, M. Schmirler, Z. Said, *J. Energy Storage* **2023**, *72*, 108781.
[88] A. Ponrouch, D. Monti, A. Boschin, B. Steen, P. Johansson, M. R. Palacín, *J. Mater. Chem. A* **2015**, *3*, 22.
[89] E. Bekaert, L. Buannic, U. Lassi, A. Llordés, J. Salminen, in *Emerging Nanotechnologies in Rechargeable Energy Storage Systems*, Elsevier, **2017**, pp. 1–43.
[90] G. G. Eshetu, M. Martinez-Ibañez, E. Sánchez-Diez, I. Gracia, C. Li, L. M. Rodriguez-Martinez, T. Rojo, H. Zhang, M. Armand, *Chemistry – An Asian Journal* **2018**, *13*, 2770.
[91] B. Mosallanejad, S. Sadeghi, M. Ershadi, A. Ahmadi, Q. Cao, F. Boorboor, S. Ramakrishna, *J. Electroanal. Chem.* **2021**, *895*, 115505.
[92] Z. Huang, X. Zhang, X.-X. Zhao, Y. Zhao, V. Aravindan, Y.-H. Liu, H. Geng, X.-L. Wu, *Inorg. Chem. Front.* **2023**, *10*, 37.
[93] Y. F. Deng, S. X. Zhao, Y. H. Xu, K. Gao, C. W. Nan, *Chem. Mater.* **2015**, *27*, 7734.
[94] X. Huang, K. Chen, Y. Liu, *J. Electrochem. Soc.* **2019**, *166*, A5081.
[95] Y. Li, F. Wu, Y. Li, M. Liu, X. Feng, Y. Bai, C. Wu, *Chem. Soc. Rev.* **2022**, *51*, 4484.
[96] K. Matsumoto, J. Hwang, S. Kaushik, C.-Y. Chen, R. Hagiwara, *Energy Environ. Sci.* **2019**, *12*, 3247.
[97] A. Basile, M. Hilder, F. Makhlooghiazad, C. Pozo-Gonzalo, D. R. MacFarlane, P. C. Howlett, M. Forsyth, *Adv. Energy Mater.* **2018**, *8*.
[98] L. Zhou, M. Cai, T. Tong, H. Wang, *Sensors (Switzerland)* **2017**, *17*.
[99] Y. Shan, H. Wang, *Chem. Soc. Rev.* **2015**, *44*, 3617.
[100] X. Gao, Z. Xing, M. Wang, C. Nie, Z. Shang, Z. Bai, S. Xue, N. Wang, *Energy Storage Mater.* **2023**, *60*, 102821.
[101] X. Feng, H. Fang, N. Wu, P. Liu, P. Jena, J. Nanda, D. Mitlin, *Joule* **2022**, *6*, 543.
[102] Y. Wang, S. Song, C. Xu, N. Hu, J. Molenda, L. Lu, *Nano Materials Science* **2019**, *1*, 91.
[103] C. Zhao, L. Liu, X. Qi, Y. Lu, F. Wu, J. Zhao, Y. Yu, Y. Hu, L. Chen, *Adv. Energy Mater.* **2018**, *8*, 14.

[104] W. Hou, X. Guo, X. Shen, K. Amine, H. Yu, J. Lu, *Nano Energy* **2018**, *52*, 279.
[105] C. Bommier, X. Ji, **2018**, *1703576*, 1.
[106] G. Åvall, J. Mindemark, D. Brandell, P. Johansson, *Adv. Energy Mater.* **2018**, *8*.
[107] K. Vignarooban, R. Kushagra, A. Elango, P. Badami, B. E. Mellander, X. Xu, T. G. Tucker, C. Nam, A. M. Kannan, *Int. J. Hydrogen Energy* **2016**, *41*, 2829.
[108] A. Bhide, J. Hofmann, A. Katharina Dürr, J. Janek, P. Adelhelm, *Phys. Chem. Chem. Phys.* **2014**, *16*, 1987.
[109] G. G. Eshetu, S. Grugeon, H. Kim, S. Jeong, L. Wu, G. Gachot, S. Laruelle, M. Armand, S. Passerini, *ChemSusChem* **2016**, *9*, 462.
[110] J. Chen, Z. Huang, C. Wang, S. Porter, B. Wang, W. Lie, H. K. Liu, *Chem. Commun.* **2015**, *51*, 9809.
[111] A. Plewa-Marczewska, T. Trzeciak, A. Bitner, L. Niedzicki, M. Dranka, G. Z. Żukowska, M. Marcinek, W. Wieczorek, *Chem. Mater.* **2014**, *26*, 4908.
[112] F. Cheng, M. Cao, Q. Li, C. Fang, J. Han, Y. Huang, *ACS Nano* **2023**, *17*, 18608.
[113] D. I. Iermakova, R. Dugas, M. R. Palacín, A. Ponrouch, *J. Electrochem. Soc.* **2015**, *162*, A7060.
[114] S. Choudhury, S. Wei, Y. Ozhabes, D. Gunceler, M. J. Zachman, Z. Tu, J. H. Shin, P. Nath, A. Agrawal, L. F. Kourkoutis, T. A. Arias, L. A. Archer, *Nat. Commun.* **2017**, *8*, 898.
[115] R. Mogensen, D. Brandell, R. Younesi, *ACS Energy Lett.* **2016**, *1*, 1173.
[116] G. Yan, D. Alves-Dalla-Corte, W. Yin, N. Madern, G. Gachot, J.-M. Tarascon, *J. Electrochem. Soc.* **2018**, *165*, A1222.
[117] Z. X. Huang, X. L. Zhang, X. X. Zhao, Y. Y. Zhao, V. Aravindan, Y. H. Liu, H. Geng, X. L. Wu, *Inorg. Chem. Front.* **2022**, *10*, 37.
[118] S. S. Zhang, *J. Power Sources* **2006**, *162*, 1379.
[119] S. Komaba, T. Ishikawa, N. Yabuuchi, W. Murata, A. Ito, Y. Ohsawa, *ACS Applied Materials and Interfaces* **2011**, *3*, 4165.
[120] R. Dugas, A. Ponrouch, G. Gachot, R. David, M. R. Palacin, J. M. Tarascon, *J. Electrochem. Soc.* **2016**, *163*, A2333.
[121] M. Dahbi, N. Yabuuchi, M. Fukunishi, K. Kubota, K. Chihara, K. Tokiwa, X. F. Yu, H. Ushiyama, K. Yamashita, J. Y. Son, Y. T. Cui, H. Oji, S. Komaba, *Chem. Mater.* **2016**, *28*, 1625.
[122] J. Shi, L. Ding, Y. Wan, L. Mi, L. Chen, D. Yang, Y. Hu, W. Chen, *J. Energy Chem.* **2021**, *57*, 650.
[123] W. Zhang, F. Zeng, H. Huang, Y. Yu, M. Xu, L. Xing, W. Li, *Nano Res.* **2023**, *16*, 3823.
[124] K. Kim, H. Ma, S. Park, N. S. Choi, *ACS Energy Lett.* **2020**, *5*, 1537.
[125] M. Li, C. Wang, Z. Chen, K. Xu, J. Lu, *Chem. Rev.* **2020**.
[126] Z. Yu, N. P. Balsara, O. Borodin, A. A. Gewirth, N. T. Hahn, E. J. Maginn, K. A. Persson, V. Srinivasan, M. F. Toney, K. Xu, K. R. Zavadil, L. A. Curtiss, L. Cheng, *ACS Energy Lett.* **2021**.
[127] K. D. Fong, J. Self, B. D. McCloskey, K. A. Persson, *Macromolecules* **2021**, *54*, 2575.
[128] A. V. Cresce, S. M. Russell, O. Borodin, J. A. Allen, M. A. Schroeder, M. Dai, J. Peng, M. P. Gobet, S. G. Greenbaum, R. E. Rogers, K. Xu, *Phys. Chem. Chem. Phys.* **2016**, *19*, 574.
[129] H. Cheng, Q. Sun, L. Li, Y. Zou, Y. Wang, T. Cai, F. Zhao, G. Liu, Z. Ma, W. Wahyudi, Q. Li, J. Ming, *ACS Energy Lett.* **2022**, *7*, 490.
[130] L. Zhou, Z. Cao, J. Zhang, Q. Sun, Y. Wu, W. Wahyudi, J.-Y. Hwang, L. Wang, L. Cavallo, Y.-K. Sun, H. N. Alshareef, J. Ming, *Nano Lett.* **2020**, *20*, 3247.
[131] K. Goloviznina, E. Bendadesse, O. Sel, J.-M. Tarascon, M. Salanne, *ACS Appl. Mater. Interfaces* **2023**, *15*, 59380.
[132] Y. Yamada, J. Wang, S. Ko, E. Watanabe, A. Yamada, *Nat. Energy* **2019**, *4*, 269.
[133] D. Wu, C. Zhu, M. Wu, H. Wang, J. Huang, D. Tang, J. Ma, *Angew. Chem., Int. Ed.* **2022**, *61*, 202214198.
[134] R. Andersson, G. Hernández, J. Mindemark, *Phys. Chem. Chem. Phys.* **2022**, *24*, 16343.
[135] M. Gouverneur, J. Kopp, L. van Wüllen, M. Schönhoff, *Phys. Chem. Chem. Phys.* **2015**, *17*, 30680.
[136] A. Zheng, S. G. Greenbaum, *Front Chem* **2023**, *11*, 1296587.
[137] M. Forsyth, H. Yoon, F. Chen, H. Zhu, D. R. MacFarlane, M. Armand, P. C. Howlett, *J. Phys. Chem. C* **2016**, *120*, 4276.
[138] A. Massaro, J. Avila, K. Goloviznina, I. Rivalta, C. Gerbaldi, M. Pavone, M. F. C. Gomes, A. A. H. Padua, *Phys. Chem. Chem. Phys.* **2020**, *22*, 20114.
[139] L. S. Domingues, H. G. de Melo, V. L. Martins, *Phys. Chem. Chem. Phys.* **2023**, *25*, 12650.
[140] N. Molinari, J. P. Mailoa, N. Craig, J. Christensen, B. Kozinsky, *J. Power Sources* **2019**, *428*, 27.
[141] T. M. Pappenfus, W. A. Henderson, B. B. Owens, K. R. Mann, W. H. Smyrl, *J. Electrochem. Soc.* **2004**, *151*, A209.
[142] D. Morales, R. E. Ruther, J. Nanda, S. Greenbaum, *Electrochim. Acta* **2019**, *304*, 239.
[143] S. G. Greenbaum, Y. S. Pak, M. C. Wintersgill, J. J. Fontanella, *Solid State Ionics* **1988**, *31*, 241.
[144] E. Flores, G. Åvall, S. Jeschke, P. Johansson, *Electrochim. Acta* **2017**, *233*, 134.
[145] J. Wang, Y. Yamada, K. Sodeyama, E. Watanabe, K. Takada, Y. Tateyama, A. Yamada, *Nat. Energy* **2018**, *3*, 22.
[146] J. Lee, Y. Lee, J. Lee, S.-M. Lee, J.-H. Choi, H. Kim, M.-S. Kwon, K. Kang, K. T. Lee, N.-S. Choi, *ACS Appl. Mater. Interfaces* **2017**, *9*, 3723.
[147] K. Takada, Y. Yamada, E. Watanabe, J. Wang, K. Sodeyama, Y. Tateyama, K. Hirata, T. Kawase, A. Yamada, *ACS Appl. Mater. Interfaces* **2017**, *9*, 33802.
[148] Y. Yamada, A. Yamada, *Chem. Lett.* **2017**, *46*, 1056.
[149] F. Chen, M. Forsyth, *Phys. Chem. Chem. Phys.* **2016**, *18*, 19336.
[150] D. T. Duncan, I. E. Gunathilaka, M. Forsyth, D. R. MacFarlane, M. Kar, *Electrochim. Acta* **2023**, *472*, 143398.
[151] J. Zheng, S. Chen, W. Zhao, J. Song, M. H. Engelhard, J.-G. Zhang, *ACS Energy Lett.* **2018**, *3*, 315.
[152] Y. Wang, R. Jiang, Y. Liu, H. Zheng, W. Fang, X. Liang, Y. Sun, R. Zhou, H. Xiang, *ACS Appl. Energy Mater.* **2021**, *4*, 7376.
[153] Z. Yuan, A. Chen, J. Liao, L. Song, X. Zhou, *Nano Energy* **2024**, *119*, 109088.
[154] S. C. Kim, J. Wang, R. Xu, P. Zhang, Y. Chen, Z. Huang, Y. Yang, Z. Yu, S. T. Oyakhire, W. Zhang, L. C. Greenburg, M. S. Kim, D. T. Boyle, P. Sayavong, Y. Ye, J. Qin, Z. Bao, Y. Cui, *Nat. Energy* **2023**, *8*, 814.
[155] J. He, A. Bhargav, L. Su, J. Lamb, J. Okasinski, W. Shin, A. Manthiram, *Nat. Energy* **2024**, *2024*, 1.
[156] F. Gebert, J. Knott, R. Gorkin, S.-L. Chou, S.-X. Dou, *Energy Storage Mater.* **2021**, *36*, 10.
[157] M. P. Rosenwinkel, R. Andersson, J. Mindemark, M. Schönhoff, *J. Phys. Chem. C* **2020**, *124*, 23588.
[158] N. M. Vargas-Barbosa, B. Roling, *ChemElectroChem* **2020**, *7*, 367.
[159] J. Evans, C. A. Vincent, P. G. Bruce, *Polymer* **1987**, *28*, 2324.
[160] C. A. Angell, Y. Ansari, Z. Zhao, *Faraday Discuss.* **2011**, *154*, 9.
[161] D. R. MacFarlane, M. Forsyth, E. I. Izgorodina, A. P. Abbott, G. Annat, K. Fraser, *Phys. Chem. Chem. Phys.* **2009**, *11*, 4962.
[162] J. Popovic, D. Brandell, S. Ohno, K. B. Hatzell, J. Zheng, Y.-Y. Hu, *J. Mater. Chem. A* **2021**, *9*, 6050.
[163] K. Matsumoto, Y. Okamoto, T. Nohira, R. Hagiwara, *J. Phys. Chem. C* **2015**, *119*, 7648.
[164] M. Watanabe, *Solid State Ionics* **1988**, *28–30*, 911.
[165] K. M. Abraham, Z. Jiang, B. Carroll, *Chem. Mater.* **1997**, *9*, 1978.
[166] X. Xu, Y. Wang, Q. Yi, X. Wang, R. A. Paredes Camacho, H. Kungl, R. A. Eichel, L. Lu, H. Zhang, *ChemSusChem* **2023**, *16*, 202202152.
[167] V. Bocharova, A. P. Sokolov, *Macromolecules* **2020**, *53*, 4141.
[168] G. B. Appetecchi, *Physical Sciences Reviews* **2019**, *4*.

[169] H. Yin, C. Han, Q. Liu, F. Wu, F. Zhang, Y. Tang, *Small* **2021**, *17*, 2006627.
[170] K.-H. Shen, L. M. Hall, *Macromolecules* **2020**, *53*, 10086.
[171] Z. Song, F. Chen, M. Martinez-Ibañez, W. Feng, M. Forsyth, Z. Zhou, M. Armand, H. Zhang, *Nat. Commun.* **2023**, *14*, 4884.
[172] E. Ruoff, S. Kmiec, A. Manthiram, *Small* n/a, 2311839.
[173] K. R. Harris, *J. Phys. Chem. B* **2019**, *123*, 7014.
[174] W. Xu, E. I. Cooper, C. A. Angell, *J. Phys. Chem. B* **2003**, *107*, 6170.
[175] O. Nordness, J. F. Brennecke, *Chem. Rev.* **2020**, *120*, 12873.
[176] Y. Horowitz, M. Lifshitz, A. Greenbaum, Y. Feldman, S. Greenbaum, A. P. Sokolov, D. Golodnitsky, *J. Electrochem. Soc.* **2020**, *167*, 160514.
[177] F. Croce, G. B. Appetecchi, L. Persi, B. Scrosati, *Nature* **1998**, *394*, 456.
[178] J.-H. Shin, W. A. Henderson, C. Tizzani, S. Passerini, S.-S. Jeong, K.-W. Kim, *J. Electrochem. Soc.* **2006**, *153*, A1649.
[179] G. B. Appetecchi, *Physical Sciences Reviews* **2019**, *4*.
[180] Z. Zou, Y. Li, Z. Lu, D. Wang, Y. Cui, B. Guo, Y. Li, X. Liang, J. Feng, H. Li, C.-W. Nan, M. Armand, L. Chen, K. Xu, S. Shi, *Chem. Rev.* **2020**, *120*, 4169.
[181] L. Mezzomo, S. Bonato, S. Mostoni, B. D. Credico, R. Scotti, M. D'Arienzo, P. Mustarelli, R. Ruffo, *Electrochim. Acta* **2022**, *411*, 140060.
[182] P. Arora, Z. Zhang, *Chem. Rev.* **2004**, *104*, 4419.
[183] M. F. Lagadec, R. Zahn, V. Wood, *Nat. Energy* **2019**, *4*, 16.
[184] C. Vaalma, D. Buchholz, M. Weil, S. Passerini, *Nat. Rev. Mater.* **2018**, *3*, 18013
[185] D. M. D. Babiker, Z. R. Usha, C. Wan, M. M. El. Hassaan, X. Chen, L. Li, *J. Power Sources* **2023**, *564*, 232853.
[186] L. Zhang, X. Li, M. Yang, W. Chen, *Energy Storage Mater.* **2021**, *41*, 522.
[187] T. Zhu, X. Zuo, X. Lin, Z. Su, J. Li, R. Zeng, J. Nan, **2022**, *2200409*, 1.
[188] J. Mun, T. Yim, Y. Gap, K. Jae, *Chem. Eng. J.* **2021**, *405*, 125844.
[189] M. S. Whittingham, *Chem. Rev.* **2020**, *120*, 6328.
[190] J. Schnell, T. Günther, T. Knoche, C. Vieider, L. Köhler, A. Just, M. Keller, S. Passerini, G. Reinhart, *J. Power Sources* **2018**, *382*, 160.
[191] P. K. Dammala, K. B. Dermenci, A. R. Kathribail, P. Yadav, J. Van Mierlo, M. Berecibar, *J. Energy Storage* **2023**, *74*, 109209.
[192] F. J. Günter, J. Keilhofer, C. Rauch, S. Rössler, M. Schulz, W. Braunwarth, R. Gilles, R. Daub, G. Reinhart, *J. Power Sources* **2022**, *517*, 230668.
[193] C. F. J. Francis, I. L. Kyratzis, A. S. Best, *Adv. Mater.* **2020**, *32*, 1904205.
[194] M. Kirchhöfer, J. Von Zamory, E. Paillard, S. Passerini, *Int. J. Mol. Sci.* **2014**, *15*, 14868.
[195] C. S. Stefan, D. Lemordant, B. Claude-Montigny, D. Violleau, *J. Power Sources* **2009**, *189*, 1174.
[196] Y. Sun, J. Wang, J. M. Prausnitz, *AIChE J.* **2021**, *67*, e17208.
[197] M. Wetjen, G.-T. Kim, M. Joost, G. B. Appetecchi, M. Winter, S. Passerini, *J. Power Sources* **2014**, *246*, 846.
[198] D. Mecerreyes, L. Porcarelli, N. Casado, *Macromol. Chem. Phys.* **2020**, *221*, 1900490.
[199] A. C. Rolandi, C. Pozo-Gonzalo, I. de Meatza, N. Casado, D. Mecerreyes, M. Forsyth, *Advanced Energy and Sustainability Research* **2023**, *4*, 2300149.
[200] M. Eftekharnia, M. Hasanpoor, M. Forsyth, R. Kerr, P. C. Howlett, *ACS Appl. Energy Mater.* **2019**, *2*, 6655.
[201] F. Wang, X. Ke, K. Shen, L. Zhu, C. Yuan, **2022**, *2100772*, 1.
[202] R. Hagiwara, K. Matsumoto, J. Hwang, T. Nohira, *Chem. Rec.* **2019**, *19*, 758.
[203] I. Hasa, S. Passerini, J. Hassoun, *J. Power Sources* **2016**, *303*, 203.
[204] H. Che, S. Chen, Y. Xie, H. Wang, K. Amine, X.-Z. Liao, Z.-F. Ma, *Energy Environ. Sci.* **2017**, *10*, 1075.
[205] C. Bommier, X. Ji, *Small* **2018**, *14*.
[206] C. H. Wang, C. H. Yang, J. K. Chang, *Chem. Commun.* **2016**, *52*, 10890.
[207] L. Otaegui, E. Goikolea, F. Aguesse, M. Armand, T. Rojo, G. Singh, *J. Power Sources* **2015**, *297*, 168.
[208] D. Monti, A. Ponrouch, M. R. Palacín, P. Johansson, *J. Power Sources* **2016**, *324*, 712.
[209] Z. Sun, B. Wang, M. G. Boebinger, A. Magasinski, S. Jhulki, Y. Zhang, W. Fu, M. T. McDowell, G. Yushin, *ACS Appl. Mater. Interfaces* **2022**, *14*, 33447.
[210] G. Maresca, A. Petrongari, S. Brutti, G. Battista Appetecchi, *ChemSusChem* **2023**, *16*.
[211] S. Wei, S. Choudhury, J. Xu, P. Nath, Z. Tu, L. A. Archer, *Adv. Mater.* **2017**, *29*.
[212] Q. Yang, Z. Zhang, X. G. Sun, Y. S. Hu, H. Xing, S. Dai, *Chem. Soc. Rev.* **2018**, *47*, 2020.
[213] P. Schmitz, R. Jakelski, M. Pyschik, K. Jalkanen, S. Nowak, M. Winter, P. Bieker, *ChemSusChem* **2017**, *10*, 876.
[214] P. Schmitz, M. Kolek, M. Pyschik, K. Jalkanen, S. Nowak, M. Winter, P. Bieker, *ChemistrySelect* **2017**, *2*, 6052.
[215] Y. Jiang, Y. Zhou, D. Chu, Z. Ye, Z. Wang, Y. Chen, A. Liu, Z. Lv, W. Sun, M. Xie, *ACS Appl. Energy Mater.* **2022**, *5*, 7822.
[216] X. Yu, T. Lu, X. Li, J. Qi, L. Yuan, Z. Man, H. Zhuo, *RSC Adv.* **2022**, *12*, 14007.
[217] J. F. Vélez, L. V. Álvarez, C. del Río, B. Herradón, E. Mann, E. Morales, *Electrochim. Acta* **2017**, *241*, 517.
[218] D. Kumar, S. A. Hashmi, *Solid State Ionics* **2010**, *181*, 416.
[219] R. Mishra, S. K. Singh, H. Gupta, R. K. Tiwari, D. Meghnani, A. Patel, A. Tiwari, V. K. Tiwari, R. K. Singh, *Energy and Fuels* **2021**, *35*, 15153.
[220] S. Parveen, P. Sehrawat, S. A. Hashmi, *ACS Appl. Energy Mater.* **2022**, *5*, 930.
[221] Y. Gao, G. Chen, X. Wang, H. Yang, Z. Wang, W. Lin, H. Xu, Y. Bai, C. Wu, *ACS Applied Materials and Interfaces* **2020**, *12*, 22981.
[222] G. Chen, Y. Bai, Y. Gao, Z. Wang, K. Zhang, Q. Ni, F. Wu, H. Xu, C. Wu, *ACS Applied Materials and Interfaces* **2019**, *11*, 43252.
[223] D. Roscher, Y. Kim, D. Stepien, M. Zarrabeitia, S. Passerini, *Batteries and Supercaps* **2023**, *6*.
[224] D. Zhou, R. Liu, J. Zhang, X. Qi, Y. B. He, B. Li, Q. H. Yang, Y. S. Hu, F. Kang, *Nano Energy* **2017**, *33*, 45.
[225] Z. Zhang, Q. Zhang, J. Shi, Y. S. Chu, X. Yu, K. Xu, M. Ge, H. Yan, W. Li, L. Gu, Y. S. Hu, H. Li, X. Q. Yang, L. Chen, X. Huang, *Adv. Energy Mater.* **2017**, *7*, 1.
[226] C. de la Torre-Gamarra, G. B. Appetecchi, U. Ulissi, A. Varzi, A. Varez, S. Passerini, *J. Power Sources* **2018**, *383*, 157.
[227] H. W. Kim, P. Manikandan, Y. J. Lim, J. H. Kim, S. C. Nam, Y. Kim, *J. Mater. Chem. A* **2016**, *4*, 17025.
[228] R. Murugan, V. Thangadurai, W. Weppner, *Angewandte Chemie – International Edition* **2007**, *46*, 7778.
[229] K. Fu, Y. Gong, J. Dai, A. Gong, X. Han, Y. Yao, C. Wang, Y. Wang, Y. Chen, C. Yan, Y. Li, E. D. Wachsman, L. Hu, *Proc. Natl. Acad. Sci. USA* **2016**, *113*, 7094.
[230] C. K. Chan, T. Yang, J. M Weller, *Electrochim. Acta* **2017**, *253*, 268.
[231] W. Liu, N. Liu, J. Sun, P. C. Hsu, Y. Li, H. W. Lee, Y. Cui, *Nano Lett.* **2015**, *15*, 2740.
[232] C. S. Martínez-Cisneros, B. Pandit, C. Antonelli, J. Y. Sanchez, B. Levenfeld, A. Varez, *J. Eur. Ceram. Soc.* **2021**, *41*, 7723.
[233] S. Elisabetta, D. F. Massimo, B. Mariangela, K. Guk-Tae, W. FangLin, P. Stefano, A. Giovanni Battista, *ChemSusChem* **2019**, *12*, 4946.
[234] C. Yuanli, Z. Hu, C. Yitao, W. Qiyuan, C. Bin, Z. Zhenlun, L. Fulu, S. Wen, D. Daogaocao, Y. Lei, *J. Power Sources* **2022**, *535*, 231481.
[235] N. Wongittharom, T. C. Lee, C. H. Wang, Y. C. Wang, J. K. Chang, *J. Mater. Chem. A* **2014**, *2*, 5655.

[236] C. Y. Chen, J. Rizell, G. M. Kanyolo, T. Masese, Y. Sassa, M. Månsson, K. Kubota, K. Matsumoto, R. Hagiwara, Q. Xu, *Chem. Commun.* **2020**, *56*, 9272.
[237] C. H. Wang, Y. W. Yeh, N. Wongittharom, Y. C. Wang, C. J. Tseng, S. W. Lee, W. S. Chang, J. K. Chang, *J. Power Sources* **2015**, *274*, 1016.
[238] M. P. Do, N. Bucher, A. Nagasubramanian, I. Markovits, T. Bingbing, P. J. Fischer, K. P. Loh, F. E. Kühn, M. Srinivasan, *ACS Applied Materials and Interfaces* **2019**, *11*, 23972.
[239] C. V. Manohar, A. Raj K, M. Kar, M. Forsyth, D. R. MacFarlane, S. Mitra, *Sustainable Energy Fuels* **2018**, *2*, 566.
[240] F. Makhlooghiazad, M. Sharma, Z. Zhang, P. C. Howlett, M. Forsyth, L. F. Nazar, *J. Phys. Chem. Lett.* **2020**, *11*, 2092.
[241] C. H. Wang, C. H. Yang, J. K. Chang, *Chem. Commun.* **2016**, *52*, 10890.
[242] J. Song, D. han Lee, S. mi Oh, H. K. Kim, S. Choi, *J. Alloys Compd.* **2023**, *941*, 169028.
[243] L. Wu, A. Moretti, D. Buchholz, S. Passerini, D. Bresser, *Electrochim. Acta* **2016**, *203*, 109.
[244] C. Y. Li, J. Patra, C. H. Yang, C. M. Tseng, S. B. Majumder, Q. F. Dong, J. K. Chang, *ACS Sustainable Chemistry and Engineering* **2017**, *5*, 8269.
[245] Y. Gao, G. Chen, X. Wang, H. Yang, Z. Wang, W. Lin, H. Xu, Y. Bai, C. Wu, *ACS Applied Materials and Interfaces* **2020**, *12*, 22981.
[246] Q. Liu, X. Zhao, Q. Yang, L. Hou, D. Mu, G. Tan, L. Li, R. Chen, F. Wu, *Adv. Mater. Technol.* **2023**, *8*.
[247] S. Kumar, R. Raghupathy, M. Vittadello, *Batteries* **2024**, *10*, 73.
[248] C. Berthier, W. Gorecki, M. Minier, M. B. Armand, J. M. Chabagno, P. Rigaud, **1983**, *11*, 91.
[249] J. L. Souquet, *Annu. Rev. Mater. Sci.* **1981**, *11*, 211.
[250] C. Zhang, S. Gamble, D. Ainsworth, A. M. Z. Slawin, Y. G. Andreev, P. G. Bruce, *Nat. Mater.* **2009**, *8*, 580.
[251] J. Feng, L. Wang, Y. Chen, P. Wang, H. Zhang, X. He, *Nano Convergence* **2021**, *8*.
[252] F. Gucci, M. Grasso, C. Shaw, G. Leighton, V. Marchante Rodriguez, J. Brighton, *Polymer-Plastics Technology and Materials* **2023**, *62*, 1019.
[253] H. M. Ragab, F. Ahmad, S. N. Radwan, *Phys. B* **2016**, *502*, 97.
[254] P. Kesharwani, D. K. Sahu, Y. K. Mahipal, R. C. Agrawal, *Mater. Chem. Phys.* **2017**, *193*, 524.
[255] L. Carbone, J. Hassoun, *Ionics* **2016**, *22*, 2341.
[256] K. West, B. Zachau-Christiansen, T. Jacobsen, S. Atlung, *J. Electrochem. Soc.* **1985**, *132*, 3061.
[257] K. West, B. Zachau-christiansen, T. Jacobsen, E. Hiort-lorenzen, **1988**, *20*, 243.
[258] Y. Ma, M. M. Doeff, S. J. Visco, L. C. D. Jonghe, **1993**, *140*, 2726.
[259] M. M. Doeff, Y. Ma, S. J. Visco, L. C. D. Jonghe, **1993**, *140*, 169.
[260] M. Science, **1995**, *34*, 18.
[261] Q. Zhang, Y. Lu, H. Yu, G. Yang, Q. Liu, Z. Wang, L. Chen, Y.-S. Hu, *J. Electrochem. Soc.* **2020**, *167*, 070523.
[262] X. Qi, Q. Ma, L. Liu, Y. Hu, H. Li, Z. Zhou, X. Huang, L. Chen, *ChemElectroChem* **2016**, *3*, 1741.
[263] A. Boschin, P. Johansson, *Electrochim. Acta* **2015**, *175*, 124.
[264] H. Zhang, C. Liu, L. Zheng, F. Xu, W. Feng, H. Li, *Electrochim. Acta* **2014**, *133*, 529.
[265] Q. Ma, J. Liu, X. Qi, X. Rong, Y. Shao, W. Feng, J. Nie, Y.-S. Hu, H. Li, X. Huang, L. Chen, Z. Zhou, *J. Mater. Chem. A* **2017**, *5*, 7738.
[266] Z. Fang, Q. Ma, P. Liu, J. Ma, Y. Hu, Z. Zhou, H. Li, X. Huang, L. Chen, *ACS Appl. Mater. Interfaces* **2017**, *9*, 4282.
[267] M. Armand, P. Johansson, M. Bukowska, P. Szczeciński, L. Niedzicki, M. Marcinek, M. Dranka, J. Zachara, G. Żukowska, M. Marczewski, G. Schmidt, W. Wieczorek, *J. Electrochem. Soc.* **2020**, *167*, 070562.
[268] A. Szczęsna-Chrzan, M. Marczewski, J. Syzdek, M. K. Kochaniec, M. Smoliński, M. Marcinek, *Applied Physics A: Materials Science and Processing* **2023**, *129*, 37.
[269] A. Bitner-Michalska, G. M. Nolis, G. Zukowska, A. Zalewska, M. Poterała, T. Trzeciak, M. Dranka, M. Kalita, P. Jankowski, L. Niedzicki, J. Zachara, M. Marcinek, W. Wieczorek, *Sci. Rep.* **2017**, *7*, 40036.
[270] F. Colò, F. Bella, J. R. Nair, M. Destro, C. Gerbaldi, *Electrochim. Acta* **2015**, *174*, 185.
[271] Y. Zheng, Q. Pan, M. Clites, B. W. Byles, E. Pomerantseva, C. Y. Li, **2018**, *1801885*, 1.
[272] Z. Osman, K. B. Md Isa, A. Ahmad, L. Othman, *Ionics* **2010**, *16*, 431.
[273] B. Sun, J. Mindemark, K. Edström, D. Brandell, *Electrochem. Commun.* **2015**, *52*, 71.
[274] J. Mindemark, E. Törmä, B. Sun, D. Brandell, *Polymer* **2015**, *63*, 91.
[275] J. Mindemark, L. Imholt, J. Montero, D. Brandell, *J. Polym. Sci., Part A: Polym. Chem.* **2016**, *54*, 2128.
[276] J. Mindemark, R. Mogensen, M. J. Smith, M. M. Silva, D. Brandell, *Electrochem. Commun.* **2017**, *77*, 58.
[277] C. Sångeland, R. Younesi, J. Mindemark, D. Brandell, *Energy Storage Mater.* **2019**, *19*, 31.
[278] Ch. V. Subba Reddy, A.-P. Jin, Q.-Y. Zhu, L.-Q. Mai, W. Chen, *The European Physical Journal E* **2006**, *19*, 471.
[279] Pritam, A. Arya, A. L. Sharma, *J. Mater. Sci.* **2019**, *54*, 7131.
[280] Y. Yang, T. Wang, Y. Guo, P. Liu, X. Han, D. Wu, *Materials Today Chemistry* **2023**, *29*, 101384.
[281] J. O. Dennis, M. F. Shukur, O. A. Aldaghri, K. H. Ibnaouf, A. A. Adam, F. Usman, Y. M. Hassan, A. Alsadig, W. L. Danbature, B. A. Abdulkadir, *Molecules* **2023**, *28*, 1781.
[282] T. M. Kanakaraj, R. F. Bhajantri, C. Chavan, V. Cyriac, S. S. Bulla, *J. Non-Cryst. Solids* **2023**, *609*, 122276.
[283] C. Yang, *Mater. Lett.* **2004**, *58*, 33.
[284] S. B. Aziz, R. T. Abdulwahid, N. M. Sadiq, R. M. Abdullah, D. A. Tahir, D. A. Jameel, S. M. Hamad, O. Gh, *Results in Physics* **2023**, *51*, 106692.
[285] T. S. Tiong, M. H. Buraidah, L. P. Teo, A. K. Arof, *Ionics* **2016**, 2133.
[286] J. Wang, S. Song, R. Muchakayala, X. Hu, R. Liu, *Ionics* **2017**, *23*, 1759.
[287] B. Karaman, A. Bozkurt, *Int. J. Hydrogen Energy* **2018**, 1.
[288] V. Duraikkan, A. B. Sultan, N. Nallaperumal, A. Shunmuganarayanan, *Ionics* **2018**, *24*, 139.
[289] P. Fan, H. Liu, V. Marosz, N. T. Samuels, S. L. Suib, L. Sun, L. Liao, *Adv. Funct. Mater.* **2021**, *31*, 1.
[290] O. Buriez, Y. B. Han, J. Hou, J. B. Kerr, J. Qiao, S. E. Sloop, M. Tian, S. Wang, *J. Power Sources* **2000**, *89*, 149.
[291] S. Tang, W. Guo, Y. Fu, *Adv. Energy Mater.* **2021**, *11*, 1.
[292] D. K. Maurya, R. Dhanusuraman, Z. Guo, S. Angaiah, *Advanced Composites and Hybrid Materials* **2022**, *5*, 2651.
[293] Z. Zhang, K. Xu, X. Rong, Y. S. Hu, H. Li, X. Huang, L. Chen, *J. Power Sources* **2017**, *372*, 270.
[294] X. Yu, L. Xue, J. B. Goodenough, A. Manthiram, *ACS Materials Letters* **2019**, *1*, 132.
[295] K. Hiraoka, M. Kato, T. Kobayashi, S. Seki, *J. Phys. Chem. C* **2020**, *124*, 21948.
[296] Y. J. Lim, J. Han, H. W. Kim, Y. Choi, E. Lee, Y. Kim, *J. Mater. Chem. A* **2020**, *8*, 14528.
[297] X. Yu, L. Xue, J. B. Goodenough, A. Manthiram, *Adv. Funct. Mater.* **2021**, *31*.
[298] L. Ran, M. Li, E. Cooper, B. Luo, I. Gentle, L. Wang, R. Knibbe, *Energy Storage Mater.* **2021**, *41*, 8.
[299] Y. Wang, Z. Wang, J. Sun, F. Zheng, M. Kotobuki, T. Wu, K. Zeng, L. Lu, *J. Power Sources* **2020**, *454*.
[300] Y. Lailun, M. Cheng, J. H. Cheng, J. Rick, B. Hwang, *J. Power Sources* **2014**.

[301] X. Zhang, X. Wang, S. Liu, Z. Tao, J. Chen, *Nano Res.* **2018**, *11*, 6244.
[302] S. Chen, F. Feng, Y. Yin, H. Che, X. Liao, Z. Ma, *J. Power Sources* **2018**, *399*, 363.
[303] H. Hong, C. Liquan, H. Xuejie, X. Rongjian, *Electrochim. Acta* **1992**, *37*, 1671.
[304] G. Appetecchi, *Electrochem. Commun.* **1999**, *1*, 83.
[305] M. Watanabe, M. Kanba, K. Nagaoka, I. Shinohara, *J. Appl. Polym. Sci.* **1982**, *27*, 4191.
[306] G. B. Appetecchi, F. Croce, B. Scrosati, *Electrochim. Acta* **1995**, *40*, 991.
[307] O. Bohnke, G. Frand, M. Rezrazi, C. Rousselot, C. Truche, *Solid State Ionics* **1993**, *66*, 105.
[308] O. Bohnke, G. Frand, M. Rezrazi, C. Rousselot, C. Truche, *Solid State Ionics* **1993**, *66*, 97.
[309] M. Alamgir, K. M. Abraham, *J. Electrochem. Soc.* **1993**, *140*, L96.
[310] S. Janakiraman, A. Surendran, R. Biswal, S. Ghosh, S. Anandhan, *J. Electroanal. Chem.* **2019**, *833*, 411.
[311] A. Perico, in *Ionic Interactions in Natural and Synthetic Macromolecules*, Wiley, **2012**, pp. 49–90.
[312] L. C. F. So, C. Capiglia, Y. Saito, H. Kataoka, T. Kodama, E. Quartarone, **2000**, *131*, 291.
[313] D. Kumar, M. Suleman, S. A. Hashmi, *Solid State Ionics* **2011**, *202*, 45.
[314] K. Yang, Z. Liao, Z. Zhang, L. Yang, S. Hirano, *Mater. Lett.* **2019**, *236*, 554.
[315] D. Mouraliraman, N. Shaji, S. Praveen, M. Nanthagopal, C. W. Ho, M. Varun Karthik, T. Kim, C. W. Lee, *Nanomaterials* **2022**, *12*, 1056.
[316] H. S. Choe, J. Giaccai, M. Alamgir, K. M. Abraham, *Electrochim. Acta* **1995**, *40*, 2289.
[317] R. Huang, R. Xu, J. Zhang, J. Wang, T. Zhou, M. Liu, X. Wang, *Nano Res.* **2023**, *16*, 9480.
[318] D. Saikia, A. Kumar, *Electrochim. Acta* **2004**, *49*, 2581.
[319] J. I. Kim, Y. Choi, K. Y. Chung, J. H. Park, *Adv. Funct. Mater.* **2017**, *27*.
[320] H. Gao, B. Guo, J. Song, K. Park, J. B. Goodenough, *Adv. Energy Mater.* **2015**, *5*, 1.
[321] Y. Zhu, Y. Yang, L. Fu, Y. Wu, *Electrochim. Acta* **2017**, *224*, 405.
[322] J. C. Barbosa, R. Gonçalves, C. M. Costa, S. Lanceros-Méndez, *ACS Omega* **2022**, *7*, 14457.
[323] M. Cheng, T. Qu, J. Zi, Y. Yao, F. Liang, W. Ma, B. Yang, Y. Dai, Y. Lei, *Nanotechnology* **2020**, *31*, 425401.
[324] J. Shi, H. Xiong, Y. Yang, H. Shao, *Solid State Ionics* **2018**, *326*, 136.
[325] Z. Liu, X. Wang, J. Chen, Y. Tang, Z. Mao, D. Wang, *ACS Appl. Energy Mater.* **2021**, *4*, 623.
[326] J. Zheng, Y. Zhao, X. Feng, W. Chen, Y. Zhao, *J. Mater. Chem. A* **2018**, *00*, 1.
[327] A. P. V Kumar, A. K. R. Saroja, B. C. Moharana, K. M., R. S., *J. Electroanal. Chem.* **2020**, *859*, 113864.
[328] S. Janakiraman, O. Padmaraj, S. Ghosh, A. Venimadhav, *J. Electroanal. Chem.* **2018**, *826*, 142.
[329] S. Janakiraman, A. Surendran, R. Biswal, S. Ghosh, S. Anandhan, A. Venimadhav, *Mater. Res. Express* **2019**, *6*, 086318.
[330] J. Manuel, X. Zhao, K. K. Cho, J. K. Kim, J. H. Ahn, *ACS Sustainable Chemistry and Engineering* **2018**, *6*, 8159.
[331] K. Vignarooban, P. Badami, M. A. K. L. Dissanayake, P. Ravirajan, A. M. Kannan, *Ionics* **2017**, *23*, 2817.
[332] A. Gabryelczyk, H. Smogór, A. Swiderska-Mocek, *Electrochim. Acta* **2023**, *439*, 141645.
[333] H. Gao, W. Zhou, K. Park, J. B. Goodenough, *Adv. Energy Mater.* **2016**, *6*, 1.
[334] F. Colò, F. Bella, J. R. Nair, C. Gerbaldi, *J. Power Sources* **2017**, *365*, 293.
[335] M. L. Lehmann, G. Yang, D. Gilmer, K. S. Han, E. C. Self, R. E. Ruther, S. Ge, B. Li, V. Murugesan, A. P. Sokolov, F. M. Delnick, J. Nanda, T. Saito, *Energy Storage Mater.* **2019**, *21*, 85.
[336] C. D. Zhao, J. Z. Guo, Z. Y. Gu, X. T. Wang, X. X. Zhao, W. H. Li, H. Y. Yu, X. L. Wu, *Nano Res.* **2022**, *15*, 925.
[337] D. Xie, M. Zhang, Y. Wu, L. Xiang, Y. Tang, *Adv. Funct. Mater.* **2020**, *30*, 1.
[338] C. Luo, T. Shen, H. Ji, D. Huang, J. Liu, B. Ke, Y. Wu, Y. Chen, C. Yan, *Small* **2020**, *16*.
[339] T. Famprikis, P. Canepa, J. A. Dawson, M. S. Islam, C. Masquelier, *Nat. Mater.* **2019**, *18*, 1278.
[340] Z. Song, F. Chen, M. Martinez-Ibañez, W. Feng, M. Forsyth, Z. Zhou, M. Armand, H. Zhang, *Nat. Commun.* **2023**, *14*, 4884.
[341] Y. Yang, S. Yang, X. Xue, X. Zhang, Q. Li, Y. Yao, X. Rui, H. Pan, Y. Yu, *Adv. Mater.* **2024**, *36*, 2308332.
[342] R. Haas, C. Pompe, M. Osenberg, A. Hilger, I. Manke, B. Mogwitz, U. Maitra, D. Langsdorf, D. Schröder, *Energy Technol.* **2019**, *7*, 1801146.
[343] Q. Ma, F. Tietz, *ChemElectroChem* **2020**, *7*, 2693.
[344] W. Zhang, C.-D. Zhao, X.-L. Wu, *Adv. Mater. Interfaces* **2020**, *7*, 2001444.
[345] L. C. De Jonghe, L. Feldman, A. Buechele, *Solid State Ionics* **1981**, *5*, 267.
[346] M. Forsyth, L. Porcarelli, X. Wang, N. Goujon, D. Mecerreyes, *Acc. Chem. Res.* **2019**, *52*, 686.
[347] E. Fan, L. Li, Z. Wang, J. Lin, Y. Huang, Y. Yao, R. Chen, F. Wu, *Chem. Rev.* **2020**, *120*, 7020.
[348] A. Banerjee, X. Wang, C. Fang, E. A. Wu, Y. S. Meng, *Chem. Rev.* **2020**, *120*, 6878.
[349] A. Hayashi, K. Noi, A. Sakuda, M. Tatsumisago, *Nat. Commun.* **2012**, *3*, 856.
[350] T. Famprikis, Ö. U. Kudu, J. A. Dawson, P. Canepa, F. Fauth, E. Suard, M. Zbiri, D. Dambournet, O. J. Borkiewicz, H. Bouyanfif, S. P. Emge, S. Cretu, J.-N. Chotard, C. P. Grey, W. G. Zeier, M. S. Islam, C. Masquelier, *J. Am. Chem. Soc.* **2020**, *142*, 18422.
[351] P. Lu, D. Wu, L. Chen, H. Li, F. Wu, *Electrochem. Energy Rev.* **2022**, *5*, 3.
[352] S. Wenzel, T. Leichtweiss, D. A. Weber, J. Sann, W. G. Zeier, J. Janek, *ACS Appl. Mater. Interfaces* **2016**, *8*, 28216.
[353] I.-H. Chu, C. S. Kompella, H. Nguyen, Z. Zhu, S. Hy, Z. Deng, Y. S. Meng, S. P. Ong, *Sci. Rep.* **2016**, *6*, 33733.
[354] E. A. Wu, C. S. Kompella, Z. Zhu, J. Z. Lee, S. C. Lee, I.-H. Chu, H. Nguyen, S. P. Ong, A. Banerjee, Y. S. Meng, *ACS Appl. Mater. Interfaces* **2018**, *10*, 10076.
[355] X. Chi, Y. Zhang, F. Hao, S. Kmiec, H. Dong, R. Xu, K. Zhao, Q. Ai, T. Terlier, L. Wang, L. Zhao, L. Guo, J. Lou, H. L. Xin, S. W. Martin, Y. Yao, *Nat. Commun.* **2022**, *13*, 2854.
[356] T. Ando, A. Sakuda, M. Tatsumisago, A. Hayashi, *Electrochem. Commun.* **2020**, *116*, 106741.
[357] L. Zhang, D. Zhang, K. Yang, X. Yan, L. Wang, J. Mi, B. Xu, Y. Li, *Adv. Sci.* **2016**, *3*, 1600089.
[358] G. Liu, X. Sun, X. Yu, W. Weng, J. Yang, D. Zhou, R. Xiao, L. Chen, X. Yao, *Chem. Eng. J.* **2021**, *420*, 127692.
[359] L. Duchêne, A. Remhof, H. Hagemann, C. Battaglia, *Energy Storage Mater.* **2020**, *25*, 782.
[360] L. Duchêne, R.-S. Kühnel, E. Stilp, E. C. Reyes, A. Remhof, H. Hagemann, C. Battaglia, *Energy Environ. Sci.* **2017**, *10*, 2609.
[361] R. Asakura, D. Reber, L. Duchêne, S. Payandeh, A. Remhof, H. Hagemann, C. Battaglia, *Energy Environ. Sci.* **2020**, *13*, 5048.
[362] S. Gandi, V. S. Chidambara Swamy Vaddadi, S. S. Sripada Panda, N. K. Goona, S. R. Parne, M. Lakavat, A. Bhaumik, *J. Power Sources* **2022**, *521*, 230930.

[363] X. Feng, H. Fang, N. Wu, P. Liu, P. Jena, J. Nanda, D. Mitlin, *Joule* **2022**, *6*, 543.
[364] K. B. Hueso, M. Armand, T. Rojo, *Energy Environ. Sci.* **2013**, *6*, 734.
[365] M.-C. Bay, R. Grissa, K. V. Egorov, R. Asakura, C. Battaglia, *Mater. Futures* **2022**, *1*, 031001.
[366] L. Duchêne, D. H. Kim, Y. B. Song, S. Jun, R. Moury, A. Remhof, H. Hagemann, Y. S. Jung, C. Battaglia, *Energy Storage Mater.* **2020**, *26*, 543.
[367] D. S Jolly, Z. Ning, J. E. Darnbrough, J. Kasemchainan, G. O. Hartley, P. Adamson, D. E. J. Armstrong, J. Marrow, P. G. Bruce, *ACS Appl. Mater. Interfaces* **2020**, *12*, 678.
[368] Z. Sun, L. Li, C. Sun, Q. Ni, Y. Zhao, H. Wu, H. Jin, *Nano Lett.* **2022**, *22*, 7187.
[369] Y. Zhao, C. Wang, Y. Dai, H. Jin, *Nano Energy* **2021**, *88*, 106293.
[370] H. Wang, G. Zhao, S. Wang, D. Liu, Z. Mei, Q. An, J. Jiang, H. Guo, *Nanoscale* **2022**, *14*, 823.
[371] T. Lan, C.-L. Tsai, F. Tietz, X.-K. Wei, M. Heggen, R. E. Dunin-Borkowski, R. Wang, Y. Xiao, Q. Ma, O. Guillon, *Nano Energy* **2019**, *65*, 104040.
[372] H. Yamauchi, J. Ikejiri, K. Tsunoda, A. Tanaka, F. Sato, T. Honma, T. Komatsu, *Sci. Rep.* **2020**, *10*, 9453.
[373] H. Yamauchi, J. Ikejiri, F. Sato, H. Oshita, T. Honma, T. Komatsu, *J. Am. Ceram. Soc.* **2019**, *102*, 6658.
[374] Y. Kato, S. Shiotani, K. Morita, K. Suzuki, M. Hirayama, R. Kanno, *J. Phys. Chem. Lett.* **2018**, *9*, 607.
[375] R. Koerver, W. Zhang, L. de Biasi, S. Schweidler, A. O. Kondrakov, S. Kolling, T. Brezesinski, P. Hartmann, W. G. Zeier, J. Janek, *Energy Environ. Sci.* **2018**, *11*, 2142.
[376] Y. Lu, J. A. Alonso, Q. Yi, L. Lu, Z. L. Wang, C. Sun, *Adv. Energy Mater.* **2019**, *9*, 1901205.
[377] W. Zhou, Y. Li, S. Xin, J. B. Goodenough, *ACS Cent. Sci.* **2017**, *3*, 52.
[378] G. Sun, X. Yang, N. Chen, S. Yao, X. Wang, X. Jin, G. Chen, Y. Xie, F. Du, *Energy Storage Mater.* **2021**, *41*, 196.
[379] Z. Zhang, Q. Zhang, J. Shi, Y. S. Chu, X. Yu, K. Xu, M. Ge, H. Yan, W. Li, L. Gu, Y.-S. Hu, H. Li, X.-Q. Yang, L. Chen, X. Huang, *Adv. Energy Mater.* **2017**, *7*, 1601196.
[380] L. Liu, X. Qi, Q. Ma, X. Rong, Y.-S. Hu, Z. Zhou, H. Li, X. Huang, L. Chen, *ACS Appl. Mater. Interfaces* **2016**, *8*, 32631.
[381] L. M. Bronstein, R. L. Karlinsey, B. Stein, Z. Yi, J. Carini, J. W. Zwanziger, *Chem. Mater.* **2006**, *18*, 708.
[382] I. Villaluenga, X. Bogle, S. Greenbaum, I. G. de Muro, T. Rojo, M. Armand, *J. Mater. Chem. A* **2013**, *1*, 8348.
[383] A. S. Shaplov, P. S. Vlasov, M. Armand, E. I. Lozinskaya, D. O. Ponkratov, I. A. Malyshkina, F. Vidal, O. V. Okatova, G. M. Pavlov, C. Wandrey, I. A. Godovikov, Y. S. Vygodskii, *Polym. Chem.* **2011**, *2*, 2609.
[384] J. L. Olmedo-Martínez, A. Fdz De Anastro, M. Martínez-Ibañez, A. J. Müller, D. Mecerreyes, *Energy Fuels* **2023**, *37*, 5519.
[385] P. Kuray, W. Mei, S. E. Sheffield, J. Sengeh, C. R. F. Pulido, C. Capparelli, R. J. Hickey, M. A. Hickner, *Front. Energy Res.* **2020**, *8*.
[386] H. B. Youcef, B. Orayech, J. M. L. Del Amo, F. Bonilla, D. Shanmukaraj, M. Armand, *Solid State Ionics* **2020**, *345*, 115168.
[387] Q. Pan, Z. Li, W. Zhang, D. Zeng, Y. Sun, H. Cheng, *Solid State Ionics* **2017**, *300*, 60.
[388] C. Simari, M. Tuccillo, S. Brutti, I. Nicotera, *Electrochim. Acta* **2022**, *410*, 139936.
[389] P. Wang, H. Zhang, J. Chai, T. Liu, R. Hu, Z. Zhang, G. Li, G. Cui, *Solid State Ionics* **2019**, *337*, 140.
[390] L. Yang, Y. Jiang, X. Liang, Y. Lei, T. Yuan, H. Lu, Z. Liu, Y. Cao, J. Feng, *ACS Appl. Energy Mater.* **2020**, *3*, 10053.
[391] X. Xu, Y. Wang, Q. Yi, X. Wang, R. A. Paredes Camacho, H. Kungl, R. A. Eichel, L. Lu, H. Zhang, *ChemSusChem* **2023**, *16*.
[392] Y. Dong, P. Wen, H. Shi, Y. Yu, Z. Wu, *Adv. Funct. Mater.* **2023**, 2213584.

Hamideh Darjazi (Ph.D. 2021) is a junior assistant professor at the Department of Applied Science and Technology (Politecnico di Torino). She has carried out multi-disciplinary research activities, encompassing synthesis of active materials, their chemical, morphological, and structural characterization (with particular attention to the crystallographic properties), and electrochemical analysis to relate the features of the materials and of the electrodes prepared with their behavior in LIBs and NIBs.

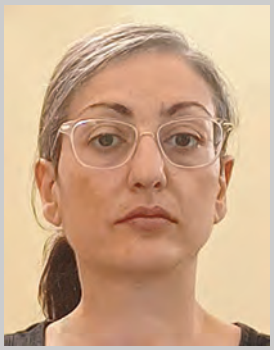

Marisa Falco (Ph.D. in materials science and technology 2023) is a post-doc researcher at the Department of Applied Science and Technology (Politecnico di Torino). Her research activity is focused on the development and electrochemical characterization of advanced polymer-based electrolytes (gels, solid, hybrids, and composites), alternative to present state-of-the-art liquid carbonates, carried out in the framework of EU/national projects. She is Topics Board Editor of *Electrochem* Journal (MDPI).

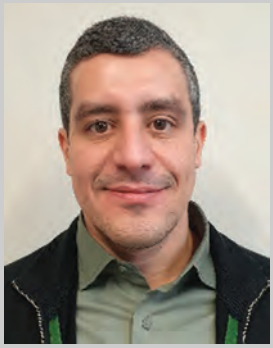

Giuseppe A. Elia (Ph.D. 2014) is a senior assistant professor at the Department of Applied Science and Technology (Politecnico di Torino), co-leading the GAME-Lab. Over the years, he focused his activity on various research topics in the field of physical chemistry, materials science, electrochemistry and its applications, particularly advanced Li-ion and Li-air batteries and beyond Li-ion systems, including sodium, calcium, zinc, and aluminium. He is the author/co-author of over 60 peer-reviewed articles and author of five book chapters and three patents.

Claudio Gerbaldi (Ph.D. 2006) is a full professor of chemistry for applied technologies at the Department of Applied Science and Technology (Politecnico di Torino). Leader of the Group for Applied Materials and Electrochemistry (GAME-Lab), he coordinates the research activity on innovative polymer electrolytes and nanostructured electrodes for high-performing, sustainable energy storage (chiefly, Li and post-Li batteries) and conversion devices in the framework of several EU-funded and industrial projects. He is (co)-author of >175 ISI articles (h-index 70) and five international patents. Among others, he has received the Piontelli Award for outstanding results in Electrochemistry from the President of the Italian Republic.